Convection in porous media and Legendre, Chebyshev Galerkin methods

Antony . Hill

Convection in Porous Media and Legendre, Chebyshev Galerkin Methods

Antony A. Hill

A Thesis presented for the degree of
Doctor of Philosophy

Numerical Analysis
Department of Mathematical Sciences
University of Durham
England

July 2005

Dedicated to

My family

Convection in Porous Media and Legendre, Chebyshev Galerkin Methods

Antony A. Hill

Submitted for the degree of Doctor of Philosophy
July 2005

Abstract

The subject of thermal convection in fluid and porous media is investigated, coupled with the development of efficient spectral finite element methods to improve on the more commonly used techniques for these types of problems.

Convection induced by the selective absorption of radiation in a porous medium is investigated in the first four chapters. For the Darcy and Brinkman models for fluid flow the thresholds of the linear and nonlinear theories are shown to be extremely close, demonstrating that the linear theory is accurate enough to predict the onset of convective motion. The exploration of a quadratically modelled internal heat source is discussed next. It is shown that the linear and nonlinear thresholds are close unless the quadratic term becomes dominant over the linear term. Developing a double-diffusive model yields a critical parameter for which no oscillatory convection occurs when it is exceeded. This is an unobserved phenomenon in the present literature.

Thermal convection in a linearly viscous fluid in a finite box is also explored. It is demonstrated that the linear and nonlinear thresholds do not coincide, which contradicts results by Georgescu & Mansutti [25].

Legendre and Chebyshev polynomial based spectral methods are also developed for the evaluation of eigenvalues and eigenfunctions inherent in stability analysis in porous media, drawing on the experience of the implementation of the well established techniques in the previous work. These generate sparse matrices, where the standard homogeneous boundary conditions for both porous and fluid media problems are contained within the method.

Declaration

The work in this thesis is based on research carried out at the Numerical Analysis Group, Department of Mathematical Sciences, University of Durham, England. No part of this thesis has been submitted elsewhere for any other degree or qualification and it all my own work with the exception of Chapters 6 and 7, which were written in collaboration with Prof B. Straughan of the University of Durham, England. The contents of Chapters 2 to 8 are published in [36] - [44].

Acknowledgements

It is with sincere gratitude that I thank my supervisor Prof Brian Straughan. His guidance and generosity have been immeasurable, making the period under his supervision both rewarding and enjoyable.

I thank everyone in the Department of Mathematical Sciences at the University of Durham for their help and support, with particular reference to the Numerical Analysis group, past and present, and Imran M for saving everyone precious time by preparing this LaTeX template. Special thanks also to Prof Ruby Krishnamurti for her correspondence with regards to the validity of some of the models I have adopted.

This work was supported by a research studentship of the Engineering and Physical Sciences Research Council.

Contents

List of Figures

List of Tables

Chapter 1

Introduction

The objective of this thesis is to investigate thermal convection in porous media and develop efficient spectral finite element methods to improve on the more commonly used techniques for these types of problems. The aim of this chapter is to present some key definitions, discuss the underlying theory of the stability and instability analyses inherent in studying flows in fluid and porous media, and to provide some motivation behind the development of each chapter.

Porous media are materials consisting of a solid matrix with an interconnected void. In our context the void is saturated by a fluid, where the interconnectedness of the void (which we refer to as the pores) allows the flow of such fluid throughout the material.

Convection in porous media is a highly active subject of research due to the immense variety of applications such as bio-remediation, geothermal reservoir systems, contaminant movement in soil, solid matrix heat exchangers, solar power converters and oil extraction. These and many other examples are described in Nield & Bejan [77], and specific references may be found on pages 238, 239 of Straughan [90]. An example of the novel use of porous media, drawn from these references, is in heat transfer mechanisms through the use of porous foams and heat pipes, see e.g. Amili & Yortsos [5].

Modeling as realistically as possible these physical phenomena is the main impetus behind the extensive research into fluid mechanics. The mathematical idealisation of the stability of these real world problems is achieved through the use

of partial differential equations to model the physical problem. The study of the stability of such systems of partial differential equations is a key aspect in their physical interpretation (see e.g. Nield & Bejan [77]; Straughan [90]), and continues to be one of the most pursued topics in fluid mechanics.

To clarify the concept of stability in the context of a system of partial differential equations, we begin with a simple illustrative example. Let $u(x,t)$ satisfy the equation

$$\frac{\partial u}{\partial t} + u\frac{\partial u}{\partial x} = \frac{\partial^2 u}{\partial x^2} + au, \tag{1.1}$$

where $x \in (0,1)$, and $u = 0$ at $x = 0, 1$. Here t and x are time and spatial point respectively, and a is some real, positive constant.

Clearly $u \equiv 0$ is a solution to equation (1.1), which is referred to as a stationary solution as none of the variables have time (t in the context of the example) dependence. It is the stability of this solution which we investigate by introducing a perturbation (i.e. disturbance) to it. If all the perturbations decay to zero as time progresses then the solution is said to be stable. Conversely if just a single disturbance grows in amplitude with time, then the solution is unstable. Let w be a perturbation to the solution $\overline{u} \equiv 0$, i.e. $u = \overline{u} + w$, such that

$$\frac{\partial w}{\partial t} + w\frac{\partial w}{\partial x} = \frac{\partial^2 w}{\partial x^2} + aw. \tag{1.2}$$

To discuss linearised instability we retain only the terms in (1.2) which are linear in w. As this is now a linear equation we may introduce exponential time dependence in w such that $w(x,t) = e^{\sigma t}y(x)$, for some, potentially complex, growth rate σ. This yields the equation

$$\sigma y = \frac{d^2 y}{dx^2} + ay. \tag{1.3}$$

By imposing the boundary conditions, ($y = 0$, $x = 0, 1$), it is possible to define

$$y(x) = C\sin(n\pi x), \qquad n = \pm 1, \pm 2, \ldots$$

for some constant C. Substituting this into (1.3) yields

$$\sigma = -n^2\pi^2 + a \qquad n = \pm 1, \pm 2, \ldots. \tag{1.4}$$

The growth rate σ can now be used to assess whether the zero solution is unstable. If $Re(\sigma) > 0$ then the perturbation will grow exponentially in time, clearly leading

to what will be referred to as linear instability. From (1.4) it is clear that $\sigma \in \mathbb{R}$. Therefore for linear instability $a > n^2\pi^2 \geq \pi^2$.

It is important to note, however, that this linear analysis approach assumes that the perturbation is small and so neglects terms of quadratic and higher order. Hence, if a system of partial differential equations contains nonlinear elements, these terms must be discarded to proceed. It has been proved that linear analysis often provides little information on the behaviour of the nonlinear system (see Straughan [90]), so in such cases only instability can be deduced from the linear thresholds, as any potential growth in the nonlinear terms is not considered.

In order to establish stability results we turn our attention to the highly adaptable energy method, cf. Straughan [90]. Nonlinear energy analysis, which is conducted throughout the thesis, is of particular importance as energy methods are creating much interest, see e.g. Kaiser & Mulone [49], Delgado *et al.* [19], and also because they delimit the parameter region of possible subcritical instability (the region between the linear instability and nonlinear stability thresholds), see e.g. Bhandar *et al.* [7], Lu & Shao [60], Herron & Ali [35].

Multiplying (1.1) by u and integrating over (0, 1) yields

$$\frac{1}{2}\frac{d}{dt}\int_0^1 u^2\,dx + \int_0^1 u^2\frac{\partial u}{\partial x}\,dx = \int_0^1 \frac{\partial^2 u}{\partial x^2}u\,dx + a\int_0^1 u^2\,dx.$$

It is possible to use the boundary conditions to derive that

$$\int_0^1 \frac{\partial^2 u}{\partial x^2}u\,dx = \left[u\frac{\partial u}{\partial x}\right]_0^1 - \int_0^1 \left(\frac{\partial u}{\partial x}\right)^2 dx = -\|u_x\|^2$$

and

$$\int_0^1 u^2\frac{\partial u}{\partial x}\,dx = \frac{1}{3}[u^3]_0^1 = 0,$$

where $\|\cdot\|$ denotes the norm on the space of square integrable functions on (0, 1) and $u_x = \partial u/\partial x$.

Defining an energy $E(t)$ by

$$E(t) = \frac{1}{2}\|u\|^2,$$

we have the inequality

$$\begin{aligned}\frac{dE}{dt} &= -\|u_x\|^2 + a\|u\|^2 \\ &= -a\|u_x\|^2\left(\frac{1}{a} - \frac{\|u\|^2}{\|u_x\|^2}\right) \\ &\leq -a\|u_x\|^2\left(\frac{1}{a} - \frac{1}{R_E}\right)\end{aligned}$$

where $1/R_E = \max_{\mathcal{H}}(\|u\|^2/\|u_x\|^2)$, and $\mathcal{H}$ is the space of admissible functions over which we seek a maximum, such that

$$\mathcal{H} = \{u \in C^2(0,1) \cap C([0,1]), \mid u = 0,\ x = 0,1\}.$$

Using the Poincaré inequality (i.e. $\|u_x\|^2 \geq \pi^2\|u\|^2$, see Appendix B.2 for further details), and assuming $c = 1/a - 1/R_E > 0$ it can be deduced that

$$\frac{dE}{dt} \leq -2\pi^2 acE$$

or, equivalently

$$\frac{d}{dt}(e^{2\pi^2 act}E) \leq 0,$$

which leads to

$$E(t) \leq e^{-2\pi^2 act}E(0).$$

Hence, by the definition of $E(t)$, $\|u\| \to 0$ at least exponentially, so the zero solution to (1.1) is stable under the maximisation problem $R_E \geq a$.

One of the aims of the thesis is to study the behaviour of the linear and non-linear thresholds and compare them to assess any potential regions of subcritical instabilities. Thus, quantifying the discrepancy between these two thresholds makes it possible to provide an assessment of the suitability of linear theory to predict the onset of convection.

Conventionally, stability calculations involve determining eigenvalues and eigenfunctions, with few of the associated eigenvalue problems solvable analytically. Two powerful existing techniques for finding eigenvalues and eigenfunctions numerically are the compound matrix (see e.g. Brown & Marletta [9]; Davies [18]; Drazin & Reid [21]; Gardner *et al.* [24]; Greenberg & Marletta [30], [31], [32]; Ivansson [46]; Straughan & Walker [91]) and the Chebyshev tau method (see e.g. Dongarra *et*

al. [20]; Gheorghiu & Pop [26]; Pop [80]; Pop [81]). The compound matrix method, which belongs to the family of shooting techniques, performs competently for stiff differential equations, with the specific purpose of reducing rounding error, as explored in Greenberg & Marletta [32], Straughan & Walker [91], see also the references therein. The Chebyshev tau technique is a spectral method. This method calculates as many eigenvalues as required as opposed to just one at a time as is done in the compound matrix method. We also refer to similar numerical techniques in Greenberg & Marletta [32], Bourne [8], Brown & Marletta [9] and Theofilis [92].

These established methods, although useful, produce a variety of computational and storage problems, as highlighted in each instance of their utilisation in the thesis. Chapters 2 to 5 have typical characteristics of the stability analysis of fluid motion in porous media with standard homogeneous boundary conditions, so the natural progression was to develop more efficient techniques based on the experience of employing the well established routines.

It was concluded through the experience of the numerical analysis of Chapters 2 to 6 that the polynomial based structure adopted by the Chebyshev tau technique was the optimal approach, if the dual problems of matrix fullness and spurious eigenvalues linked to boundary conditions inherent in this method could be addressed. A full discussion of the limitations of both the compound matrix method and Chebyshev tau technique and the resulting numerical methods designed to improve on them is given in Chapters 7 and 8.

A brief outline of each chapter now follows.

In Chapter 2 convection induced by the selective absorption of radiation in a porous medium is explored. This is a modification to a porous medium of the system modelled by Krishnamurti [55], which showed that penetrative convection could occur in a stably stratified fluid layer by internal heating through the absorption of radiation. Employing this adapted model we show the growth rate for the linearised system is real. A linear instability analysis is performed and global stability thresholds are also found using nonlinear energy theory. An excellent agreement is found between the linear instability and nonlinear stability Rayleigh numbers, so that the region of potential subcritical instabilities is very small, demonstrating that

the linear theory accurately emulates the physics of the onset of convection.

In Chapter 3 convection induced by the selective absorption of radiation in a porous medium is studied analytically and numerically using the Brinkman model. The motivation behind this adaptation is based on the observation that as the internal heating is provided by the introduction of radiation, a highly packed porous medium (such as glass beads) could potentially cause refraction of the radiation, resulting in an uneven internal heating throughout the layer. Both linear and nonlinear stability analyses are employed. The thresholds show excellent agreement so that the region of potential subcritical instabilities is very small, demonstrating that linear theory is accurate enough to predict the onset of convective motion. A surprising result shows that the critical Rayleigh number increases linearly as λ (Darcy number $\times$ Brinkman coefficient / dynamic viscosity of the fluid) increases. Employing the compound matrix method in both the linear and nonlinear numerical analysis became problematic due to the high order of the equations, with the Chebyshev tau technique also being restrictive due to the heavy computational cost in solving full matrix eigenvalue problems required over several parameter ranges. This leads to the development of the numerical methods in Chapters 7 and 8 to overcome these difficulties.

It is stated in Krishnamurti [55] in reference to the internal heat source that 'This linear relationship is a first order approximation and may need modification for high concentrations of [thymol] blue'. Chapter 4 is motivated by the exploration of the validity of an alternative quadratic model. A linear instability analysis is performed. To establish conditional and unconditional nonlinear stability results, both the Darcy and Forchheimer models are employed to describe fluid flow. Due to the presence of significant regions of potential subcritical instabilities, the results indicate that linear theory may only be accurate enough to predict the onset of convective motion when the model for the internal heat source is predominantly linear.

An interesting and significant aspect of the Krishnamurti model, unexamined in Chapters 2 to 4, is the effect of the concentration of the thymol blue on the density of the model. Each of these bodies of work define the state equation to be linear in

temperature, with the effect of concentration on density assumed negligible. Chapter 5 explores the use of a double-diffusive convection model in a porous medium, with fixed boundary conditions employed throughout. Both the numerical and analytical analysis for the linear theory strongly suggest the presence of a critical value γ_c, where γ is essentially a measure of the internal heat source, for which no oscillatory convection occurs when $\gamma_c \leq \gamma$. This, in the present literature, appears to be an unobserved phenomenon. A nonlinear energy stability analysis demonstrates more comparable linear and nonlinear thresholds when the linear theory predicts the onset of fully stationary convection. However, irrespective of the γ value, the agreement of the thresholds does deteriorate as the solute Rayleigh number R_c increases. Similarly to Chapter 3, the Chebyshev tau technique was found to be restrictive due to the heavy computational cost in solving full matrix eigenvalue problems required over several parameter ranges.

In Chapter 6 the linear instability and nonlinear stability bounds for thermal convection in a linearly viscous fluid in a finite box are analysed. The linear instability threshold is found to be well above the global stability boundary, which contradicts previous work on this model by Georgescu and Mansutti [25]. This problem is an interesting example for which the methods developed in Chapters 7 and 8 would not be directly applicable due to complicated boundary conditions.

In response to the limitations of the well established numerical methods used in Chapters 2 to 6, Chapter 7 presents a Legendre polynomial based spectral technique to be applicable to solving eigenvalue problems which arise in linear and nonlinear stability questions in porous media, (although there is potential for application to other areas of Continuum Mechanics). The matrices produced in the corresponding generalised eigenvalue problem are sparse, reducing the computational and storage costs, where the superimposition of the standard homogeneous boundary conditions which arise in porous media is not needed due to the structure of the method. This improves on the computational and storage difficulties encountered with the Chebyshev tau method in Chapters 2 to 6. Several eigenvalue problems are solved using both the Legendre polynomial based and Chebyshev tau techniques. In each example the Legendre polynomial based spectral technique converges to the required

accuracy utilising fewer polynomials than the Chebyshev tau method, and with much greater computational efficiency.

Although the Legendre polynomial based spectral method developed in Chapter 7 was shown to overcome the dual problems of matrix fullness and boundary conditions, providing a viable, more efficient, alternative to the Chebyshev tau technique, drawbacks appeared which resulted in the development of Chapter 8. Namely, the introduction of large order polynomials into the system of partial differential equations under evaluation yields a problematic assessment of the inner product of the Legendre bases with the polynomial, and bandwidth growth within the Legendre method (see the introduction of Chapter 8 for specific details). This is mainly overcome with the use of Chebyshev polynomials. Thus, in Chapter 8 a Chebyshev polynomial based spectral technique is presented which is applicable to solving eigenvalue problems which arise in linear and nonlinear stability analysis. Although, in the present literature, the basis functions explored are stated to lead to full matrices in the associated generalised eigenvalue problem, it is shown that by utilising a weighted Chebyshev space, sparse matrices are produced. The structure of the method also negates the need for the superimposition of the standard homogeneous boundary conditions. A selection of eigenvalue problems are presented, which are solved using both the Chebyshev polynomial based and Chebyshev tau techniques. The results clearly demonstrate the computational advantages of utilising the Chebyshev spectral method. This chapter is concluded with comparisons between the Legendre and Chebyshev polynomial based methods from Chapters 7 and 8.

Chapter 9 contains some concluding remarks on the results and implications of the thesis, with suggestions on the development of future work.

Standard indicial notation is utilised throughout the thesis, with the Einstein summation convention for repeated indices. For example,

$$u_t \equiv \frac{\partial u}{\partial t} \equiv u_{,t}, \qquad u_{i,t} \equiv \frac{\partial u_i}{\partial t}, \qquad u_{i,i} \equiv \frac{\partial u_i}{\partial x_i} \equiv \sum_{i=1}^{3} \frac{\partial u_i}{\partial x_i},$$

$$u_j u_{i,j} \equiv u_j \frac{\partial u_i}{\partial x_j} \equiv \sum_{j=1}^{3} u_j \frac{\partial u_i}{\partial x_j}, \quad i = 1, 2 \text{ or } 3.$$

The standard Laplacian is represented by $\triangle$, with the Lebesgue space $L^2(\Omega)$ being defined as

$$L^2(\Omega) = \left\{ v : \Omega \to \mathbb{C} \,\middle|\, \int_\Omega |v|^2 dx < \infty \right\}.$$

Chapter 2

Convection induced by the selective absorption of radiation in a porous medium

The object of this chapter is to explore convection induced by the selective absorption of radiation in a porous medium. This is a modification of the system modelled by Krishnamurti [55], which showed that penetrative convection could occur in a stably stratified fluid layer by internal heating through the absorption of radiation. This model has not been particularly well explored in the current literature even though it provides a closer model of cumulus convection as it occurs in the atmosphere.

Krishnamurti's experiment involves the use of a layer of water containing thymol blue, a substance commonly used to visualise fluid motion. The thymol blue has the characteristic of colouring the water orange when the pH is low, and blue when the pH is high. With a positive electrode along the bottom layer hydroxyl ions are produced forcing the pH to increase, which in turn makes this area of the fluid blue. When a sodium lamp is introduced the predominantly orange light acts as an internal heat source as the radiation travels through the orange part of the fluid layer with negligible absorption, but is strongly absorbed by the conjugated blue fluid near the positive electrode at the bottom of the layer. Buoyancy driven flows can be propagated from the resultant heating.

The convection mechanism is a penetrative one effectively modelled via an internal heat source. Penetrative convection occurs when vertical buoyancy driven motion, originally in an unstably stratified layer of fluid, penetrates into surrounding stably stratified layers. There is extensive literature on penetrative convection with relevant material including Carr & de Putter [13] who provide linear and nonlinear analysis for penetrative convection in a horizontally isotropic porous layer, Chasnov & Tse [15] who explore turbulent penetrative convection with an internal heat source in a fluid layer, and McKay [67] who studies the onset of buoyancy-driven convection in superposed reacting fluid and porous layers. Further novel recent contributions are those of Straughan [88], Tse & Chasnov [96] and Zhang & Schubert [99], [100].

The system we consider is essentially the same as that given in Krishnamurti [55], but with the crucial exception of exploring the model for penetrative convection in a porous medium (see e.g. McKay [68], Carr & de Putter [13]), with boundary surfaces as there would be in the experiment.

The development of both linear instability and nonlinear stability theories in this chapter allows for the study of any potential regions of subcritical instabilities, so that an assessment of the suitability of linear theory to predict the physics of the onset of convection can be made.

The numerical solutions of the linear and nonlinear theories constitute generalised eigenvalue problems, which are evaluated using the Chebyshev tau technique and the compound matrix numerical techniques (see Appendices A.2 and A.1).

It is interesting to note that the porosity ε is found to have no effect on the linear and nonlinear analysis, so that ε can take any value, (within acceptable range $0 < \varepsilon < 1$), with the results remaining the same.

The results in this chapter have been published in the article Hill [36].

2.1 Governing Equations

Let us consider a fluid saturated porous layer occupying the three dimensional layer $\{(x, y) \in \mathbb{R}^2\} \times \{z \in (0, d_z)\}$, where $Oxyz$ is a cartesian frame of reference with unit

vectors **i**, **j**, **k** respectively.

The porosity ε of a porous medium is defined as the fraction of the total volume of the medium that is occupied by the fluid volume, assuming that all the fluid space is connected. With this in mind, if we define $\mathbf{v}$ to be the velocity averaged over all the pores of the porous medium, and $\mathbf{V}$ to be the actual fluid velocity in a pore, then we have the Dupuit-Forcheimer relationship $\mathbf{v} = \varepsilon\mathbf{V}$ (see Nield & Bejan [77]).

From Nield & Bejan [77] we see that relationships between aspects of the porous medium can be split into their fluid and solid components respectively. Those presented in Nield & Bejan [77] which are relevant to this body of work consist of

$$(\rho_0 h)_m = (1-\varepsilon)(\rho_0 h)_s + \varepsilon(\rho_0 h_p)_f$$

where ρ_0 denotes density, h_p is the specific heat of the fluid at constant pressure, and h is the specific heat of the solid. The subscripts s, f and m denote the solid, fluid, and porous medium respectively. Similarly

$$\kappa_m = (1-\varepsilon)\kappa_s + \varepsilon\kappa_f$$

where κ is the thermal diffusivity (i.e. thermal conductivity) of the component, with subscripts as above.

Darcy's law for convection in a porous medium (see Nield and Bejan [77]) is taken to govern the flow. Defining v_i to be the pore averaged velocity in the direction i,

$$\frac{\mu}{k} v_i = -p_{,i} - b_i g \rho(T). \tag{2.1}$$

Here g is acceleration due to gravity in the negative z direction, $\mathbf{b} = (0,0,1)$, $p_{,i}$ is the pressure gradient, μ is the dynamic viscosity of the fluid, and k is the permeability of the porous medium. We make the simplifying assumption that the density ρ is a linear function in the temperature T, so that

$$\rho(T) = \rho_0(1 - \alpha(T - T_0))$$

for initial pressure ρ_0 and initial temperature T_0. The effect of the concentration of the conjugated form of the thymol blue on the density function $\rho(T)$ is assumed negligible in this chapter, although this is addressed in Chapter 5.

The incompressibility condition for this system is derived from an equation that expresses the fact that the rate of change of mass contained in a fixed volume (F) of fluid is given by the rate at which the fluid flows out of it across the boundary ∂F. Namely, letting $\mathbf{n}$ be a normal vector of F and utilising the divergence theorem,

$$\begin{aligned} \frac{d}{dt}\int_F \rho \, dF &= -\oint_{\partial F} (\rho v_i) \cdot \mathbf{n} \, dS \\ &= -\int_F (\rho v_i)_{,i} \, dF. \end{aligned}$$

As F can be taken arbitrarily,

$$\frac{\partial \rho}{\partial t} + (\rho v_i)_{,i} = 0.$$

The Boussinesq approximation (see Chandrasekhar [14]) is taken, where ρ (as defined previously) is treated as a constant in all terms in the equations of motion except in the external force term. This leads to the incompressibility condition

$$v_{i,i} = 0. \tag{2.2}$$

We now turn our attention to the heat equation. From Joseph [48] the heat equation is defined as

$$(\rho_0 h)_m T_{,t} + (\rho_0 h_p)_f \varepsilon \mathbf{V} \cdot \nabla T = \nabla(\kappa_m \nabla T) + (\rho_0 h_p)_f Q \tag{2.3}$$

where κ_m, $(\rho_0 h_p)_f$, and $(\rho_0 h)_m$ are as before, and the term Q is introduced as the internal heat source created by the absorbed radiation. Dividing (2.3) by $(\rho_0 h_p)_f$, and recalling $v_i = \varepsilon V_i$, we have

$$\frac{1}{M} T_{,t} + v_i T_{,i} = \kappa \triangle T + Q,$$

where $\kappa = \kappa_m/(\rho_0 h_p)_f$ and $M = (\rho_0 h_p)_f/(\rho_0 h)_m$.

Assuming a linear relationship between the concentration of the conjugated form c and the internal heat source produced by the radiation, we define $Q = \beta c$ where β is some constant of proportionality. Hence we have

$$\frac{1}{M} T_{,t} + v_i T_{,i} = \kappa \triangle T + \beta c. \tag{2.4}$$

The concentration c is taken to obey the diffusion equation, with the porosity multiplied throughout (see Nield & Bejan [77]), resulting in

$$\varepsilon c_{,t} + \varepsilon \mathbf{V} \cdot \nabla c = \varepsilon \nabla (D_c \nabla c)$$

where D_c is the diffusivity of the conjugated form. Thus, defining $\kappa_c = D_c \varepsilon$, we have

$$\varepsilon c_{,t} + v_i c_{,i} = \kappa_c \triangle c. \tag{2.5}$$

The model now consists of the six partial differential equations (2.1), (2.2), (2.4), and (2.5), with the boundary conditions

$$\left.\begin{array}{l} T = T_L \\ c = c_L \\ v_3 = 0 \end{array}\right\} \quad z = 0, \qquad \left.\begin{array}{l} T = T_U \\ c = 0 \\ v_3 = 0 \end{array}\right\} \quad z = d_z.$$

The experimental realisation of the concentration related boundary conditions can be achieved by applying fixed voltages to the conducting upper and lower boundaries, as is shown by Krishnamurti [55].

Let us now consider the basic steady state solution ($\overline{v}_i$, $\overline{p}$, $\overline{T}$, $\overline{c}$) of the system, where, as there is no fluid flow, $\overline{v}_i = 0$. Utilising the boundary conditions and assuming that the basic steady state solutions are functions of z only

$$\overline{c}(z) = (d_z - z)\frac{c_L}{d_z}. \tag{2.6}$$

$$\overline{T}(z) = -\frac{\beta c_L}{\kappa d_z}(d_z \frac{z^2}{2} - \frac{z^3}{6}) + z\left[-\frac{H\delta T}{d_z} + \frac{\beta c_L d_z}{3\kappa}\right] + T_L, \tag{2.7}$$

where $T_L - T_U = H\delta T$ with $H = \text{sign}(T_L - T_U)$ and $\delta T = |T_L - T_U|$.

The steady pressure $\overline{p}$ may then be found from (2.1) which reduces to

$$-\overline{p}_{,i} - b_i g \rho_0 (1 - \alpha(\overline{T} - T_0)) = 0. \tag{2.8}$$

To study the stability of (2.1), (2.2), (2.4) and (2.5) we introduce a perturbation (u_i, θ, π, ϕ) to the steady state solution $(\overline{v_i}, \overline{T}, \overline{p}, \overline{c})$, where

$$v_i = \overline{v}_i + u_i \qquad T = \overline{T} + \theta \qquad p = \overline{p} + \pi \qquad c = \overline{c} + \phi.$$

Using (2.6), (2.7) and (2.8) and letting $u_3 = w$ the perturbed system is

$$\frac{\mu}{k}u_i = -\pi_{,i} + b_i g\rho_0\alpha\theta,$$
$$\frac{1}{M}\theta_{,t} + u_i\theta_{,i} = w\left[\frac{H\delta T}{d_z} - \frac{\beta c_L d_z}{3\kappa} + \frac{\beta c_L}{\kappa d_z}(d_z z - \frac{z^2}{2})\right] + \kappa\triangle\theta + \beta\phi,$$
$$\varepsilon\phi_{,t} + u_i\phi_{,i} = \frac{c_L}{d_z}w + \kappa_c\triangle\phi,$$

where u_i is solenoidal, i.e. $u_{i,i} = 0$.

We now introduce non-dimensionalised variables with scalings of

$$u_i = \frac{\kappa}{d_z}u_i^*,\ \pi_i = \frac{\mu\kappa}{k}\pi_i^*,\ \theta = \sqrt{\frac{\mu\kappa(\delta T)}{g\alpha d_z k\rho_0}}\theta^*,\ \phi = c_L\phi^*,\ x_i = d_z x_i^*,$$
$$t = \frac{d_z^2}{M\kappa}t^*,\ \eta = \frac{\kappa_c}{\kappa},\ R = \sqrt{\frac{g\rho_0\alpha k d_z(\delta T)}{\mu\kappa}}$$

where d_z is the porous layer depth, and $R_a = R^2$ is the Rayleigh number. After dropping the stars the perturbation equations become

$$\begin{aligned} u_i &= -\pi_{,i} + b_i R\theta, \\ \theta_{,t} + u_i\theta_{,i} &= wRF(z) + \triangle\theta + \gamma R\phi, \\ \hat{\phi}\phi_{,t} + u_i\phi_{,i} &= w + \eta\triangle\phi, \end{aligned} \tag{2.9}$$

where u is solenoidal, $\gamma = \beta c_L d_z^2/\kappa(\delta T)$, $\hat{\phi} = \varepsilon M$ and $F(z) = H - \gamma/3 + \gamma(z - z^2/2)$. The spatial domain of the porous layer is now $\{(x, y) \in \mathbb{R}^2\} \times \{z \in (0, 1)\}$. The perturbed boundary conditions are given by

$$w = 0,\ \theta = 0,\ \phi = 0, \qquad z = 0, 1.$$

We will denote V to be the period cell for the perturbations.

2.2 Linear Instability Analysis

To proceed with the linear analysis the nonlinear terms from (2.9) are discarded. Since the resulting system is linear we may seek solutions of the form $u_i = e^{\sigma t}u_i(\mathbf{x})$, $\theta = e^{\sigma t}\theta(\mathbf{x})$, $\phi = e^{\sigma t}\phi(\mathbf{x})$, and $\pi = e^{\sigma t}\pi(\mathbf{x})$, where σ is the growth rate and a complex constant. Equations $(2.9)_2$ and $(2.9)_3$ become

$$(\triangle - \sigma)\theta = -Rw F - \gamma R\phi \tag{2.10}$$

$$(\eta\triangle - \hat{\phi}\sigma)\phi = -w. \tag{2.11}$$

Taking the double *curl* of the linearised version of $(2.9)_1$, using the third component, (and the fact that u is solenoidal) we have

$$\begin{aligned} \triangle w &= \pi_{,333} - \pi_{,333} + R(\triangle\theta - \theta_{,33}) \\ &= R\triangle^*\theta \end{aligned} \tag{2.12}$$

where $\triangle^* = \partial^2/\partial x^2 + \partial^2/\partial y^2$.

We shall now show that the growth rate σ is real. If we assume $\sigma = \sigma_r + i\sigma_i$, σ_r, $\sigma_i \in \mathbb{R}$, then we expect to have complex solutions u_i, θ and ϕ with associated complex conjugates u_i^*, θ^* and ϕ^* respectively. Operating on (2.10) by $R\triangle^*$ and substituting in (2.12) yields

$$(\triangle - \sigma)\triangle w = -R^2 F\triangle^* w - \gamma R^2\triangle^*\phi.$$

Multiplying by the complex conjugate w^*, integrating over V, and recalling u_i is solenoidal (i.e. $u_{i,i} = 0$) leads to

$$\|\triangle w\|^2 + \sigma\|\nabla w\|^2 = R^2\langle F\nabla^* w^*, \nabla^* w\rangle + \gamma R^2\langle\nabla^* w^*, \nabla^*\phi\rangle$$

where $\nabla^* = \mathbf{i}\,\partial/\partial x + \mathbf{j}\,\partial/\partial y$, and $\|\cdot\|$ and $\langle\cdot\rangle$ denote the norm and inner product on $L^2(V)$.

Applying $\gamma R^2\phi^*\triangle^*$ to (2.11) with similar arguments yields

$$\gamma R^2\eta\|\nabla\nabla^*\phi\|^2 + \gamma R^2\hat{\phi}\sigma\|\nabla^*\phi\|^2 = \gamma R^2\langle\nabla^*\phi^*, \nabla^* w\rangle.$$

Combining the last two identities we have

$$\begin{aligned} &\|\triangle w\|^2 + \gamma R^2\eta\|\nabla\nabla^*\phi\|^2 + \sigma(\|\nabla w\|^2 + \gamma R^2\hat{\phi}\|\nabla^*\phi\|^2) \\ &= R^2\textstyle\int_V F|\nabla^* w|^2\,dV + \gamma R^2(\langle\nabla^* w^*, \nabla^*\phi\rangle + \langle\nabla^*\phi^*, \nabla^* w\rangle). \end{aligned} \tag{2.13}$$

Since $R^2\int_V F|\nabla^* w|^2\,dV \in \mathbb{R}$ as $F(z) \in \mathbb{R}$, and

$$\begin{aligned} \langle\nabla^* w^*, \nabla^*\phi\rangle + \langle\nabla^*\phi^*, \nabla^* w\rangle &= \langle\nabla^*(w_r - iw_i), \nabla^*(\phi_r + i\phi_i)\rangle \\ &\quad + \langle\nabla^*(\phi_r - i\phi_i), \nabla^*(w_r + iw_i)\rangle \\ &= 2(\nabla^*\langle w_r, \phi_r\rangle + \nabla^*\langle w_i, \phi_i\rangle) \in \mathbb{R}, \end{aligned}$$

taking the imaginary parts of (2.13) we deduce

$$\sigma_i(\|\nabla w\|^2 + \gamma R^2\hat{\phi}\|\nabla^*\phi\|^2) = 0.$$

Clearly, as all norms are ≥ 0, $\sigma_i \equiv 0$. Our system of equations now satisfy the *Principle of exchange of stabilities* (see Straughan [90]). This is said to hold if the system in question has a growth rate σ such that $\sigma \in \mathbb{R}$ or $\sigma_i \neq 0$ implies $\sigma_r < 0$. Recalling the time dependent solutions defined at the beginning of the section, it is clear that the solutions grow exponentially in time when $\sigma > 0$, and are thus unstable. So to find the instability boundary, we solve the linearised system for the smallest R^2 value (R_L^2) with $\sigma = 0$. It is important to recall, however, that this gives a boundary for which all $R^2 > R_L^2$ result in instability, but no claim can be made about stability when $R^2 < R_L^2$, until further nonlinear analysis is made.

We now introduce normal modes of the form $w = W(z)f(x,y)$, $\theta = S(z)f(x,y)$, and $\phi = \Phi(z)f(x,y)$ where $f(x,y)$ is a plan-form which tiles the plane $(x,\ y)$ with

$$\triangle^* f = -a^2 f. \tag{2.14}$$

The plan-forms represent the horizontal shape of the convection cells formed at the onset of instability. These cells from a regular horizontal pattern tiling the $(x,\ y)$ plane, where the wavenumber a (see Christopherson [16]) is a measure of the width of the convection cell.

Letting $D = d/dz$, using (2.14), and applying the normal mode representations to (2.10), (2.11), and (2.12) we find

$$\begin{aligned} &(D^2 - a^2)W + a^2 RS = 0 \\ &(D^2 - a^2)S + RWF + \gamma R\Phi = \sigma S \\ &(D^2 - a^2)\Phi + \frac{W}{\eta} = \frac{\hat{\phi}\sigma}{\eta}\Phi \end{aligned} \tag{2.15}$$

where the boundary conditions become

$$W = 0,\ S = 0,\ \Phi = 0, \qquad z = 0, 1. \tag{2.16}$$

It is interesting to note that with the introduction of $\sigma = 0$ into the system, the term $\hat{\phi}$, which includes the porosity ε and the value M, has no affect on the critical boundary.

The system (2.15) constitutes a generalised eigenvalue problem which has been solved using the two entirely different numerical methods referenced in Chapter

1, namely the compound matrix method, and the Chebyshev tau-QZ algorithm. Both methods are explained in detail in Appendices A.1 and A.2, although brief descriptions are given in this chapter to clarify the use of the methods in the context of the system of the second order coupled equations being explored. The limitations of these methods are discussed in Chapters 7 and 8, where alternative approachs are presented.

To solve (2.15) with $\sigma = 0$ by the compound matrix method we let $\mathbf{U} = (W, W', S, S', \Phi, \Phi')$, and then suppose $\mathbf{U_1}$, $\mathbf{U_2}$ and $\mathbf{U_3}$ are independent solutions to (2.15), with values at $z = 0$ of (0,1,0,0,0,0), (0,0,0,1,0,0), and (0,0,0,0,0,1) respectively. The three initial value problems can be integrated numerically between 0 and 1, and the solution found by writing it as a linear combination of the three solutions obtained i.e. $W = \varphi W_1 + \chi W_2 + \omega W_3$, $S = \varphi S_1 + \chi S_2 + \omega S_3$, and $\Phi = \varphi \Phi_1 + \chi W_2 + \omega \Phi_3$ for some constants φ, χ, ω. Then, the correct boundary conditions $W = S = \Phi = 0$ at $z = 1$ are imposed which require

$$\det \begin{pmatrix} W_1 & W_2 & W_3 \\ S_1 & S_2 & S_3 \\ \Phi_1 & \Phi_2 & \Phi_3 \end{pmatrix} = 0.$$

The variables $y_1, ..., y_{20}$ are introduced to be the 3×3 minors of the 6×3 solution matrix whose columns are $\mathbf{U_1}$, $\mathbf{U_2}$, and $\mathbf{U_3}$. Thus,

$$\begin{aligned} y_1 &= W_1(W_2'S_3 - S_2W_3') - W_2(W_1'S_3 - S_1W_3') + W_3(W_1'S_2 - S_1W_2') \\ y_2 &= W_1(W_2'S_3' - S_2'W_3') - W_2(W_1'S_3' - S_1'W_3') + W_3(W_1'S_2' - S_1'W_2') \\ y_3 &= W_1(W_2'\Phi_3 - \Phi_2W_3') - W_2(W_1'\Phi_3 - \Phi_1W_3') + W_3(W_1'\Phi_2 - \Phi_1W_2') \\ &\textit{etc.} \end{aligned}$$

Differentiating the y's and using (2.15) (and noting that $D^2W = W''$) the differential

equations for the compound matrix variables are

$$y_1' = y_2, \qquad y_2' = a^2 y_1 + B y_3 + A y_5, \qquad y_3' = y_4 + A y_6,$$
$$y_4' = A y_7 + a^2 y_3, \qquad y_5' = y_{11} + B y_6, \qquad y_6' = y_{12} + y_8 + y_7,$$
$$y_7' = y_{13} + y_9 + a^2 y_6, \qquad y_8' = y_{14} + y_9 + a^2 y_6,$$
$$y_9' = y_{15} + a^2 y_7 + B y_{10} + a^2 y_8, \qquad y_{10}' = y_{16},$$
$$y_{11}' = a^2 y_5 - RF y_1 + B y_{12}, \qquad y_{12}' = a^2 y_6 + y_{14} + y_{13},$$
$$y_{13}' = a^2 y_7 + y_{15} + a^2 y_{12} + C y_1,$$
$$y_{14}' = a^2 y_8 + A y_{17} + a^2 y_{12} + RF y_3 + y_{15},$$
$$y_{15}' = a^2 y_9 + A y_{18} + a^2 y_{13} + RF y_4 + B y_{16} + a^2 y_{14} + C y_2,$$

$$y_{16}' = a^2 y_{10} + A y_{19} + C y_3, \qquad y_{17}' = RF y_6 + y_{18},$$
$$y_{18}' = RF y_7 + B y_{19} + a^2 y_{17} + C y_5, \qquad y_{19}' = y_{20} + C y_6,$$
$$y_{20}' = a^2 y_{19} - RF y_{10} + C y_8,$$

where $A = -a^2 R$, $B = -\gamma R$, and $C = -1/\eta$. This system was numerically integrated subject to the initial condition $y_{15}(0) = 1$, and the final condition $y_6(1) = 0$, and the eigenvalue R was varied until these conditions were met to some pre-defined degree of accuracy. Keeping $a^2 > 0$ fixed, a golden section search was employed to numerically find

$$R_a = \min_{a^2} R^2(a^2). \tag{2.17}$$

The numerical results are presented for values of $\eta = 10^{-3}$ to 10^{-2} with a step of 10^{-3} and $\gamma = 1$ to 10 in Figures 2.1 - 2.2. The values of η and γ are those suggested by Krishnamurti [55], and are also used by Straughan [89].

Although the Rayleigh numbers are different, as would be expected from a different medium, we can see that the results from Figures 2.1 and 2.2 follow a similar pattern to that of Straughan [89], although the quantitative effect is different. It is observed that the effect of increasing the radiation parameter γ is to greatly reduce the critical Rayleigh number and, therefore, to allow convection to commence more easily.

To confirm these results numerically we turn our attention to the Chebyshev tau-QZ algorithm, which adopts an entirely different strategy. As highlighted in

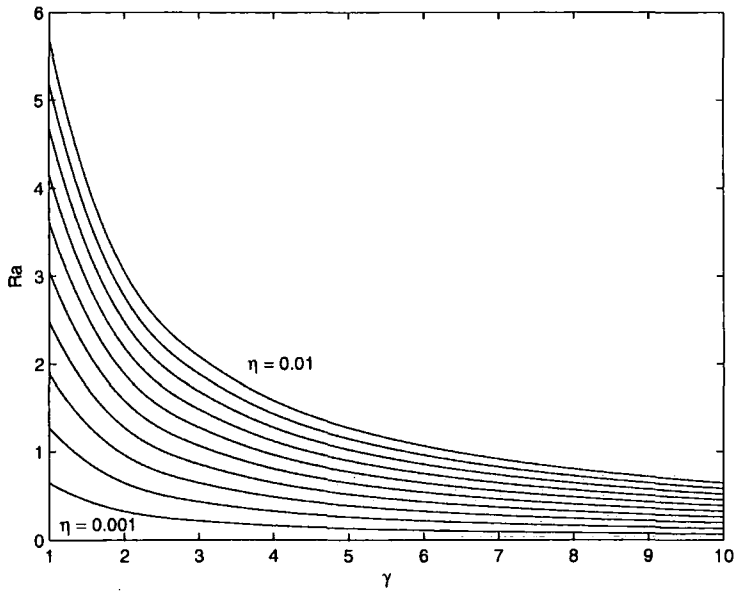

Figure 2.1: Critical Rayleigh number R_a against γ, for various η. The graph corresponds to heating from below ($H = +1$).

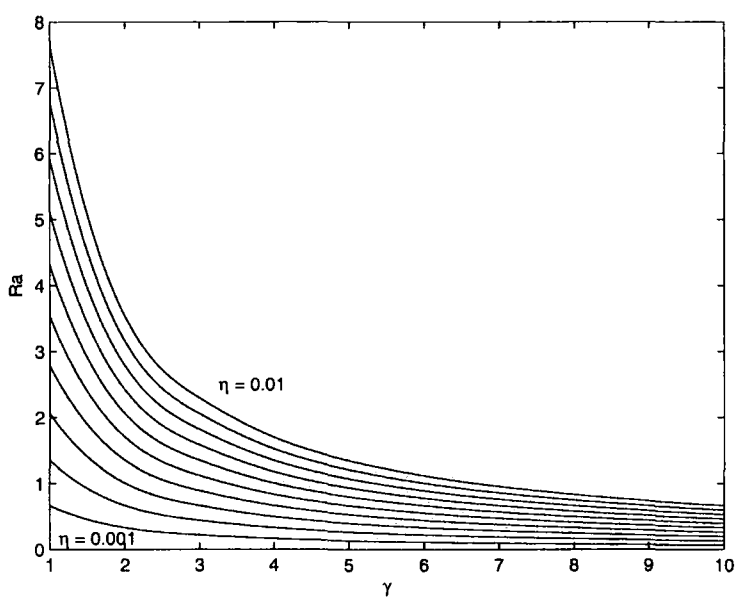

Figure 2.2: Critical Rayleigh number R_a against γ, for various η. The graph corresponds to heating from above ($H = -1$).

Chapter 1, the compound matrix technique belongs to the family of shooting methods, whereas the Chebyshev tau method is a spectral technique coupled with the QZ algorithm. By reintroducing the σ term back into the system we can use the Rayleigh numbers given by the compound matrix method to assess whether the σ term is effectively zero, as required. To employ the Chebyshev tau technique system (2.15) is converted to the Chebyshev domain $(-1, 1)$, and then W, S and Φ are written as a finite series of Chebyshev polynomials

$$W = \sum_{k=0}^{N+2} W_k T_k(z) \qquad S = \sum_{k=0}^{N+2} S_k T_k(z) \qquad \Phi = \sum_{k=0}^{N+2} \Phi_k T_k(z).$$

The weighted inner product of each equation is taken with some T_k and the orthogonality of the Chebyshev polynomials is utilised to form the generalised eigenvalue problem

$$\begin{pmatrix} 4D^2 - a^2 & a^2 R & 0 \\ RF^* & 4D^2 - a^2 & \gamma R \\ \dfrac{1}{\eta} & 0 & 4D^2 - a^2 \end{pmatrix} \begin{pmatrix} \mathbf{W} \\ \mathbf{S} \\ \mathbf{\Phi} \end{pmatrix} = \sigma \begin{pmatrix} 0 & 0 & 0 \\ 0 & 1 & 0 \\ 0 & 0 & \dfrac{\hat{\phi}}{\eta} \end{pmatrix} \begin{pmatrix} \mathbf{W} \\ \mathbf{S} \\ \mathbf{\Phi} \end{pmatrix}$$

where $\mathbf{W} = (W_0, ..., W_N)^T$, $\mathbf{S} = (S_0, ..., S_N)^T$, $\mathbf{\Phi} = (\Phi_0, ..., \Phi_N)^T$, D^2 is the Chebyshev representation of $\partial^2/\partial z^2$, and $F^* = H + \gamma/24 + Z\gamma/4 - Z^2\gamma^2/8$, where Z and Z^2 are the matrix representations of z and z^2 respectively. The F^* term does not correspond with the original $F(z)$ term as we have transformed z to $2z - 1$ for the Chebyshev domain, and thus changed $F(z)$ accordingly.

Using the boundary conditions (2.16) and the fact that $T_n(\pm 1) = (\pm 1)^n$ we replaced the last two rows of each $(N + 2) \times (N + 2)$ segment, (see Appendix A.2 for further clarification). The QZ algorithm (see Moler & Stewart [73]) was then employed to solve this system. Results were taken at $\gamma = 1, 10$ for all η values. All σ values were of a magnitude less than 10^{-6}, an acceptable value within the constraint of the accuracy of the Rayleigh number.

Although the linear analysis has been completed numerically, it is possible to use analytic methods to provide an approximation of the results. The problem that arises when dealing with (2.15) analytically is the $F(z)$ term, as it clearly varies over

the $z \in [0,1]$ range. However, by taking the average of $F(z)$ over this range we can proceed analytically, although accuracy is clearly lost.

$$\begin{aligned} F_{av} &= \int_0^1 H - \frac{\gamma}{3} + \gamma(z - \frac{z^2}{2})\, dz \\ &= [(H - \frac{\gamma}{3})z + \frac{\gamma}{2}z^2 - \frac{\gamma}{6}z^3]_0^1 \\ &= H - \frac{\gamma}{3} + \frac{\gamma}{2} - \frac{\gamma}{6} \\ &= H. \end{aligned}$$

Hence, letting $L = D^2 - a^2$, taking $\sigma = 0$, re-applying L to $(2.15)_1$, and using $(2.15)_2$, $(2.15)_3$ we have

$$\begin{aligned} LW &= -a^2 RS \\ L^{(2)}W &= -a^2 RLS = -a^2 R(-RF_{av}W - \gamma R\Phi) \\ L^{(3)}W &= a^2R^2HLW + a^2R^2\gamma L\Phi = a^2R^2HLW - \frac{1}{\eta}a^2R^2\gamma W \\ L^{(4)}W &= AL^{(2)}W + BLW \end{aligned}$$

for constants A and B. Using the boundary conditions (2.16) we can see that $L^{(4)}W = 0$ on $z = 0$, 1 (as LW and $L^{(2)}W$ can be written in terms of W, S, and Φ). By repeated application of L and relevant substitution of lower powers we can intuitively see that $L^{(n)}W = 0$ for $n > 4$, $z = 0$, 1. Hence we may write $W = W_0 \sin(n\pi z)$ for some constant W_0. Substituting this into the $L^{(3)}$; equation (as it contains an R^2 term which is what we want), after some canceling we find

$$R^2 = \frac{(n^2\pi^2 + a^2)^3}{a^2[H(n^2\pi^2 + a^2) + \frac{\gamma}{\eta}]}. \tag{2.18}$$

Now we need to minimise with respect to n^2. Letting $\Omega = n^2\pi^2 + a^2$, and differentiating (2.18) with respect to n^2 we have

$$\begin{aligned} \frac{\partial R^2}{\partial n^2} &= \frac{3\Omega^2\pi^2}{a^2[\Omega H + \frac{\gamma}{\eta}]} + \frac{-\pi^2\Omega^3 H}{a^2[\Omega H + \frac{\gamma}{\eta}]^2} \\ &= \frac{3\Omega^2\pi^2[\Omega H + \frac{\gamma}{\eta}] - \pi^2\Omega^3 H}{a^2[\Omega H + \frac{\gamma}{\eta}]^2} \\ &= \frac{3\Omega^2\pi^2\frac{\gamma}{\eta} + 2\pi^2\Omega^3 H}{a^2[\Omega H + \frac{\gamma}{\eta}]^2} \\ &> 0 \end{aligned}$$

where we have taken $H = +1$ to ensure the positivity of the differential. As the differential is > 0 we can take $n = 1$. We must similarly minimise (2.18) with respect to a^2. Thus letting $n = 1$ (with $\Omega = \pi^2 + a^2$) leads to

$$R^2 = \frac{\Omega^3}{a^2[\Omega + \frac{\gamma}{\eta}]}$$

$$\frac{\partial R^2}{\partial a^2} = \frac{3\Omega^2}{a^2[\Omega + \frac{\gamma}{\eta}]} - \frac{\Omega^3}{(a^2)^2[\Omega + \frac{\gamma}{\eta}]} - \frac{\Omega^3}{a^2[\Omega + \frac{\gamma}{\eta}]^2}.$$

Thus, setting $\partial R^2/\partial a^2 = 0$,

$$(\pi^2 + a^2)^2[3a^2\pi^2 + 3(a^2)^2 + \frac{3a^2\gamma}{\eta} - \pi^4 - a^2\pi^2 - \frac{\pi^2\gamma}{\eta} - a^2\pi^2 - (a^2)^2$$
$$-a^2\frac{\gamma}{\eta} - a^2\pi^2 - (a^2)^2] = 0.$$

Since $a^2 \geq 0$ we have

$$(a^2)^2 + 2\frac{a^2\gamma}{\eta} - \pi^2(\pi^2 + \frac{\gamma}{\eta}) = 0$$

$$a^2 = -\frac{\gamma}{\eta} + \sqrt{\frac{\gamma^2}{\eta^2} + \pi^4 + \frac{\pi^2\gamma}{\eta}}. \tag{2.19}$$

Substituting this a^2 value into (2.18) we can calculate R^2 for given η and γ. Using (2.19) and the compound method results we display solutions for the six cases $\gamma = 1, 10$, $\eta = 0.001, 0.005, 0.01$ for the approximate analytical and exact numerical R^2 values.

γ	η	R_A	R_N
1	0.001	0.64790	0.64767
10	0.001	0.06565	0.06563
1	0.005	3.05972	3.05432
10	0.005	0.32639	0.32573
1	0.01	5.71883	5.69974
10	0.01	0.64791	0.64550

Table 2.1: Comparison of the approximate analytical and exact numerical critical Rayleigh numbers R_A and R_N.

From Table 2.1 we see that the approximate analytical results are a very useful guide to their numerical counterparts. Hence, we have produced the linear critical

Rayleigh numbers for which any R^2 greater than these critical values will result in instability.

2.3 Nonlinear Stability Analysis

To obtain sufficient conditions on the stability of the solution we need to consider the nonlinear equations. Our aim is to show that the thresholds of the nonlinear theory are close enough to those of the linear theory, so that we can conclude that linear instability theory is accurate enough to predict the onset of convective motion. In order to establish the stability of the solution we must show that the solutions tend to 0 as $t \to \infty$, in some suitable mathematical measure. We will achieve this by using the *energy method* (see Straughan [90] and Drazin & Reid [21]), utilising the coupling method of Joseph explained in Straughan [90]

Let us recall the original system (2.9)

$$\begin{aligned} u_i &= -\pi_{,i} + b_i R\theta \\ \theta_{,t} + u_i\theta_{,i} &= wRF(z) + \triangle\theta + \gamma R\phi \\ \hat{\phi}\phi_{,t} + u_i\phi_{,i} &= w + \eta\triangle\phi. \end{aligned}$$

Firstly we multiply $(2.9)_1$ by u_i and integrate over V to find

$$\|\mathbf{u}\|^2 = R\langle\theta, w\rangle \tag{2.20}$$

where $\|\cdot\|$ and $\langle\cdot\rangle$ denote the norm and inner product on $L^2(V)$. Multiplying $(2.9)_2$ by θ and using similar arguments, noting $u_{i,i} = 0$,

$$\frac{1}{2}\frac{d}{dt}\|\theta\|^2 = R\langle wF, \theta\rangle - \|\nabla\theta\|^2 + \gamma R\langle\phi, \theta\rangle. \tag{2.21}$$

Using the same processes again for $(2.9)_3$, this time multiplying through by ϕ, we have

$$\frac{\hat{\phi}}{2}\frac{d}{dt}\|\phi\|^2 = \langle w, \phi\rangle - \eta\|\nabla\phi\|^2. \tag{2.22}$$

Letting λ_1 and λ_2 be positive coupling parameters to be selected at our discretion, we multiply (2.22) by λ_1 and (2.20) by λ_2. Adding these two equations to (2.21)

yields

$$\begin{aligned}\frac{1}{2}\frac{d}{dt}\|\theta\|^2+\frac{\lambda_1\hat{\phi}}{2}\frac{d}{dt}\|\phi\|^2 &= R\langle wF,\theta\rangle-\|\nabla\theta\|^2+\gamma R\langle\phi,\theta\rangle\\ &\quad+\lambda_1\langle w,\phi\rangle-\eta\lambda_1\|\nabla\phi\|^2\\ &\quad-\lambda_2\|\mathbf{u}\|^2+\lambda_2 R\langle\theta,w\rangle.\end{aligned}\tag{2.23}$$

Define

$$\begin{aligned}E(t) &= \frac{\lambda_1\hat{\phi}}{2}\|\phi\|^2+\frac{1}{2}\|\theta\|^2\\ \mathcal{D} &= \|\nabla\theta\|^2+\eta\lambda_1\|\nabla\phi\|^2+\lambda_2\|\mathbf{u}\|^2\\ \mathcal{I} &= R\langle wF,\theta\rangle+\gamma R\langle\phi,\theta\rangle+\lambda_1\langle w,\phi\rangle+\lambda_2 R\langle\theta,w\rangle.\end{aligned}$$

Adopting these definitions for (2.23) we find

$$\begin{aligned}\frac{dE}{dt} &= \mathcal{I}-\mathcal{D}\\ \frac{dE}{dt} &\leq -\mathcal{D}\left(1-\frac{1}{R_E}\right)\end{aligned}$$

where $1/R_E=\max_{\mathcal{H}}(\mathcal{I}/\mathcal{D})$ and $\mathcal{H}$ is the space of admissible functions, namely

$$\mathcal{H}=\{u_i,\,\theta,\,\phi\in C^2(0,1)\,|\,w=\theta=\phi=0,\;z=0,1\}.$$

If $R_E>1$ then by the Poincaré inequality (see Appendix B.2) and using the fact that $\|\mathbf{u}\|^2\geq 0$, it follows that $\mathcal{D}\geq cE$ for some constant $c>0$. Hence

$$\frac{dE}{dt}\leq -cE\left(\frac{R_E-1}{R_E}\right).$$

Thus, letting $\hat{a}=c(R_E-1)/R_E>0$ and integrating we have

$$E(t)\leq E(0)e^{-\hat{a}t}.$$

As $t\to\infty$, $E(t)$ tends to zero, so we have shown the decay of θ and ϕ. We now need to determine the decay of $\mathbf{u}$ to show global nonlinear stability. Defining some constant $\alpha>0$, from (2.20) we have

$$\begin{aligned}\|\mathbf{u}\|^2=R\langle w,\theta\rangle &\leq \frac{R}{2\alpha}\|w\|^2+\frac{R\alpha}{2}\|\theta\|^2\\ &\leq \frac{R}{2\alpha}\|\mathbf{u}\|^2+\frac{R\alpha}{2}\|\theta\|^2+\frac{\lambda_1\alpha^2}{2}\hat{\phi}\|\phi\|^2\end{aligned}$$

as $\lambda_1\alpha^2\hat{\phi}\|\phi\|^2 \geq 0$. Letting $\alpha = R$,

$$\begin{aligned}\|\mathbf{u}\|^2 &\leq R^2\|\theta\|^2 + \lambda_1 R^2\hat{\phi}\|\phi\|^2 \\ &\leq R^2 2E \\ &\leq 2R^2E(0)e^{-\hat{a}t} \quad \to 0 \qquad as \quad t \to \infty.\end{aligned}$$

The decay of $\mathbf{u}$ then clearly follows.

Now that global stability has been established we must study the maximisation problem $1/R_E = \max_{\mathcal{H}}(\mathcal{I}/\mathcal{D})$ together with the condition $R_E > 1$. To solve the maximisation problem we study the Euler Lagrange equations which are derived as follows.

Let $\eta_1(x_j)$, $\eta_2(x_j)$, and $\eta_3(x_j)$ be arbitrary, fixed $C^2(0,1)$ functions which satisfy the boundary conditions

$$\eta_i(0) = \eta_i(1) = 0 \qquad i = 1,2,3. \tag{2.24}$$

We now consider neighbouring functions $\overline{u}_i = u_i + \alpha\eta_1(x_j)$, $\overline{\theta} = \theta + \alpha\eta_2(x_j)$ and $\overline{\phi} = \phi + \alpha\eta_3(x_j)$ and then define

$$\mathcal{I}(\alpha) = \int R\overline{w}F\overline{\theta} + \gamma R\overline{\phi\theta} + \lambda_1\overline{w}\overline{\phi} + \lambda_2 R\overline{\theta}\overline{w}\; dV = \int \mathcal{I}_1(\overline{u}_i, \overline{\theta}, \overline{\phi}, \overline{u}_{i,j}, \overline{\theta}_{,j}, \overline{\phi}_{,j})\; dV$$

$$\mathcal{D}(\alpha) = \int \overline{\theta}_{,j}\overline{\theta}_{,j} + \eta\lambda_1\overline{\phi}_{,j}\overline{\phi}_{,j} + \lambda_2\overline{u}_i\overline{u}_i\; dV = \int \mathcal{D}_1(\overline{u}_i, \overline{\theta}, \overline{\phi}, \overline{u}_{i,j}, \overline{\theta}_{,j}, \overline{\phi}_{,j})\; dV.$$

If $\delta\mathcal{I}$ is $\partial\mathcal{I}/\partial\alpha$ evaluated at $\alpha = 0$ then

$$\delta\mathcal{I} = \int (\frac{\partial\mathcal{I}_1}{\partial u_i}\eta_1 + \frac{\partial\mathcal{I}_1}{\partial\theta}\eta_2 + \frac{\partial\mathcal{I}_1}{\partial\phi}\eta_3 + \frac{\partial\mathcal{I}_1}{\partial u_{i,j}}\eta_1' + \frac{\partial\mathcal{I}_1}{\partial\theta_{,j}}\eta_2' + \frac{\partial\mathcal{I}_1}{\partial\phi_{,j}}\eta_3')\; dV$$

Integrating by parts and using (2.24) yields

$$\begin{aligned}\delta\mathcal{I} \;=\; &\int \eta_1\left[\frac{\partial\mathcal{I}_1}{\partial u_i} - \frac{d}{dx_j}\left(\frac{\partial\mathcal{I}_1}{\partial u_{i,j}}\right)\right] dV + \int \eta_2\left[\frac{\partial\mathcal{I}_1}{\partial\theta} - \frac{d}{dx_j}\left(\frac{\partial\mathcal{I}_1}{\partial\theta_{,j}}\right)\right] dV \\ &+ \int \eta_3\left[\frac{\partial\mathcal{I}_1}{\partial\phi} - \frac{d}{dx_j}\left(\frac{\partial\mathcal{I}_1}{\partial\phi_{,j}}\right)\right] dV.\end{aligned} \tag{2.25}$$

For the stationary value, $\delta\mathcal{I} = \mathcal{I}'(0) = 0$, and so (2.25) $= 0$. As η_1, η_2 and η_3 can be chosen arbitrarily it follows that

$$\begin{aligned}\frac{\partial\mathcal{I}_1}{\partial u_i} - \frac{d}{dx_j}\left(\frac{\partial\mathcal{I}_1}{\partial u_{i,j}}\right) &= 0 \\ \frac{\partial\mathcal{I}_1}{\partial\theta} - \frac{d}{dx_j}\left(\frac{\partial\mathcal{I}_1}{\partial\theta_{,j}}\right) &= 0 \\ \frac{\partial\mathcal{I}_1}{\partial\phi} - \frac{d}{dx_j}\left(\frac{\partial\mathcal{I}_1}{\partial\phi_{,j}}\right) &= 0\end{aligned} \tag{2.26}$$

Similar results hold for $\delta\mathcal{D}$. The original maximisation problem was $1/R_E = \max_{\mathcal{H}}(\mathcal{I}/\mathcal{D})$, hence we study

$$\delta\left(\frac{\mathcal{I}}{\mathcal{D}}\right) = \frac{\delta\mathcal{I}}{\mathcal{D}} - \frac{\mathcal{I}}{\mathcal{D}^2}\delta\mathcal{D} = \frac{1}{\mathcal{D}}(\delta\mathcal{I} - \frac{\mathcal{I}}{\mathcal{D}}\delta\mathcal{D}) = 0$$

This yields

$$R_E\delta\mathcal{I} - \delta\mathcal{D} = 0. \tag{2.27}$$

For u_i using $(2.26)_1$

$$\delta\mathcal{I} = \frac{d}{du_i}(RwF\theta + \gamma R\phi\theta + \lambda_1 w\phi + \lambda_2 R\theta w) = RF\theta + \lambda_1\phi + \lambda_2 R\theta$$
$$\delta\mathcal{D} = \frac{d}{du_i}(\lambda_2 u_i u_i) = 2\lambda_2 u_i.$$

Similarly for θ using $(2.26)_2$ we have

$$\delta\mathcal{I} = RwF + \gamma R\phi + \lambda_2 Rw.$$
$$\delta\mathcal{D} = -\frac{d}{dx_j}\left(\frac{\partial}{\partial\theta_{,j}}(\theta_{,i}\theta_{,i})\right) = -\frac{d}{dx_j}(2\theta_{,j}) = -2\triangle\theta.$$

Using $(2.26)_3$ for ϕ we have

$$\delta\mathcal{I} = \gamma R\theta + \lambda_1 w$$
$$\delta\mathcal{D} = -\frac{d}{dx_j}\left(\frac{\partial}{\partial\phi_{,j}}(\eta\lambda_1\phi_{,i}\phi_{,i})\right) = -\frac{d}{dx_j}(2\eta\lambda_1\phi_{,j}) = -2\eta\lambda_1\triangle\phi.$$

Hence using (2.27) and the previous $\delta\mathcal{I}$ and $\delta\mathcal{D}$ values we have the Euler Lagrange equations

$$\begin{aligned} &RF\theta + \lambda_1\phi + \lambda_2 R\theta + 2\lambda_2 u_i = \omega_{,i} \\ &RwF + \gamma R\phi + \lambda_2 Rw + 2\triangle\theta = 0 \\ &\gamma R\theta + \lambda_1 w - 2\eta\lambda_1\triangle\phi = 0 \end{aligned} \tag{2.28}$$

where we are looking at the sharpest boundary condition, $R_E = 1$. As we need to include the constraint $u_{i,i} = 0$ we have introduced the Lagrange multiplier ω, where $\int_V \omega u_{i,i}\, dV = 0$, so that

$$\frac{d}{dx_i}\left(\frac{\partial}{\partial u_{i,i}}(\omega u_{i,i})\right) = \omega_{,i}.$$

Taking the third component of the double *curl* of $(2.28)_1$ (to remove the Lagrange

multiplier), and introducing the normal mode representations and notation as presented in Section 2.2, system (2.28) then becomes

$$\begin{aligned}
&(D^2-a^2)W+\frac{R}{2\lambda_2}(F+\lambda_2)a^2S+\frac{a^2\lambda_1}{2\lambda_2}\Phi=0\\
&(D^2-a^2)S+\frac{R}{2}(F+\lambda_2)W+\frac{\gamma R}{2}\Phi=0\\
&(D^2-a^2)\Phi+\frac{\gamma R}{2\eta\lambda_1}S+\frac{1}{2\eta}W=0.
\end{aligned} \tag{2.29}$$

We can now determine the critical Rayleigh number given by

$$Ra_E=\max_{\lambda_1,\lambda_2}\min_{a^2}R^2(a^2,\lambda_1,\lambda_2)$$

where for all $R^2<Ra_E$ we have stability. To solve the eigenvalue problem presented by the system (2.29) the compound matrix method was utilised (see Section 2.2 and Appendix A.1) where the compound matrix equations are now

$$\begin{aligned}
&y_1'=-By_6+y_2, \qquad y_2'=Ay_5-By_8+a^2y_1+Dy_3, \qquad y_3'=Ay_6+y_4,\\
&y_4'=Ay_7+By_{10}+a^2y_3+Ey_1, \qquad y_5'=y_{11}+Dy_6,\\
&y_6'=y_{12}+y_8+y_7, \qquad y_7'=y_{13}+y_9+a^2y_6, \qquad y_8'=y_{14}+a^2y_6+y_9,\\
&y_9'=y_{15}+Dy_{10}+a^2y_7+a^2y_8-Ey_5, \qquad y_{10}'=y_{16}-Ey_6,\\
&y_{11}'=a^2y_5+By_{17}+Cy_1+Dy_{12}, \qquad y_{12}'=a^2y_6+y_{14}+y_{13},\\
&y_{13}'=a^2y_7-By_{19}+y_{15}+a^2y_{12}+Fy_1,\\
&y_{14}'=a^2y_8+Ay_{17}+a^2y_{12}-Cy_3+y_{15},\\
&y_{15}'=a^2y_9+Ay_{18}-By_{20}+a^2y_{13}-Cy_4+Dy_{16}+a^2y_{14}-Ey_{11}+Fy_2,\\
&y_{16}'=a^2y_{10}+Ay_{19}-Ey_{12}+Fy_3, \qquad y_{17}'=-Cy_6+y_{18},\\
&y_{18}'=a^2y_{17}-Cy_7+Dy_{19}+Fy_5, \qquad y_{19}'=y_{20}+Fy_6,\\
&y_{20}'=a^2y_{19}+Cy_{10}+Ey_{17}+Fy_8,
\end{aligned}$$

with $A=-R(F+\lambda_2)a^2/2\lambda_2$, $B=-a^2\lambda_1/2\lambda_2$, $C=-R(F+\lambda_2)/2$, $D=-\gamma R/2$, $E=-\gamma R/2\eta\lambda_1$ and $F=-1/2\eta$. As in Section 2.2, this system was numerically integrated subject to $y_{15}(0)=1$, and $y_6(1)=0$.

In Table 2.2 we display the numerical results for both the nonlinear and the linear (see Section 2.2) critical Rayleigh numbers with $\gamma=1,\,5,\,10$, $\eta=0.001,\,0.005,\,0.01$, $H=+1$ and -1. The critical parameters of linear and nonlinear theory are denoted L and E respectively, with the critical wavenumbers denoted by a_L^2 and a_E^2. Clearly we see an excellent agreement between the nonlinear and linear results.

γ	η	H	Ra_E	Ra_L	a_E^2	a_L^2
1	0.001	+1	0.6476675739	0.6476676880	4.9720	4.9720
5	0.001	+1	0.1310648838	0.1310649075	4.9430	4.9430
10	0.001	+1	0.065629321	0.0656293327	4.9393	4.9393
1	0.005	+1	3.054308651	3.054321113	5.1174	5.1174
5	0.005	+1	0.6467036386	0.646706499	4.9758	4.9758
10	0.005	+1	0.3257283587	0.325729815	4.9576	4.9577
1	0.01	+1	5.699650645	5.699734754	5.2908	5.2908
5	0.01	+1	1.272411967	1.272433956	5.0163	5.0164
10	0.01	+1	0.645491451	0.645502832	4.9805	4.9805
1	0.001	−1	0.667125663	0.6671257863	4.8990	4.8990
5	0.001	−1	0.131843079	0.1318431026	4.9284	4.9284
10	0.001	−1	0.065823869	0.065823880	4.931	4.9321
1	0.005	−1	3.541425057	3.541442825	4.7526	4.7525
5	0.005	−1	0.666107901	0.666110972	4.9028	4.9028
10	0.005	−1	0.330578799	0.330580307	4.9212	4.9212
1	0.01	−1	7.666604583	7.666775544	4.5618	4.5617
5	0.01	−1	1.349797705	1.349823027	4.8707	4.8706
10	0.01	−1	0.664827927	0.664840142	4.9077	4.9076

Table 2.2: Comparison of the nonlinear and linear critical Rayleigh numbers Ra_E and Ra_L.

2.4 Conclusions

In Sections 2.2 and 2.3 we have provided a full linear and nonlinear analysis of the adaption of the Krishnamurti [55] model for convection induced by selective absorption of radiation in a fluid, to a porous medium. A graphical representation of the linear instability results is given in Figures 2.1 and 2.2, with a comparison to approximate analytic results in Table 2.1. The results of the nonlinear energy analysis are presented in Table 2.2, with the corresponding linear results adjacent. The thresholds of the nonlinear theory, which guarantee stability when the Rayleigh

number is below them, are shown to be extremely close to the thresholds of the linear energy theory which guarantee instability. As the region of potential subcritical instabilities is extremely small we can conclude that linear theory is accurate enough to predict the onset of convective motion.

It is interesting to note that the porosity ε has no effect on the linear and nonlinear analysis, so that ε can take any value, (within acceptable range $0 < \varepsilon < 1$), with the results remaining the same.

Chapter 3

Convection induced by the selective absorption of radiation for the Brinkman model

The object of this chapter is to explore convection induced by the selective absorption of radiation in a porous medium, as presented in Chapter 2, with the introduction of the Brinkman model.

In Chapter 1, the Darcy model for fluid flow in porous media was adopted. However, Amahmid *et al.* [4] propose that for sparsely packed porous media (more appropriate to the physical problem as potential refraction is decreased) the Brinkman model, which accounts for friction due to macroscopic shear, is more appropriate to describe fluid flows in a porous matrix, which forms the motivation behind the development of this chapter.

The Brinkman model has been employed by Mamou *et al.* [64] and Amahmid *et al.* [3] to investigate the stability of a porous layer when the buoyancy thermal and solutal forces have opposing effects and equal intensity. Poulikakos [82] also relies on the Brinkman model to investigate the onset of thermohaline convection in a horizontal porous layer.

In this chapter we present a detailed linear and nonlinear analysis for this system with the Brinkman model describing fluid flow in the porous matrix, with the bounding surfaces being fixed. The linear and nonlinear results are derived using

the Chebyshev tau and compound matrix numerical techniques (see Appendices A.2 and A.1), and compared to assess the region of potential subcritical instabilities as a direct indicator of the suitability of linear instability theory in the prediction of the onset of penetrative convection. Employing the compound matrix method in both the linear and nonlinear numerical analysis was found to be problematic due to the high order of the equations, with the Chebyshev tau technique being restrictive due to the heavy computational cost in solving full matrix eigenvalue problems required over two parameter ranges. This leads to the development of the methods in Chapters 7 and 8 to overcome these difficulties.

The results in this chapter were published in the article Hill [37].

3.1 Governing Equations

Let us consider a fluid saturated porous layer occupying the three dimensional layer $\{(x,y) \in \mathbb{R}^2\} \times \{z \in (0,d_z)\}$, where $Oxyz$ is a Cartesian frame of reference with unit vectors **i**, **j**, **k** respectively. Adopting the same boundaries as in Chapter 2, the upper and lower planes are held fixed at temperatures T_U and T_L, and concentrations 0 and c_L respectively.

The Brinkman model for convection in a porous medium is taken to govern flow, (see Straughan [90]), where v_i is the pore averaged velocity in the direction i, leading to the equations

$$\frac{\mu}{k}v_i = -p_{,i} + \overline{\lambda}\triangle v_i - b_i g\rho(T),$$
$$v_{i,i} = 0,$$

with the second equation being the incompressibility condition. Here $p_{,i}$ is the pressure gradient, μ is the dynamic viscosity of the fluid, $\overline{\lambda}$ is the Brinkman coefficient (or effective viscosity), k is the permeability, g is the acceleration due to gravity, and $\mathbf{b} = (0,0,1)$. The density ρ is taken to be a linear function in the temperature T, where the effect of the conjugated blue form of the thymol blue on the density function is assumed negligible. Hence

$$\rho(T) = \rho_0(1 - \alpha(T - T_0)),$$

where ρ_0 and T_0 are reference density and temperature values and α is the coefficient of thermal expansion.

In addition to the Brinkman model, the governing equations consist of the equations of conservation of energy and mass. Similarly to Chapter 2, the internal heat source is modelled linearly with respect to concentration, which is represented by the introduction of the βc term in the heat equation, where c represents the concentration of the conjugated form of the thymol blue and β is some constant of proportionality. Combining these equations with Brinkman's model the governing system of equations is as follows:

$$\begin{aligned}
&\frac{\mu}{k}v_i = -p_{,i} + \bar{\lambda}\triangle v_i - b_i g\rho_0(1-\alpha(T-T_0)),\\
&v_{i,i} = 0,\\
&\frac{1}{M}T_{,t} + v_i T_{,i} = \kappa\triangle T + \beta c,\\
&\varepsilon c_{,t} + v_i c_{,i} = \kappa_c \triangle c,
\end{aligned} \tag{3.1}$$

where κ_c and κ_m are the solute and thermal diffusivities respectively, ϵ is the porosity, with

$$(\rho_0 h)_m = (1-\epsilon)(\rho_0 h)_s + \epsilon(\rho_0 h_p)_f$$

where h_p is the specific heat of the fluid, and h is the specific heat of the solid, with the subscripts f, s, and m referring to the fluid, solid and porous components of the medium respectively. The remaining terms of system (5.1) are defined as $\kappa = \kappa_m/(\rho_0 h_p)_f$ and $M = (\rho_0 h_p)_f/(\rho_0 h)_m$.

Let us now consider the basic steady state solution $(\overline{v}_i, \overline{p}, \overline{T}, \overline{c})$ of the system, where, as there is no fluid flow, $\overline{v}_i = 0$. Utilising the boundary conditions, the equations contained in (3.1) show that

$$\begin{aligned}
&\overline{T}(z) = -\frac{\beta c_L}{\kappa d_z}\left(d_z\frac{z^2}{2} - \frac{z^3}{6}\right) + z\left[-\frac{H\delta T}{d_z} + \frac{\beta c_L d_z}{3\kappa}\right] + T_L,\\
&\overline{c} = (d_z - z)\frac{c_L}{d_z},
\end{aligned} \tag{3.2}$$

where $H = \text{sign}(T_L - T_U)$ and $\delta T = |T_L - T_U|$.

To study the stability of (3.1) we introduce a perturbation (u_i, θ, π, ϕ) to the steady state solution as follows

$$v_i = \overline{v}_i + u_i, \qquad T = \overline{T} + \theta, \qquad p = \overline{p} + \pi, \qquad c = \overline{c} + \phi,$$

and introduce non-dimensionalised variables with scalings of

$$u_i = \frac{\kappa}{d_z} u_i^*,\ \pi_i = \frac{\mu\kappa}{k}\pi_i^*,\ \theta = \sqrt{\frac{\mu\kappa(\delta T)}{g\alpha d_z k\rho_0}}\theta^*,\ \phi = c_L\phi^*,\ x_i = d_z x_i^*,$$
$$t = \frac{d_z^2}{M\kappa}t^*,\ \eta = \frac{\kappa_c}{\kappa},\ R = \sqrt{\frac{g\rho_0\alpha k d_z(\delta T)}{\mu\kappa}}$$

where d_z is the porous layer depth, and $R_a = R^2$ is the Rayleigh number. After dropping the stars, the perturbed equations are

$$\begin{aligned} &u_i - \lambda\triangle u_i = -\pi_{,i} + b_i R\theta, \\ &u_{i,i} = 0, \\ &\theta_{,t} + u_i\theta_{,i} = wRF(z) + \triangle\theta + \gamma R\phi, \\ &\hat{\phi}\phi_{,t} + u_i\phi_{,i} = w + \eta\triangle\phi, \end{aligned} \tag{3.3}$$

where $\lambda = \overline{\lambda}k/\mu d_z^2$, $\gamma = \beta c_L d_z^2/\kappa(\delta T)$, $\hat{\phi} = \varepsilon M$ and $F(z) = H - \gamma/3 + \gamma(z - z^2/2)$. The spatial domain of the porous layer is now $\{(x,y) \in \mathbb{R}^2\} \times \{z \in (0,1)\}$. The perturbed boundary conditions are given by

$$u_i = \theta = \phi = 0, \qquad z = 0, 1,$$

where $(u_i,\ \theta,\ \pi,\ \phi)$ have a periodic plan-form tiling the (x,y) plane. Two additional fixed boundary conditions are also required, so from $(3.3)_2$ it can be deduced that

$$w_z = 0, \qquad z = 0, 1.$$

We will denote V to be the period cell for the perturbations.

3.2 Linear Instability Analysis

The linearised equations are derived from (3.3) by discarding the nonlinear terms. Since the resulting system is linear we may seek solutions of the form $u_i = e^{\sigma t}u_i(\mathbf{x})$, $\theta = e^{\sigma t}\theta(\mathbf{x})$, $\phi = e^{\sigma t}\phi(\mathbf{x})$, and $\pi = e^{\sigma t}\pi(\mathbf{x})$, where σ is a complex constant. Taking the double *curl* of $(3.3)_1$, an eighth order system of equations in w, θ and ϕ can be derived, such that

$$\begin{aligned} &\triangle w - \lambda\triangle^2 w = R\triangle^*\theta, \\ &(\triangle - \sigma)\theta = -RwF - \gamma R\phi, \\ &(\eta\triangle - \hat{\phi}\sigma)\phi = -w, \end{aligned} \tag{3.4}$$

where $\triangle^* = \partial^2/\partial x^2 + \partial^2/\partial y^2$.

We assume a normal mode representation for w, θ and ϕ of the form $w = W(z)f(x,y)$, $\theta = S(z)f(x,y)$, and $\phi = \Phi(z)f(x,y)$ where $f(x,y)$ is a horizontal plan-form satisfying $\triangle^* f = -a^2 f$ (see Christopherson [16]). The system (3.4) then becomes four second order equations, namely

$$\begin{aligned}
&(D^2 - a^2)W - A = 0,\\
&(D^2 - a^2)A - \frac{1}{\lambda}A - \frac{a^2 R}{\lambda}S = 0,\\
&(D^2 - a^2)S + RWF + \gamma R\Phi = \sigma S,\\
&(D^2 - a^2)\Phi + \frac{1}{\eta}W = \frac{\hat{\phi}\sigma}{\eta}\Phi,
\end{aligned} \tag{3.5}$$

where $D^2 = \partial^2/\partial z^2$, and A is introduced by $(3.5)_1$. The boundary conditions are now

$$W = DW = S = \Phi = 0 \qquad z = 0, 1. \tag{3.6}$$

This eighth order system for R has been solved using the Chebyshev tau D^2 algorithm. A brief description of the application of this method to (3.5) is presented, although there are more explicit details in the references in Chapter 1 and Appendix A.2.

The system (3.5) is transformed onto the Chebyshev domain $(-1, 1)$ and the solutions W, A, S, and Φ are expanded as Chebyshev polynomials so that

$$\begin{aligned}
W &= \sum_{k=0}^{N+2} W_k T_k(z), \qquad A = \sum_{k=0}^{N+2} A_k T_k(z),\\
S &= \sum_{k=0}^{N+2} S_k T_k(z), \qquad \Phi = \sum_{k=0}^{N+2} \Phi_k T_k(z).
\end{aligned}$$

Taking the weighted inner product with T_i, and defining D^2 to be the Chebyshev representation of $\partial^2/\partial z^2$, the eigenvalue problem (3.5) now becomes

$$\begin{pmatrix}
4D^2 - a^2 & -1 & 0 & 0\\
0 & 4D^2 - a^2 - \frac{1}{\lambda} & -\frac{a^2 R}{\lambda} & 0\\
RF^* & 0 & 4D^2 - a^2 & \gamma R\\
\frac{1}{\eta} & 0 & 0 & 4D^2 - a^2
\end{pmatrix} \mathbf{B} = \sigma \begin{pmatrix}
0 & 0 & 0 & 0\\
0 & 0 & 0 & 0\\
0 & 0 & 1 & 0\\
0 & 0 & 0 & \frac{\hat{\phi}}{\eta}
\end{pmatrix} \mathbf{B}.$$

Here $\mathbf{B} = (\mathbf{W}, \mathbf{A}, \mathbf{S}, \mathbf{\Phi})^{\mathrm{T}}$, with $\mathbf{W} = (W_0, ..., W_N)$, $\mathbf{A} = (A_0, ..., A_N)$, $\mathbf{S} = (S_0, ..., S_N)$, $\mathbf{\Phi} = (\Phi_0, ..., \Phi_N)$, and $F^* = H + \gamma/24 + \gamma Z/4 - \gamma Z^2/8$, where Z and Z^2 are the matrix representations of z and z^2 respectively. The last two rows of each $(N+2)\times(N+2)$ block are removed and replaced by the discrete form of the boundary conditions (3.6). The QZ algorithm is then used to solve this matrix system. This technique, however, is restrictive due to the heavy computational cost in solving full matrix eigenvalue problems required over two parameter ranges (namely γ and λ). The natural progression was to develop the techniques in Chapters 7 and 8 to overcome these difficulties.

The range of values for η and γ suggested by Krishnamurti [55] and Straughan [89] are 10^{-3} to 10^{-2} and 1 to 10, respectively. The value $\lambda = (\overline{\lambda}/\mu) \times (k/d^2)$, however, need to be quantified.

The value k/d_z^2, where k is the permeability and d_z is the depth of the porous layer, is often referred to as the Darcy number. Numerous papers involve the use of Darcy numbers including Tien & Chiang [93] and Merrikh & Mohamad [71]. We will take similar values as Amahmid *et al.* [4] with the Darcy number ranging from 0 to 1. A Darcy number with a magnitude close to 1 is relatively large compared with those used in Carr & de Putter [13], Tien & Chiang [93] and Merrikh & Mohamad [71], but since we are considering a sparsely packed porous medium we would expect a high permeability, and thus a corresponding high Darcy number.

Martys [65] states that although the Brinkman model is capable of describing the case when $\overline{\lambda}/\mu \neq 1$, it is usually assumed to be 1 in the absence of any definitive knowledge about this ratio. However, theoretical studies (see Kim & Russel [53]) and numerical studies (see Martys *et al.* [66]) have shown that this case is only true as $\varepsilon \to 1$, and that $\overline{\lambda}/\mu$ increases in relation to the solid fraction. Martys *et al.* [66] shows that when $\varepsilon = 0.5$, $\overline{\lambda}/\mu$ was approximately 4 for an overlapping sphere model of porous media.

Taking $0 \leq \lambda \leq 1$ incorporates the characteristics of both the Darcy number and $\overline{\lambda}/\mu$, as since the porosity is high $\overline{\lambda}/\mu$ should not deviate too much from 1, and any increase would only require a smaller Darcy number, which as we are taking relatively large values seems an acceptable variation.

Numerical results generated via the Chebyshev tau routine are displayed for λ fixed at 0.01 and 0.1 (corresponding to Figures 3.1 and 3.2), $\eta = 10^{-3}$ to 10^{-2} in steps of 10^{-3}, and $\gamma = 1$ to 10.

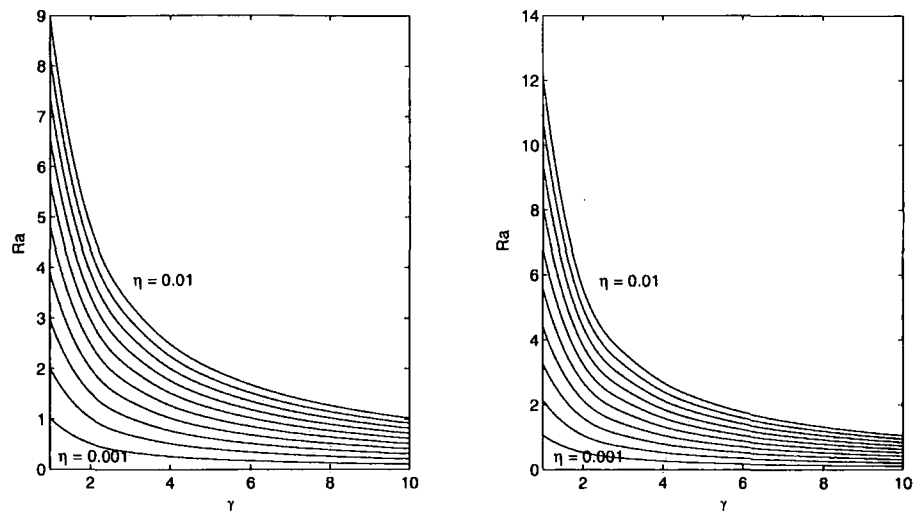

Figure 3.1: Critical Rayleigh number R_a plotted against γ with $\lambda = 0.01$. The left and right graphs correspond to heating from below ($H = +1$) and heating from above ($H = -1$) respectively

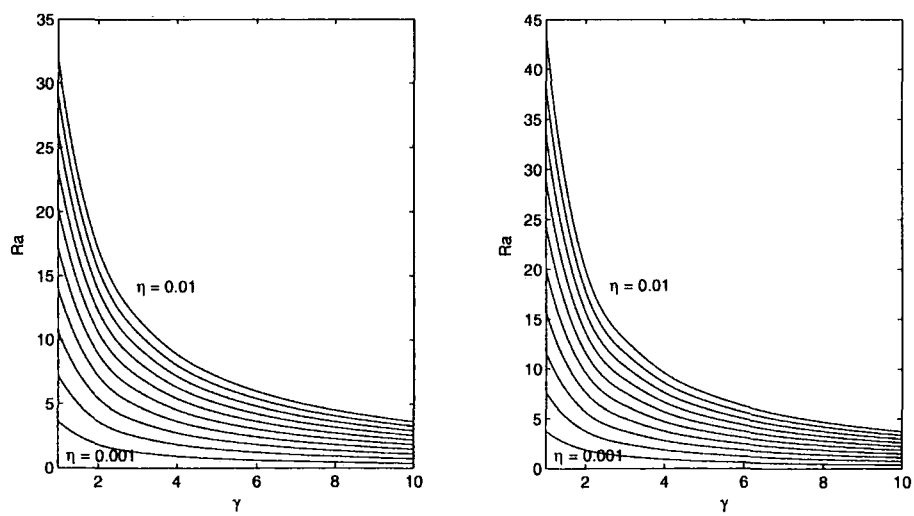

Figure 3.2: Critical Rayleigh number R_a plotted against γ with $\lambda = 0.1$. The left and right graphs correspond to heating from below ($H = +1$) and heating from above ($H = -1$) respectively

The results in Figures 3.1 and 3.2 for fixed λ follow a similar pattern to those of Chapter 1 and Straughan [89]. The results show that for the range specified increasing the radiation parameter γ greatly reduces the Rayleigh number, allowing convection to commence more easily.

We will now explore the effect of the λ term on the results by keeping η and γ fixed and varying λ. Figure 3.3 shows results for $\eta = 0.001, 0.005, 0.01$, and $\gamma = 1$, to 10, with λ varying from 0 to 1.

From Figure 3.3 it would appear there exists a linear relationship between the Rayleigh number and λ. This relationship is a somewhat unexpected result implying that increasing the λ term increases the Rayleigh number linearly, which makes the commencement of convection more difficult.

The spectrum of σ is found numerically to be always real, which is predicted by analysis on free boundaries, but is an interesting result considering the lack of symmetry of the linearised system.

3.3 Nonlinear Stability Analysis

As stated in Chapters 1 and 2, linear instability analysis provides a boundary for which all R^2 greater than the critical Rayleigh number will result in instability, where no assumptions can be made about stability when R^2 is below this boundary, as the solution may become unstable before the threshold predicted by the linear theory is reached. A nonlinear energy analysis produces stability boundaries with our aim being to show that these thresholds are close enough to those of linear theory, so that we can conclude that linear instability theory effectively captures the physics of the onset of convection.

As in Chapter 2 the nonlinear results are achieved by using the *energy method* (see Straughan [90] and Drazin & Reid [21]).

Let $\| \cdot \|$ and $\langle \cdot \rangle$ denote the norm and inner product on $L^2(V)$. Then by multiplying $(3.3)_1$ by u_i, $(3.3)_3$ by θ, and $(3.3)_4$ by ϕ and integrating over V we

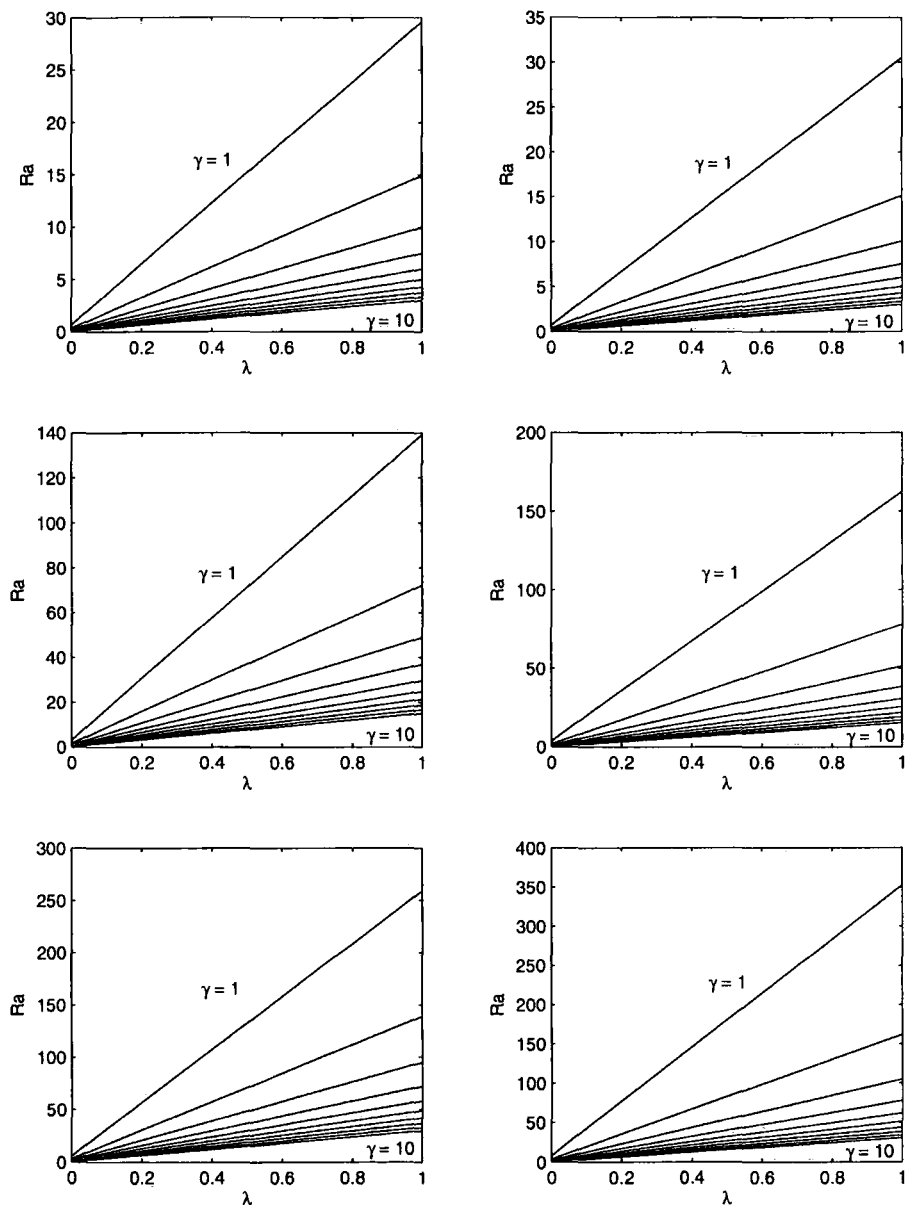

Figure 3.3: Critical Rayleigh number R_a plotted against λ for $\eta = 0.001$, 0.005, 0.01, and $\gamma = 1$, 5, 10. The three left hand side graphs correspond to heating from below ($H = +1$) with the remaining graphs corresponding to heating from above ($H = -1$)

derive the following nonlinear equations

$$\begin{aligned} &\|\mathbf{u}\|^2 + \lambda\|\nabla\mathbf{u}\|^2 = R\langle\theta, w\rangle, \\ &\frac{1}{2}\frac{d}{dt}\|\theta\|^2 = R\langle wF, \theta\rangle - \|\nabla\theta\|^2 + \gamma R\langle\phi, \theta\rangle, \\ &\frac{\hat{\phi}}{2}\frac{d}{dt}\|\phi\|^2 = \langle w, \phi\rangle - \eta\|\nabla\phi\|^2. \end{aligned} \tag{3.7}$$

We introduce coupling parameters λ_1, λ_2, and define

$$\begin{aligned} E(t) &= \frac{\lambda_1\hat{\phi}}{2}\|\phi\|^2 + \frac{1}{2}\|\theta\|^2, \\ \mathcal{D} &= \|\nabla\theta\|^2 + \eta\lambda_1\|\nabla\phi\|^2 + \lambda_2\|\mathbf{u}\|^2 + \lambda\lambda_2\|\nabla\mathbf{u}\|^2, \\ \mathcal{I} &= R\langle wF, \theta\rangle + \gamma R\langle\phi, \theta\rangle + \lambda_1\langle w, \phi\rangle + \lambda_2 R\langle\theta, w\rangle. \end{aligned}$$

From (3.7) we derive

$$\begin{aligned} \frac{dE}{dt} &= \mathcal{I} - \mathcal{D} \\ &\leq -\mathcal{D}\left(1 - \frac{1}{R_E}\right) \end{aligned}$$

where $1/R_E = \max_{\mathcal{H}}(\mathcal{I}/\mathcal{D})$ and $\mathcal{H}$ is the space of admissible functions to (3.3). If $R_E > 1$ then by the Poincaré inequality, $\mathcal{D} \geq cE$ for some positive constant c. Hence it follows that

$$\frac{dE}{dt} \leq -cE\left(\frac{R_E - 1}{R_E}\right).$$

Thus letting $a = c(R_E - 1)/R_E > 0$ we have $E(t) \leq E(0)e^{-at}$ which tends to 0 as $t \to \infty$, showing the decay of θ and ϕ. To show the decay of $\mathbf{u}$ we define some positive constant $\alpha > 0$, and use $(3.7)_1$ and the Poincaré inequality so that

$$(1 + \lambda\pi^2)\|\mathbf{u}\|^2 \leq R\langle w, \theta\rangle.$$

We let b equal $1/(1 + \lambda\pi^2) \in [0, 1]$ (as $\lambda \geq 0$), which leads to

$$\|\mathbf{u}\|^2 \leq \frac{Rb}{2\alpha}\|\mathbf{u}\|^2 + \frac{R\alpha b}{2}\|\theta\|^2 + \frac{\lambda_1\alpha^2 b}{2}\hat{\phi}\|\phi\|^2$$

as $\lambda_1\alpha^2 b\hat{\phi} \geq 0$. Hence defining $f = b/(1 - b/2) \in [0, 2]$ and letting $\alpha = R$

$$\|\mathbf{u}\|^2 \leq R^2 fE \leq R^2 fE(0)e^{-at} \quad \to 0 \qquad as \quad t \to \infty.$$

The decay of $\mathbf{u}$ clearly follows.

We now turn our attention to the maximisation problem $1/R_E = \max_{\mathcal{H}}(\mathcal{I}/\mathcal{D})$ with $R_E > 1$. We do this for the threshold case $R_E = 1$ which yields the sharpest stability boundary.

The arising Euler Lagrange equations (see Section 2.3 for an explicit example of the derivation of Euler Lagrange equations) are

$$\begin{aligned} &RF\theta + \lambda_1\phi + \lambda_2 R\theta - 2\lambda_2 u_i = \omega_{,i}, \\ &RwF + \gamma R\phi + \lambda_2 Rw + 2\triangle\theta = 0, \\ &\gamma R\theta + \lambda_1 w + 2\eta\lambda_1\triangle\phi = 0, \end{aligned} \tag{3.8}$$

where we have introduced the Lagrange multiplier ω, where $\int_V \omega u_{i,i}\, dV = 0$, such that

$$\frac{d}{dx_i}\left(\frac{\partial}{\partial u_{i,i}}(\omega u_{i,i})\right) = \omega_{,i}.$$

Taking the double *curl* of the third component of $(3.8)_1$ and introducing the normal mode representations as presented in Section 3.1, (3.8) is converted to a system of four second order equations, namely

$$\begin{aligned} &(D^2 - a^2)W - A = 0, \\ &(D^2 - a^2)A - \frac{1}{\lambda}A - \frac{R(F+\lambda_2)a^2}{2\lambda\lambda_2}S - \frac{a^2\lambda_1}{2\lambda\lambda_2}\Phi = 0, \\ &(D^2 - a^2)S + \frac{R(F+\lambda_2)}{2}W + \frac{\gamma R}{2}\Phi = 0, \\ &(D^2 - a^2)\Phi + \frac{\gamma R}{2\eta\lambda_1}S + \frac{1}{2\eta}W = 0, \end{aligned} \tag{3.9}$$

where the boundary conditions are

$$W = DW = S = \Phi = 0, \qquad z = 0, 1. \tag{3.10}$$

System (3.9) was solved using the compound matrix method, as discussed in Chapter 1, with further details in Appendix A.1. A brief description of the method is provided, with any further required explicit details in the aforementioned references.

Define a vector $\mathbf{W} = (W, W', A, A', S, S', \Phi, \Phi')$, and suppose $\mathbf{W_1}$, $\mathbf{W_2}$, $\mathbf{W_3}$, and $\mathbf{W_4}$ are independent solutions obtained by replacing the boundary conditions (3.10) at $z = 1$ by the initial conditions

$$\begin{aligned} &\mathbf{W}_1(0) = (0,0,1,0,0,0,0,0)^T, \qquad &&\mathbf{W}_2(0) = (0,0,0,1,0,0,0,0)^T, \\ &\mathbf{W}_3(0) = (0,0,0,0,0,1,0,0)^T, \qquad &&\mathbf{W}_4(0) = (0,0,0,0,0,0,0,1)^T. \end{aligned}$$

By defining the variables $y_1, ..., y_{70}$ to be the 4×4 minors of the 8×4 matrix where the columns are $\mathbf{W_1}$, $\mathbf{W_2}$, $\mathbf{W_3}$, and $\mathbf{W_4}$ respectively, this system was numerically integrated subject to the initial condition

$$y_{60}(0) = A_1(0)A_2'(0)S_3'(0)\Phi_4'(0) + \ldots = 1,$$

and the final condition

$$y_{11}(1) = W_1(1)W_2'(1)S_3(1)\Phi_4(1) + \ldots = 0,$$

and the eigenvalue R was varied until these conditions were met to some pre-defined degree of accuracy. The critical Rayleigh number was then located by a golden section search to minimise with respect to a^2, and was maximised over the coupling parameters λ_1, λ_2, so that

$$Ra_E = \max_{\lambda_1,\lambda_2} \min_{a^2} R^2(a^2, \lambda_1, \lambda_2).$$

The compound matrix equations (i.e. the differentials of each of the minors of the solution matrix) which had to be calculated before any numerical analysis was attempted, were found to be highly time consuming. An automated program had to be written to evaluate all 256 of them, which was deemed to be excessive as this must be completed before numerical analysis is attempted, resulting in the alternative approach in Chapters 7 and 8.

Table 3.1 displays the critical values (R_L, R_E, a_E^2), where the subscripts L and E refer to linear and non-linear results, respectively. (a^2 refers to the critical wavelength number). The results are given for $\gamma = 1$, $\eta = 0.001$, 0.005, 0.01, and $\lambda = 0.001$, 0.1.

We can conclude from Table 3.1 that for this parameter range the critical values obtained from the linear analysis are very close to those obtained via the nonlinear energy analysis (i.e. the linear instability and nonlinear stability thresholds are very close).

3.4 Conclusions

The Brinkman model is used to analytically and numerically study convection induced by the selective absorption of radiation in a porous medium, a modification

λ	η	H	Ra_E	Ra_L	a_E^2
0.01	0.001	+1	1.021673795	1.022415867	5.3628
0.1	0.001	+1	3.631695736	3.636379071	5.4820
0.01	0.005	+1	4.810092189	4.813258929	5.5264
0.1	0.005	+1	17.08957809	17.10973686	5.6413
0.01	0.01	+1	8.958983607	8.964409432	5.7304
0.1	0.01	+1	31.81324678	31.84701031	5.8336
0.01	0.001	−1	1.053194836	1.053990687	5.2804
0.1	0.001	−1	3.744680628	3.749746613	5.4004
0.01	0.005	−1	5.599061666	5.603666549	5.1146
0.1	0.005	−1	19.91750142	19.94685489	5.2406
0.01	0.01	−1	12.14503142	12.15634931	4.9008
0.1	0.01	−1	43.23434653	43.30622631	5.0192

Table 3.1: Comparison of the nonlinear and linear critical Rayleigh numbers Ra_E and Ra_L, with $\gamma = 1$.

of the Darcy model used in Chapter 1 for fixed bounding surfaces.

Figures 3.1 and 3.2 provide a graphical representation of the results of the linear instability analysis with λ fixed and varying η and γ. By contrast Figure 3.3 shows the results when λ varies between 0 and 1. A linear relationship between the critical Rayleigh number R_a and λ is predicted. This implies a dependence on the specific porous medium due to the permeability k and the term $\overline{\lambda}/\mu$ (see Martys [65]).

Table 3.1 presents the nonlinear stability and corresponding linear instability results for various η and λ. The thresholds of the linear and nonlinear theory are extremely close, so that the potential region of subcritical instabilities is extremely small, showing that for the range with respect to the parameters given, the linear theory effectively captures the physics of the onset of convection.

Chapter 4

Conditional and unconditional stability for convection in a porous medium with a concentration based internal heat source

In Chapters 2 and 3 the assumption is made that the internal heat source is linear with respect to concentration in the model for convection induction by the selective absorption of radiation in a porous medium. However, it is stated in Krishnamurti [55] that 'This linear relationship is a first order approximation and may need modification for high concentrations of [thymol] blue'. This chapter is motivated by the exploration of the validity of an alternative quadratic model.

The Darcy equation (see Straughan [90]) is first employed as the standard approach to describe fluid flow in the porous medium. The nonlinear stability results that are achieved are conditional, so that they are undesirably bounded by the initial data thresholds. McKay & Straughan [69] also derive conditional results for a porous medium in a similar fashion to those presented in this paper.

In the case when fluid flow is not small it is possible to modify the Darcy equations by introducing Forchheimer drag coefficients (see Forchheimer [22] and Nield & Bejan [77]), with the idea being that the pressure gradient is no longer proportional to the velocity itself. Extensive literature exists on Forchheimer theory including

significant recent contributions from Giorgi [27], Whitaker [97], Payne *et al.* [78], and Andrade *et al.* [6].

To establish unconditional nonlinear results we found it necessary to introduce Forchheimer drag coefficients. Payne & Straughan [79] and Carr [12] use Forchheimer theory to establish unconditional nonlinear results for flow in a porous medium, where density is assumed to vary constantly and cubically with temperature respectively. In this paper a similar approach to Payne & Straughan [79] is adopted, where the density is assumed linear in temperature.

In this chapter we present a detailed linear and nonlinear analysis for this system with a quadratically modelled internal heat source, with the bounding surfaces being fixed. The linear and nonlinear results are derived using using Chebyshev-tau and compound matrix numerical techniques (see Appendices A.2 and A.1), and compared to assess the region of potential subcritical instabilities as a direct indicator of the suitability of linear instability theory in the prediction of the onset of penetrative convection. Although details are not given in this chapter, the methods developed in Chapters 7 and 8 are ideal candidates to evaluate the linear and nonlinear results.

The results in this chapter were published in the article Hill [38]. A further paper, Hill [39], has also been published where a fluid, as opposed to a porous, medium is taken with a quadratically modelled heat source. This lent much credence to the use of a linearly modelled internal heat source as used by Krishnamurti [55], within the constraints of the parameter range.

4.1 Governing Equations

Let us consider a fluid saturated porous layer occupying the three dimensional layer $\{(x,y) \in \mathbb{R}^2\} \times \{z \in (0,d_z)\}$, where $Oxyz$ is a Cartesian frame of reference with unit vectors $\mathbf{i}$, $\mathbf{j}$, $\mathbf{k}$ respectively. Adopting the same boundaries as in Chapters 2 and 3 the upper and lower planes are held fixed at temperatures T_U and T_L, and concentrations 0 and c_L respectively. Gravity acts in the negative z direction and

we assume that the density has a linear temperature dependence of the form

$$\rho(T) = \rho_0(1 - \alpha(T - T_0)),$$

where ρ_0 and T_0 are reference density and temperature values and α is the coefficient of thermal expansion.

Denote v_i, p, μ, and k to be the pore averaged velocity, pressure gradient, dynamic viscosity of the fluid and permeability respectively. We are studying two separate models to govern the flow in the porous medium, with the first satisfying Darcy's law (see Straughan [90]) of the form

$$\frac{\mu}{k}v_i = -p_{,i} - b_i g\rho(T), \tag{4.1}$$

$$v_{i,i} = 0. \tag{4.2}$$

The second is that of Forchheimer (see Nield & Bejan [77]) with non-linear drag terms $|\mathbf{v}|v_i$ and $|\mathbf{v}|^2 v_i$ such that

$$\frac{\mu}{k}v_i = -p_{,i} - b_i g\rho(T) - \hat{b}|\mathbf{v}|v_i - \hat{c}|\mathbf{v}|^2 v_i, \tag{4.3}$$

$$v_{i,i} = 0, \tag{4.4}$$

where $\hat{b}$ and $\hat{c}$ are some positive constants.

Using Joseph [48] to derive the heat equation governing the temperature of the porous medium, and introducing internal heat source Q, we have

$$\frac{1}{M}T_{,t} + v_i T_{,i} = \kappa\triangle T + Q, \tag{4.5}$$

where κ_m is the thermal diffusivity of the porous medium, h_p is the specific heat of the fluid, and h is the specific heat of the solid, with $\kappa = \kappa_m/(\rho_0 h_p)_f$ and $M = (\rho_0 h_p)_f/(\rho_0 h)_m$. Denoting c to be the concentration of the conjugated blue form of the thymol blue, we define the internal heat source Q quadratically in terms of c such that

$$Q = \beta_1 c + \beta_2 c^2, \tag{4.6}$$

where β_1 and β_2 are some constants of proportionality.

The concentration c is taken to obey the diffusion equation (see Lombardo *et. al.* [59]) of the form

$$\epsilon c_{,t} + v_i c_{,i} = \kappa_c \triangle c, \tag{4.7}$$

where ϵ is the porosity and D_c is the diffusivity of the conjugated form with $\kappa_c = \epsilon D_c$.

The two models under consideration now consist of the partial differential equations (4.1), (4.2), (4.5), (4.7) and (4.3), (4.4), (4.5), (4.7) respectively, with (4.6) defining the form of the internal heat source Q.

For each model the basic steady state solution, in whose stability we are interested in, is

$$\overline{c}(z) = (d_z - z)\frac{c_L}{d_z}, \tag{4.8}$$

$$\overline{T}(z) = T_L + z\left(-\frac{H\delta T}{d_z} + \frac{d_z}{12}(4\tau_1 + 3\tau_2)\right) - \frac{z^2}{2}(\tau_1 + \tau_2) + \frac{z^3}{6d_z}(\tau_1 + 2\tau_2) - \frac{z^4\tau_2}{12d_z^2}, \tag{4.9}$$

where $H = sign(T_L - T_U)$, $\delta T = |T_L - T_U|$, $\tau_1 = \beta_1 c_L/\kappa$, and $\tau_2 = \beta_2 c_L^2/\kappa$. The hydrostatic pressure $\overline{p}$ for each model may be found from (4.1) and (4.3) respectively, but since we eliminate $\overline{p}$ from our analysis later, we do not include a derivation here.

To study the stability of each system we introduce a perturbation (u_i, θ, π, ϕ) to the steady state solution as follows

$$v_i = \overline{v}_i + u_i, \qquad T = \overline{T} + \theta, \qquad p = \overline{p} + \pi, \qquad c = \overline{c} + \phi.$$

and introduce non-dimensionalised variables with scalings of

$$u_i = \frac{\kappa}{d_z}u_i^*,\ \pi_i = \frac{\mu\kappa}{k}\pi_i^*,\ \theta = \sqrt{\frac{\mu\kappa(\delta T)}{g\alpha d_z k\rho_0}}\theta^*,\ \phi = c_L\phi^*,\ x_i = d_z x_i^*,$$

$$t = \frac{d_z^2}{M\kappa}t^*,\ \eta = \frac{\kappa_c}{\kappa},\ R = \sqrt{\frac{g\rho_0\alpha k d_z(\delta T)}{\mu\kappa}}$$

where d_z is the porous layer depth, and $R_a = R^2$ is the Rayleigh number. Substituting the perturbations and non-dimensionalised variables into (4.1), (4.3), (4.2), (4.5), and (4.7), letting $u_3 = w$, imposing (4.8) and (4.9), and dropping the stars we obtain

$$\begin{aligned}
&u_i = -\pi_{,i} + b_i R\theta,\\
&u_i = -\pi_{,i} + b_i R\theta - b|\mathbf{u}|u_i - c|\mathbf{u}|^2 u_i,\\
&u_{i,i} = 0,\\
&\theta_{,t} + u_i\theta_{,i} = RF_1(z)w + \triangle\theta + RF_2(z)\phi + \gamma_2 R\phi^2,\\
&\hat{\phi}\phi_{,t} + u_i\phi_{,i} = w + \eta\triangle\phi,
\end{aligned} \tag{4.10}$$

where $b = k\hat{b}\kappa/d_z\mu$, $c = k\hat{c}\kappa^2/d_z^2\mu$, $\gamma_1 = d_z^2\tau_1/\delta T$, $\gamma_2 = d_z^2\tau_2/\delta T$, and

$$\begin{aligned} F_1(z) &= H - \gamma_1/3 - \gamma_2/4 + z(\gamma_1 + \gamma_2) - z^2(\gamma_1/2 + \gamma_2) + z^3\gamma_2/3, \\ F_2(z) &= \gamma_1 + 2\gamma_2(1 - z). \end{aligned}$$

The Darcy and Forchheimer flow governing equations are $(4.10)_1$ and $(4.10)_2$ respectively.

The spatial domain of the porous layer is now $\{(x, y) \in \mathbb{R}^2\} \times \{z \in (0, 1)\}$. The perturbed boundary conditions for both models are given by

$$w = \theta = \phi = 0, \qquad z = 0, 1,$$

where $(u_i,\ \theta,\ \phi)$ have a periodic plan-form tiling the (x, y) plane. We will denote V to be the period cell for the perturbations.

4.2 Linear Instability Analysis

The linearised equations are derived from (4.10) by discarding the nonlinear terms. Both models produce the same linearised equations as the non linear drag coefficients from $(4.10)_2$ are removed, such that the equation reduces to $(4.10)_1$. Assuming a temporal growth rate like $e^{\sigma t}$, where σ is a complex constant, taking the double *curl* of $(4.10)_1$ and looking at the third component, we obtain the linearised system

$$\begin{aligned} &\triangle w = R\triangle^*\theta, \\ &\sigma\theta = RF_1(z)w + \triangle\theta + RF_2(z)\phi, \\ &\hat{\phi}\sigma\phi = w + \eta\triangle\phi, \end{aligned} \tag{4.11}$$

where $\triangle^* = \partial^2/\partial x^2 + \partial^2/\partial y^2$.

Assuming a normal mode representation for w, θ, and ϕ of the form $w = W(z)f(x, y)$, $\theta = S(z)f(x, y)$, and $\phi = \Phi(z)f(x, y)$ where $f(x, y)$ is a horizontal plan-form satisfying $\triangle^* f = -a^2 f$ (see Christopherson [16]), (4.11) becomes

$$\begin{aligned} &(D^2 - a^2)W + a^2RS = 0, \\ &(D^2 - a^2)S + RF_1(z)W + RF_2(z)\Phi = \sigma S, \\ &(D^2 - a^2)\Phi + \frac{1}{\eta}W = \frac{\hat{\phi}\sigma}{\eta}\Phi, \end{aligned} \tag{4.12}$$

where $D^2 = \partial^2/\partial z^2$, with boundary conditions

$$W = S = \Phi = 0, \qquad z = 0, 1. \tag{4.13}$$

We have solved this eighth order system for R using the the Chebyshev tau technique, as described in Dongarra *et al.* [20] and Appendix A.2. A brief description is not included in this chapter as it follows a very similar implementation to that of Chapters 2 and 3.

As γ_1 and γ_2 are not explicitly defined experimentally, we present a numerical assessment of their affects on the Rayleigh number in comparison to each other. Two specific ranges of 0.1 to 1 and 1 to 10 are studied for both γ_1 and γ_2 with the opposing γ term set at 1, 10 and 100. The value η remains fixed at 0.01.

Although the Rayleigh numbers are different, as would be expected from a different model, we can see that the results from Figures 4.1 and 4.2, for γ_1 and γ_2 varying from 1 to 10, with the opposing γ term fixed at 1, follow a similar pattern to that of Chapters 2 and 3 and Straughan [89], although the quantitative effect is different. It is observed that an increase in either γ_1 or γ_2 causes the Rayleigh number to decrease. More interestingly though is the observation that γ_1 and γ_2 have an almost identical effect on the Rayleigh number in relation to each other. This demonstrates that a variation change in γ_2 will be as equally significant to a change in the Rayleigh number as a variational change to γ_1.

To attempt to further explore the effects of the parameters γ_1 and γ_2 we turn our attention to analytical methods. The main problem when dealing with (4.11) analytically are the $F_1(z)$ and $F_2(z)$ terms, as they vary over the $z \in [0, 1]$ range. However, by taking the average of both polynomials over this range we can proceed analytically so that $F_{1(av)} = \int_0^1 H - \gamma_1/3 - \gamma_2/4 + z(\gamma_1 + \gamma_2) - z^2(\gamma_1/2 + \gamma_2) + z^3\gamma_2/3 \, dz = H$, and $F_{2(av)} = \gamma_1 + \gamma_2$. Furthermore, the spectrum of σ was found numerically to be always real, so this is assumed for the analysis. It must be stressed that the analysis is only heuristic as σ has not been proved to be real (it is only suggested by the numerical analysis).

Letting $L = D^2 - a^2$, taking $\sigma = 0$, re-applying L to $(4.12)_1$, and using $(4.12)_2$,

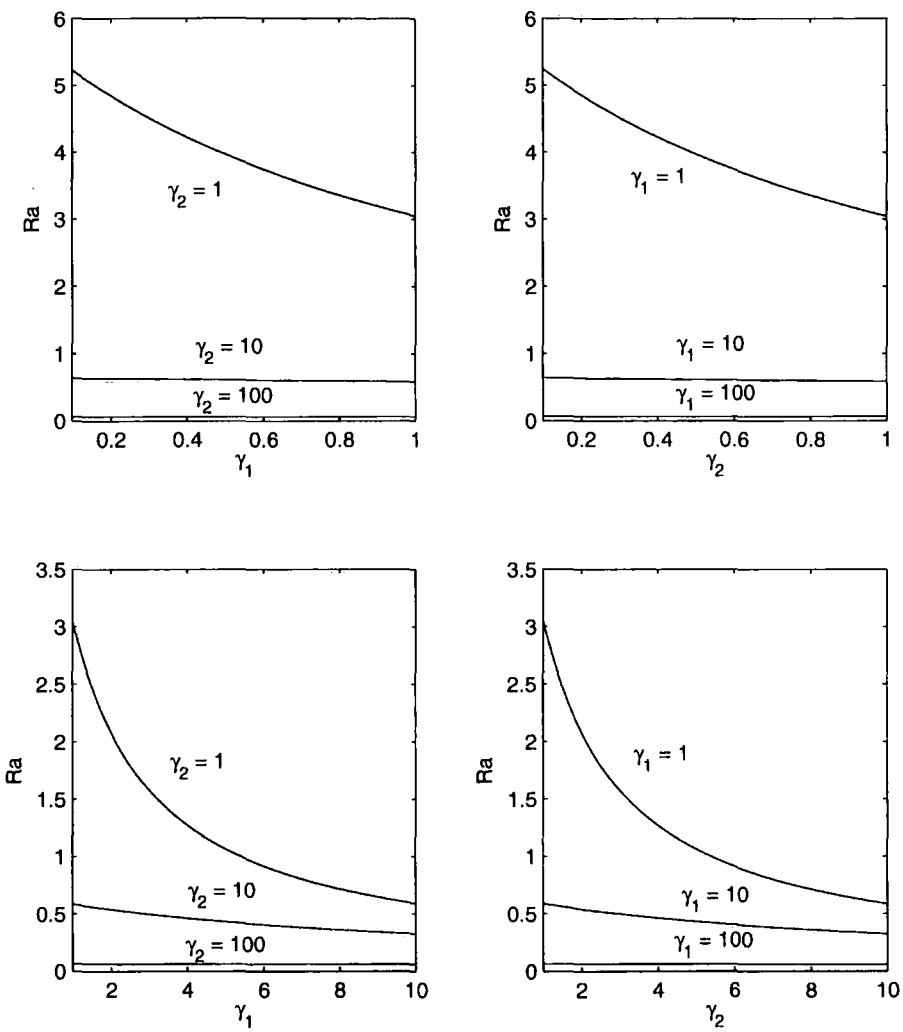

Figure 4.1: Critical Rayleigh number R_a plotted against γ_1 for left hand graphs and γ_2 for right hand graphs. These graphs correspond to heating from below ($H = +1$) with η fixed at 0.01.

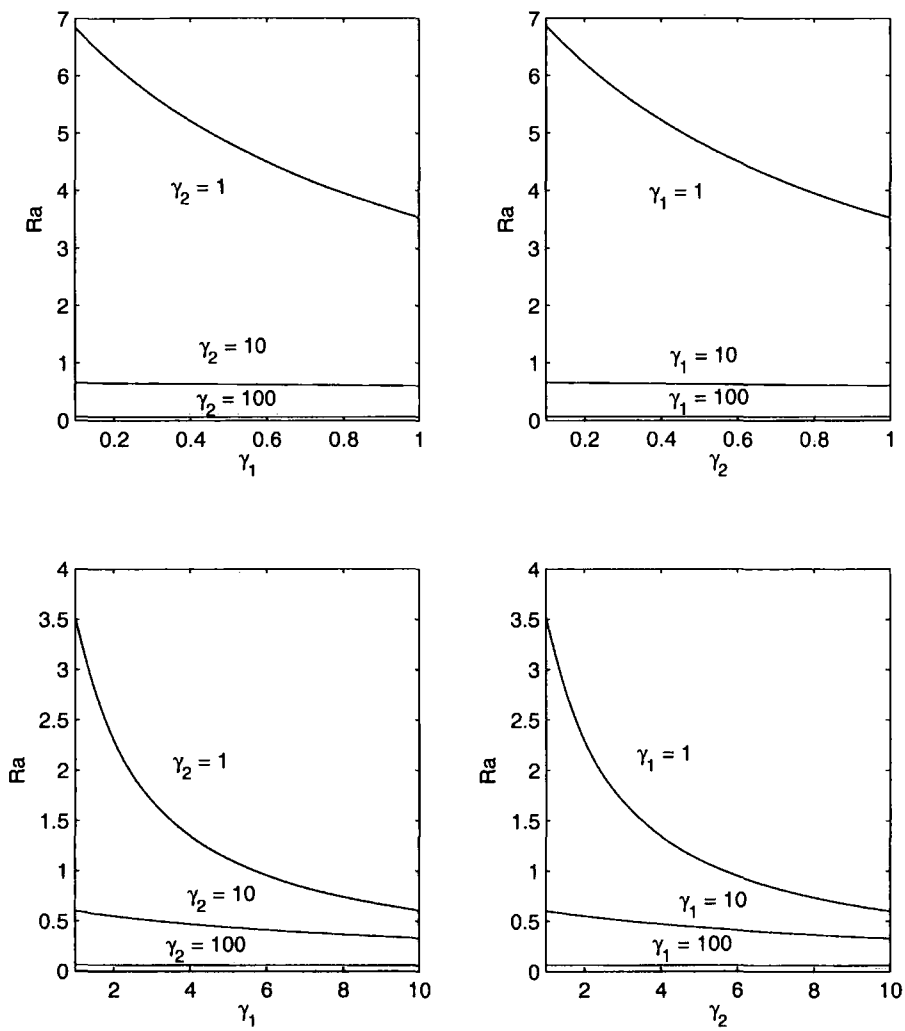

Figure 4.2: Critical Rayleigh number R_a plotted against γ_1 for left hand graphs and γ_2 for right hand graphs. These graphs correspond to heating from above ($H = -1$) with η fixed at 0.01.

$(4.12)_3$ we have

$$\begin{aligned} LW &= -a^2RS, \\ L^{(2)}W &= -a^2R(-RWH - \gamma_1 R\Phi), \\ L^{(3)}W &= a^2R^2HLW - \frac{(\gamma_1+\gamma_2)a^2R^2}{\eta}W, \\ L^{(4)}W &= a^2R^2HL^2W - \frac{(\gamma_1+\gamma_2)a^2R^2}{\eta}LW. \end{aligned}$$

Using the boundary conditions $W = 0$, $S = 0$, $\Phi = 0$, at $z = 0$, 1 we can see that $L^{(4)}W = 0$ on $z = 0, 1$ (as LW and L^2W can be written in terms of W, S, and Φ). By repeated application of L and relevant substitution of lower powers we can see that $L^{(n)}W = 0$ for $n \geq 1$, $z = 0$, 1. Hence we may write $W = W_0 \sin(n\pi z)$ for some constant W_0. Substituting this into the $L^{(3)}$ equation, after some cancelling we find

$$R^2 = \frac{(n^2\pi^2 + a^2)^3}{a^2[H(n^2\pi^2 + a^2) + \frac{\gamma_1+\gamma_2}{\eta}]}. \tag{4.14}$$

Letting $\Omega = n^2\pi^2 + a^2$, and differentiating (4.14) with respect to n^2 we have

$$\frac{\partial R^2}{\partial n^2} = \frac{2\Omega^3\pi^2 H + 3\Omega^2\pi^2(\gamma_1+\gamma_2)/\eta}{a^2[H\Omega + \frac{\gamma_1+\gamma_2}{\eta}]^2} \quad > \quad 0,$$

where we have taken $H = +1$ to ensure the positivity of the differential. As the differential is > 0 we can take $n = 1$. Hence

$$R^2 = \frac{(\pi^2 + a^2)^3}{a^2[\pi^2 + a^2 + \frac{\gamma_1+\gamma_2}{\eta}]}. \tag{4.15}$$

Thus setting $\partial R^2/\partial a^2 = 0$ we derive a quadratic for a^2 and since $a^2 \geq 0$ we find the a^2 value which minimises R^2 is given by

$$a^2 = -\frac{\gamma_1+\gamma_2}{\eta} + \sqrt{\frac{(\gamma_1+\gamma_2)^2}{\eta^2} + \pi^4 + \frac{\pi^2(\gamma_1+\gamma_2)}{\eta}}.$$

Substituting this a^2 value into (4.15) we can calculate R^2 for given η and γ. The main impetus behind this analytic work is to highlight that γ_1 and γ_2 have equal importance in the resulting analytical equation, as reflected in the numerical results. Using (4.15) and the compound method results we display solutions for the seven distinct cases of varying proportial magnitudes between γ_1 and γ_2, for the approximate analytical and exact numerical R^2 values.

From Table 4.1 we see that the approximate analytical results are a very useful guide to their numerical counterparts.

γ_1	γ_2	R_A	R_N
1	1	3.0597	3.0463
0.1	1	5.2618	5.2284
1	0.1	5.2618	5.2442
0.1	10	0.6416	0.6364
10	0.1	0.6416	0.6392
0.1	100	0.0656	0.0650
100	0.1	0.0656	0.0653

Table 4.1: Comparison of the approximate analytical and exact numerical critical Rayleigh numbers R_A and R_N

4.3 Conditional Nonlinear Stability Analysis

In this section we employ the Darcy model. Due to this we are only able to derive conditional nonlinear stability results. To obtain a global nonlinear stability bound in the stability measure $L^2(V)$ we proceed as follows for the Darcy model consisting of $(4.10)_1$, $(4.10)_4$, and $(4.10)_5$. First we multiply $(4.10)_1$, $(4.10)_4$, and $(4.10)_5$ by u_i, θ, and ϕ respectively and integrate over V to obtain

$$\begin{aligned} &\|\mathbf{u}\|^2 = R\langle\theta, w\rangle, \\ &\frac{1}{2}\frac{d}{dt}\|\theta\|^2 = R\langle F_1 w, \theta\rangle - \|\nabla\theta\|^2 + R\langle F_2\phi, \theta\rangle + \gamma_2 R\langle\phi^2, \theta\rangle, \\ &\frac{\hat{\phi}}{2}\frac{d}{dt}\|\phi\|^2 = \langle w, \phi\rangle - \eta\|\nabla\phi\|^2. \end{aligned} \tag{4.16}$$

Adding equations $(4.16)_1$, $(4.16)_2$, and $(4.16)_3$ leads to

$$\begin{aligned} \frac{d}{dt}\left(\frac{1}{2}\|\theta\|^2 + \frac{\hat{\phi}}{2}\|\phi\|^2\right) = &-\|\mathbf{u}\|^2 - \|\nabla\theta\|^2 - \eta\|\nabla\phi\|^2 + R\langle\theta, w\rangle \\ &+R\langle F_1 w, \theta\rangle + R\langle F_2\phi, \theta\rangle + \gamma_2 R\langle\phi^2, \theta\rangle + \langle w, \phi\rangle, \end{aligned} \tag{4.17}$$

where $\|\cdot\|$ and $\langle\cdot\rangle$ denote the norm and inner product on $L^2(V)$.

However, due to the higher order terms in the right hand side of (4.17) a standard energy technique in $L^2(V)$ fails to provide a meaningful unconditional nonlinear stability bound. To quantify this we follow a similar argument as that presented in

Payne and Straughan [79]. We define

$$\mathcal{I} = R\langle\theta, w\rangle + R\langle F_1 w, \theta\rangle + R\langle F_2\phi, \theta\rangle + \gamma_2 R\langle\phi^2, \theta\rangle + \langle w, \phi\rangle,$$
$$\mathcal{D} = \|\mathbf{u}\|^2 + \|\nabla\theta\|^2 + \eta\|\nabla\phi\|^2.$$

Then we deduce from (4.17)

$$\frac{d}{dt}\left(\frac{1}{2}\|\theta\|^2 + \frac{\hat{\phi}}{2}\|\phi\|^2\right) \leq -\mathcal{D}\left(1 - \max_{\mathcal{H}}\frac{\mathcal{I}}{\mathcal{D}}\right), \tag{4.18}$$

where $\mathcal{H}$ is the space of admissible functions. The usual energy argument then states that if $\max_{\mathcal{H}}(\mathcal{I}/\mathcal{D}) < 1$ then we may conclude nonlinear stability (see Straughan [90]). However, $\mathcal{I}/\mathcal{D}$ in this system is not bounded by 1. To see this we note that since the space $\mathcal{H}$ is linear we can write u_i, θ, and ϕ as αu_i, $\beta\theta$, and $\delta\phi$ respectively for arbitrary real numbers α, β, δ. Then

$$\frac{\mathcal{I}}{\mathcal{D}} = \frac{A_1\alpha\beta + A_2\beta\delta + A_3\delta^2\beta + A_4\alpha\delta}{A_5\alpha^2 + A_6\beta^2 + A_7\delta^2},$$

where $A_1, \ldots, A_7$ are the appropriate integrals from the definitions of I and $\mathcal{D}$. If we fix u_i, θ, and ϕ we may treat $A_1, \ldots, A_7$ as constants. Letting $\beta = \delta = \alpha^{1+\omega}$ for some positive number ω leads to

$$\frac{\mathcal{I}}{\mathcal{D}} = \frac{A_1\alpha^{\omega+2} + A_2\alpha^{2\omega+2} + A_3\alpha^{3\omega+3} + A_4\alpha^{\omega+2}}{A_5\alpha^2 + A_6\alpha^{2\omega+2} + A_7\alpha^{2\omega+2}}.$$

Setting $\omega = 1/2$ we see that

$$\frac{\mathcal{I}}{\mathcal{D}} = \alpha^{\frac{3}{2}}\left[\frac{A_1\alpha^{-2} + A_2\alpha^{-\frac{3}{2}} + A_3 + A_4\alpha^{-2}}{A_5\alpha^{-1} + A_6 + A_7}\right] \quad \to \infty \quad as \quad \alpha \to \infty.$$

Hence the maximum of $\mathcal{I}/\mathcal{D}$ in $\mathcal{H}$ can not be achieved, so any standard approach to derive global nonlinear stability using $L^2(V)$ will not succeed.

To overcome this problem we derive conditional nonlinear bounds (see McKay & Straughan [69]). We take the system (4.16) and include another equation whose derivation occurs when $(4.10)_5$ is multiplied by ϕ^3 and integrated over V. Letting $\alpha = \phi^2$ we now have the system

$$\begin{aligned}
&\|\mathbf{u}\|^2 = R\langle\theta, w\rangle,\\
&\frac{1}{2}\frac{d}{dt}\|\theta\|^2 = R\langle F_1 w, \theta\rangle - \|\nabla\theta\|^2 + R\langle F_2\phi, \theta\rangle + \gamma_2 R\langle\alpha, \theta\rangle,\\
&\frac{\hat{\phi}}{2}\frac{d}{dt}\|\phi\|^2 = \langle w, \phi\rangle - \eta\|\nabla\phi\|^2,\\
&\frac{\hat{\phi}}{4}\frac{d}{dt}\|\alpha\|^2 = \langle w, \phi^3\rangle - \frac{3\eta}{4}\|\nabla\alpha\|^2.
\end{aligned} \tag{4.19}$$

By repeated use of the Cauchy-Schwarz and Sobolev inequalities (see Appendix B.3) we find

$$\begin{aligned}\langle w, \phi^3 \rangle &\leq (\int_V w^2\, dV)^{\frac{1}{2}} (\int_V \alpha^3\, dV)^{\frac{1}{2}} \\ &\leq (\int_V w^2\, dV)^{\frac{1}{2}} (\int_V \alpha^2\, dV)^{\frac{1}{4}} (\int_V \alpha^4\, dV)^{\frac{1}{4}} \\ &\leq (\int_V w^2\, dV)^{\frac{1}{2}} (\int_V \alpha^2\, dV)^{\frac{1}{4}} (\int_V |\nabla\alpha|^2\, dV)^{\frac{1}{2}}. \end{aligned} \tag{4.20}$$

After introducing coupling parameters $\lambda_1, \lambda_2, \lambda_3 > 0$ we define

$$\begin{aligned} E(t) &= \frac{1}{2}\|\theta\|^2 + \frac{\lambda_1\hat{\phi}}{2}\|\phi\|^2 + \frac{\lambda_2\hat{\phi}}{4}\|\alpha\|^2, \\ \mathcal{D} &= \|\nabla\theta\|^2 + \eta\lambda_1\|\nabla\phi\|^2 + \frac{3\eta}{4}\lambda_2\|\nabla\alpha\|^2 + \lambda_3\|\mathbf{u}\|^2, \\ \mathcal{I} &= R\langle F_1 w, \theta\rangle + R\langle F_2\phi, \theta\rangle + \gamma_2 R\langle\alpha, \theta\rangle + \lambda_1\langle w, \phi\rangle + \lambda_3 R\langle\theta, w\rangle. \end{aligned}$$

From (4.19) and (4.20), using the Poincaré inequality we derive that

$$\begin{aligned}\frac{dE}{dt} &\leq \mathcal{I} - \mathcal{D} + m\mathcal{D}^{\frac{1}{2}}E^{\frac{1}{4}}\mathcal{D}^{\frac{1}{2}} \\ &\leq -\mathcal{D}(\hat{a} - mE^{\frac{1}{4}}),\end{aligned}$$

where m is some positive constant and $\hat{a} = 1 - 1/R_E$ where $1/R_E = \max_{\mathcal{H}}(\mathcal{I}/\mathcal{D})$. If $R_E > 1$ then by the Poincaré inequality, $\mathcal{D} \geq cE$ for some positive constant c. Hence it follows that

$$\frac{dE}{dt} \leq -cE(\hat{a} - mE^{\frac{1}{4}}). \tag{4.21}$$

We will show that (4.21) ensures nonlinear stability as long as

$$(a) \quad R_E > 1, \qquad (b) \quad E^{\frac{1}{4}}(0) < \frac{\hat{a}}{m}. \tag{4.22}$$

For (4.22)(b) to hold there are two possibilities which are that

$$E^{\frac{1}{4}}(t) < \frac{\hat{a}}{m}, \quad t \geq 0, \tag{4.23}$$

or there exists an $\zeta > 0$ such that $E^{\frac{1}{4}}(\zeta) = \hat{a}/m$, and $E^{\frac{1}{4}}(t) < \hat{a}/m$, for any $t \in [0, \zeta)$. Therefore, from (4.21) it follows that $dE/dt \leq 0$ for $t \in [0, \zeta)$, hence, $E^{\frac{1}{4}}(t) \leq E^{\frac{1}{4}}(0) < \hat{a}/m$ for any $t \in [0, \zeta)$. As $E(t)$ is a continuous function of t on $[0, \zeta]$ then it is impossible that $E^{\frac{1}{4}}(\zeta) = \hat{a}/m$. This contradiction implies (4.23)

and consequently $dE/dt \leq 0$ for $t \geq 0$ such that $E^{\frac{1}{4}}(t) \leq E^{\frac{1}{4}}(0)$. Letting $k = \hat{a} - mE^{\frac{1}{4}}(0) > 0$ with (4.22)(a) and (4.22)(b) holding

$$\frac{dE}{dt} \leq -cE(\hat{a} - mE^{\frac{1}{4}}(t)) \leq -kcE.$$

Integrating we have

$$E(t) \leq E(0)e^{kct} \quad \to 0 \qquad as \quad t \to \infty,$$

which shows the decay of θ and ϕ. To show the decay of $\mathbf{u}$ we define some positive constant α and use $(4.16)_1$ and the Poincaré inequality such that

$$\|\mathbf{u}\|^2 \leq \frac{R}{2\alpha}\|\mathbf{u}\|^2 + \frac{R\alpha}{2}\|\theta\|^2.$$

Hence letting $\alpha = R$

$$\|\mathbf{u}\|^2 \leq 2R^2E \leq 2R^2E(0) \quad \to 0 \qquad as \quad t \to \infty,$$

where the decay of $\mathbf{u}$ clearly follows.

The Euler Lagrange equations (see Section 2.3 for an explicit example of the derivation of Euler Lagrange equations) for the maximisation problem $1/R_E = \max_{\mathcal{H}}(\mathcal{I}/\mathcal{D})$ (with the threshold case when $R_E = 1$) are found to be

$$\begin{aligned}
&RF_1\theta + \lambda_1\phi + \lambda_3 R\theta - 2\lambda_3 u_i = \omega_{,i},\\
&RF_1 w + RF_2\phi + \gamma_2 R\alpha + \lambda_3 Rw + 2\triangle\theta = 0,\\
&RF_2\theta + \lambda_1 w + 2\eta\lambda_1\triangle\phi = 0,\\
&\gamma_2 R\theta + \frac{3\eta\lambda_2}{2}\triangle\alpha = 0.
\end{aligned} \tag{4.24}$$

As we need to include the constraint $u_{i,i} = 0$ we have introduced the Lagrange multiplier ω, where $\int_V \omega u_{i,i}\, dV = 0$, so that

$$\frac{d}{dx_i}\left(\frac{\partial}{\partial u_{i,i}}(\omega u_{i,i})\right) = \omega_{,i}.$$

As λ_2 only appears in the $\mathcal{D}$ term in the maximisation problem, we set it equal to 1 so that we can assess solutions over the maximisation of λ_1 and λ_3 only.

We now take the third component of the double *curl* of $(4.24)_1$ (to remove the Lagrange multiplier), and introduce the normal mode representations and notation

as presented in Section 4.2, with $\alpha = \alpha(z)f(x,y)$. The system (4.24) then becomes

$$\begin{aligned}
&(D^2 - a^2)W + \frac{R(F_1 + \lambda_3)a^2}{2\lambda_3}S + \frac{a^2\lambda_1}{2\lambda_3}\Phi = 0,\\
&(D^2 - a^2)S + \frac{R(F_1 + \lambda_3)}{2}W + \frac{RF_2}{2}\Phi + \frac{\gamma_2 R}{2}\alpha = 0,\\
&(D^2 - a^2)\Phi + \frac{RF_2}{2\eta\lambda_1}S + \frac{1}{2\eta}W = 0,\\
&(D^2 - a^2)\alpha + \frac{2\gamma_2 R}{3\eta\lambda_2}S = 0,
\end{aligned} \tag{4.25}$$

where the boundary conditions are

$$W = S = \Phi = \alpha = 0 \qquad z = 0, 1. \tag{4.26}$$

System (4.25) was solved using the compound matrix method (see Appendix A.1) in an analogous manner to previous chapters, where there is maximisation over the coupling parameters λ_1, λ_3 to find

$$Ra_E = \max_{\lambda_1,\lambda_3} \min_{a^2} R^2(a^2, \lambda_1, \lambda_2),$$

where for all $R^2 < Ra_E$ we have stability.

The compound matrix equations (i.e. the differentials of each of the minors of the solution matrix) which had to be calculated before any numerical analysis was attempted, were found to be highly time consuming. An automated program had to be written to evaluate all 256 of them, which was deemed to be excessive, resulting in the alternative approach in Chapters 7 and 8.

Table 4.2 displays the critical values (R_L, R_E, a_E^2) where the linear and nonlinear results correspond to the subscripts L and E respectively. The results are given for η fixed at 0.01, $\gamma_1 = 1$, 5, 10 and $\gamma_2 = 0.1$, 1.

From Table 4.2 we can see acceptable agreement when γ_1 is the dominant term. There is, however, the development of a large region of potential subcritical instabilities when γ_1 and γ_2 are equal.

4.4 Unconditional Nonlinear Stability Analysis

Conditional nonlinear stability analysis is inherently restricted due to the bounding of initial data, where in this body of work $E^{\frac{1}{4}}(0) < \hat{a}/m$ (see (4.22) in Section 4.3),

γ_1	γ_2	H	Ra_E	Ra_L	a_E^2
1	0.1	+1	4.8512	5.2442	4.8359
5	0.1	+1	1.2244	1.2482	4.9196
10	0.1	+1	0.6329	0.6392	4.9317
1	1	+1	0.4106	3.0463	7.2806
1	0.1	−1	6.1515	6.8650	4.1592
5	0.1	−1	1.2954	1.3226	4.7758
10	0.1	−1	0.6514	0.6582	4.8594
1	1	−1	0.4191	3.5305	7.7454

Table 4.2: Comparison of the nonlinear and linear critical Rayleigh numbers Ra_E and Ra_L

where $\hat{a} = 1 - 1/R_E$. Clearly as $R_E \to 1$, $\hat{a} \to 0$ which restricts all initial data by 0. The motivation in introducing a second model for fluid flow in Section 4.1 was to provide the opportunity of a full unconditional analysis, leading to a less restricted and more mathematically pleasing assessment of the suitability of linear theory to predict the onset of convective motion.

When the fluid velocity becomes larger, a Forchheimer system is thought to be appropriate for porous flow. Hence, its use in an energy analysis, which does deal with nonlinear terms, is justified.

The system we now consider is $(4.10)_2$, $(4.10)_4$, and $(4.10)_5$. To show that a standard energy technique in $L^2(V)$ can not be used we follow an analogous argument to Section 4.3, choosing

$$\mathcal{I} = R\langle\theta, w\rangle + R\langle F_1 w, \theta\rangle + R\langle F_2\phi, \theta\rangle + \gamma_2 R\langle\phi^2, \theta\rangle + \langle w, \phi\rangle,$$
$$\mathcal{D} = \|\mathbf{u}\|^2 + \|\nabla\theta\|^2 + \eta\|\nabla\phi\|^2 + b\int_V |\mathbf{u}|^3\, dV + c\int_V |\mathbf{u}|^4\, dV,$$

for the maximisation problem $\max_{\mathcal{H}}(\mathcal{I}/\mathcal{D})$, where $\mathcal{H}$ is the space of admissible functions. As $\mathcal{H}$ is linear we can write u_i, θ, and ϕ as αu_i, $\beta\theta$, and $\delta\phi$ respectively for arbitrary real numbers α, β, δ. We fix u_i, θ, and ϕ and let $\beta = \delta = \alpha^{\frac{3}{2}}$, which yields

$$\frac{\mathcal{I}}{\mathcal{D}} = \alpha^{\frac{1}{2}}\left[\frac{A_1\alpha^{-2} + A_2\alpha^{-\frac{3}{2}} + A_3 + A_4\alpha^{-2}}{A_5\alpha^{-2} + A_6\alpha^{-1} + A_7\alpha^{-1} + A_8\alpha^{-1} + A_9}\right] \to \infty \quad as \quad \alpha \to \infty,$$

as $A_1, \ldots, A_9$ are treated as constants. Hence the maximum of $\mathcal{I}/\mathcal{D}$ in $\mathcal{H}$ can not be achieved, so any standard approach to derive global nonlinear stability using $L^2(V)$ will not succeed.

In order to establish unconditional results we introduce norms of higher order. Let $\|\cdot\|_p$ denote the norm on $L^p(V)$ where $p > 2$. Using $(4.10)_5$, the fact that the derivative of $sign\,\phi$ is a Dirac delta function, and using the properties of the delta function we derive that

$$\begin{aligned}
\frac{d}{dt}\frac{\hat{\phi}}{3}\|\phi\|_3^3 &= \frac{d}{dt}\frac{\hat{\phi}}{3}\int_V \phi^3(sign\,\phi)\,dV \\
&= \int_V w\phi^2(sign\,\phi)\,dV + \eta\int_V \triangle\phi\phi^2(sign\,\phi)\,dV \\
&= \int_V w\phi^2(sign\,\phi)\,dV - 2\eta\int_V |\phi|(\phi_{,i})^2\,dV \\
&= \int_V w\phi^2(sign\,\phi)\,dV - \frac{8\eta}{9}\int_V |\phi|_{,i}^{\frac{3}{2}}|\phi|_{,i}^{\frac{3}{2}}\,dV.
\end{aligned}$$

Using both the Poincaré and Young inequalities we find

$$\frac{d}{dt}\frac{\hat{\phi}}{3}\|\phi\|_3^3 \leq \left(\frac{2}{3\beta} - \frac{8\pi^2\eta}{9}\right)\int_V |\phi|^3\,dV + \frac{\beta^2}{3}\int_V |\mathbf{u}|^3\,dV, \tag{4.27}$$

for some positive constant β.

Again using $(4.10)_5$ we derive an identity for L^4 such that

$$\frac{d}{dt}\frac{\hat{\phi}}{4}\|\phi\|_4^4 \leq \frac{3}{4}(\zeta - \pi^2\eta)\int_V |\phi|^4\,dV + \frac{1}{4\zeta^3}\int_V |\mathbf{u}|^4\,dV, \tag{4.28}$$

for some positive constant ζ.

We now define an *energy* $E(t)$ by

$$E(t) = \frac{\lambda_1}{2}\|\theta\|^2 + \frac{\lambda_2\hat{\phi}}{2}\|\phi\|^2 + \frac{\lambda_3\hat{\phi}}{3}\|\phi\|_3^3 + \frac{\lambda_4\hat{\phi}}{4}\|\phi\|_4^4, \tag{4.29}$$

for coupling parameters $\lambda_1, \lambda_2, \lambda_3, \lambda_4 > 0$.

Then using our system $(4.10)_2$, $(4.10)_4$, $(4.10)_5$ and (4.27) and (4.28) we derive

that

$$\begin{aligned}\frac{dE}{dt} \leq\ & \lambda_1 R\langle F_1 w, \theta\rangle - \lambda_1\|\nabla\theta\|^2 + \lambda_1 R\langle F_2\phi, \theta\rangle + \gamma_2\lambda_1 R\langle\phi^2, \theta\rangle \\ & +\lambda_2\langle w, \phi\rangle - \eta\lambda_2\|\nabla\phi\|^2 \\ & +\lambda_3\left(\frac{2}{3\beta} - \frac{8\pi^2\eta}{9}\right)\int_V |\phi|^3\, dV + \frac{\lambda_3\beta^2}{3}\int_V |\mathbf{u}|^3\, dV \\ & +\frac{3\lambda_4}{4}(\zeta - \pi^2\eta)\int_V |\phi|^4\, dV + \frac{\lambda_4}{4\zeta^3}\int_V |\mathbf{u}|^4\, dV \\ & -\|\mathbf{u}\|^2 + R\langle\theta, w\rangle - b\int_V |\mathbf{u}|^3\, dV - c\int_V |\mathbf{u}|^4\, dV.\end{aligned}$$

To bound the $\langle\phi^2, \theta\rangle$ term we use Young's inequality to deduce

$$\int_V \phi^2\theta\, dV \leq \frac{1}{2}\int_V \phi^4\, dV + \frac{1}{2}\int_V \theta^2\, dV.$$

Let

$$\begin{aligned}\mathcal{I} &= \lambda_1 R\langle F_1 w, \theta\rangle + \lambda_1 R\langle F_2\phi, \theta\rangle + \frac{\gamma_2\lambda_1 R}{2}\|\theta\|^2 + \lambda_2\langle w, \phi\rangle + R\langle\theta, w\rangle, \\ \mathcal{D} &= \lambda_1\|\nabla\theta\|^2 + \eta\lambda_2\|\nabla\phi\|^2 + \|\mathbf{u}\|^2,\end{aligned}$$

and define $1/R_E = \max_{\mathcal{H}}(\mathcal{I}/\mathcal{D})$. Then

$$\begin{aligned}\frac{dE}{dt} \leq -\left(\frac{R_E - 1}{R_E}\right)\mathcal{D} \ &+ \int_V |\mathbf{u}|^3\left(\frac{\lambda_3\beta^2}{3} - b\right) dV \\ &+ \int_V |\phi|^3\left(\lambda_3\left(\frac{2}{3\beta} - \frac{8\pi^2\eta}{9}\right)\right) dV \\ &+ \int_V |\mathbf{u}|^4\left(\frac{\lambda_4}{4\zeta^3} - c\right) dV \\ &+ \int_V |\phi|^4\left(\frac{\lambda_4 3}{4}(\zeta - \pi^2\eta) + \frac{\gamma_2\lambda_1 R}{2}\right) dV.\end{aligned}$$

We choose $\lambda_3 = k_3\epsilon_3$ and $\lambda_4 = \lambda_4' + k_4\epsilon_4$, where ϵ_3, ϵ_4 are arbitrarily small and λ_4' is free to select. We set

$$\frac{3\lambda_4'}{4}(\zeta - \pi^2\eta) + \frac{\gamma_2\lambda_1 R}{2} = 0,$$

so that $\lambda_4' = (2\gamma_2 R\lambda_1)/3(\pi^2\eta - \zeta)$. Minimising $\lambda_4'/4\zeta^3$ with respect to ζ leads to

$$\zeta = \frac{3\pi^2\eta}{4}, \qquad \lambda_4' = \frac{8\gamma_2 R\lambda_1}{3\pi^2\eta}.$$

We now choose $k_3 = 9\beta/(\eta 8\pi^2\beta - 6)$, $k_4 = 16/3\pi^2\eta$ and minimise $\beta^2\lambda_3/3$ with respect to β. This yields the selection

$$\beta = \frac{9}{8\pi^2\eta}, \qquad k_3 = \frac{27}{8\pi^2\eta}.$$

Hence we have

$$\frac{dE}{dt} \leq -\left(\frac{R_E-1}{R_E}\right)\mathcal{D} - \bar{b}\int_V |\mathbf{u}|^3\,dV - \epsilon_3\int_V |\phi|^3\,dV - \bar{c}\int_V |\mathbf{u}|^4\,dV - \epsilon_4\int_V |\phi|^4\,dV. \tag{4.30}$$

where

$$\bar{b} = b - \left(\frac{9}{8\pi^2\eta}\right)^3\epsilon_3, \qquad \bar{c} = c - \frac{128\gamma_2 R\lambda_1}{81\pi^8\eta^4} - \frac{256}{81\pi^8\eta^4}\epsilon_4.$$

Since ϵ_3 and ϵ_4 can be taken to be arbitrarily small, we can ensure the positivity of $\bar{b}$ and $\bar{c}$ by setting

$$b > 0, \qquad c > \frac{128\gamma_2 R\lambda_1}{81\pi^8\eta^4}. \tag{4.31}$$

Thus, letting $\hat{a} = (R_E - 1)/R_E$ and supposing (4.31) is satisfied, then for $R_E > 1$

$$\begin{aligned}\frac{dE}{dt} &\leq -\hat{a}\mathcal{D} - \epsilon_3\int_V |\phi|^3\,dV - \epsilon_4\int_V |\phi|^4\,dV,\\ &\leq -kE,\end{aligned}$$

where

$$k = \min\left\{2\hat{a}\pi^2,\ 2\hat{a}\eta\pi^2,\ \frac{3\epsilon_3}{\lambda_3\hat{\phi}},\ \frac{4\epsilon_4}{\lambda_4\hat{\phi}}\right\}.$$

After integrating we have $E(t) \leq E(0)e^{-kt} \to 0$ as $t \to \infty$ where the decay of θ and ϕ is shown.

However, to have global nonlinear energy stability we need to show the convergence of $\|\mathbf{u}\|^2$, $\|\mathbf{u}\|_3^3$, and $\|\mathbf{u}\|_4^4$. Using $(4.10)_2$ we have

$$\begin{aligned}\|\mathbf{u}\|^2 + b\|\mathbf{u}\|_3^3 + c\|\mathbf{u}\|_4^4 &= R\langle\theta, w\rangle\\ &\leq \frac{R\alpha}{2}\|\theta\|^2 + \frac{R}{2\alpha}\|\mathbf{u}\|^2.\end{aligned}$$

Letting $\alpha = R$

$$\frac{1}{2}\|\mathbf{u}\|^2 + b\|\mathbf{u}\|_3^3 + c\|\mathbf{u}\|_4^4 \leq \frac{R^2}{\lambda_1}E \to 0 \quad as \quad t \to \infty,$$

where the decay of $\mathbf{u}$ clearly follows.

The Euler Lagrange equations (see Section 2.3 for an explicit example of the derivation of Euler Lagrange equations) for the maximisation problem $1/R_E = \max_{\mathcal{H}}(\mathcal{I}/\mathcal{D})$ (with the threshold case when $R_E = 1$) are found to be

$$\begin{aligned}&\lambda_1 RF_1\theta + \lambda_2\phi + R\theta - 2u_i = \omega_{,i},\\ &\lambda_1 RF_1 W + \lambda_1 RF_2\theta + \gamma_2\lambda_1 R\theta + RW + 2\lambda_1\triangle\theta = 0,\\ &\lambda_1 RF_2\theta + \lambda_2 w + 2\eta\lambda_2\triangle\phi = 0,\end{aligned} \tag{4.32}$$

where ω is the Lagrange multiplier. Taking the third component of the double *curl* of $(4.32)_1$, and introducing the normal mode representations and notation as presented in Section 4.2, system (4.32) then becomes

$$\begin{aligned}
&(D^2 - a^2)W + \frac{R(F_1\lambda_1 + 1)a^2}{2}S + \frac{a^2\lambda_2}{2}\Phi = 0,\\
&(D^2 - a^2)S + \frac{R(F_1\lambda_1 + 1)}{2\lambda_1}W + \frac{RF_2}{2}\Phi + \frac{\gamma_2 R}{2}S = 0,\\
&(D^2 - a^2)\Phi + \frac{\lambda_1 RF_2}{2\eta\lambda_2}S + \frac{1}{2\eta}W = 0,
\end{aligned} \tag{4.33}$$

where the boundary conditions are

$$W = S = \Phi = 0 \qquad z = 0, 1.$$

System (4.33) was solved in an entirely analogous fashion to (4.12) in Section 4.2 using the compound matrix method, with identical initial and final conditions, but also maximising over the coupling parameters λ_1, λ_2.

Table 4.3 displays the critical values (R_L, R_E, a_E^2) where the linear and nonlinear results correspond to the subscripts L and E respectively. The results are for η fixed at 0.01, $\gamma_1 = 1$, 5, 10, and $\gamma_2 = 0.1$, 5, 10.

Table 4.3 shows a similar pattern of results to the conditional analysis in Section 4.3, such that there is excellent agreement between the linear and nonlinear thresholds when γ_1 is the dominant term, but the closeness of the agreement collapses the magnitude of γ_2 becomes similar or greater to γ_1.

Clearly from Table 4.3 we can see that the linear results fail to emulate the nonlinear ones when $\gamma_2 > \gamma_1$, so we turn our attention to the case when the value of γ_2 approaches and then exceeds that of γ_1, to assess the behaviour of both the linear and nonlinear Rayleigh numbers. Figure 4.3 provides a visual representation of the formation of these potential subcritical regions, (i.e. when the agreement between the linear and nonlinear theory is not with an acceptable range), where γ_1 is fixed at 0.1 and 10 and γ_2 varies between 1 and 10.

Figure 4.3 shows that when $\gamma_1 = 10$ the linear and nonlinear thresholds show excellent agreement for $\gamma_2 = 1$ to 10, although the region of potential subcritical instabilities does increase as γ_2 approaches the same magnitude as γ_1. In contrast

γ_1	γ_2	H	Ra_E	Ra_L	a_E^2
1	0.1	+1	5.2040	5.2442	5.2380
5	0.1	+1	1.2435	1.2482	5.006
10	0.1	+1	0.6375	0.6392	4.9732
1	1	+1	2.8601	3.0463	4.9755
0.1	1	+1	4.7797	5.2283	5.0753
0.1	5	+1	1.0118	1.2430	4.5673
0.1	10	+1	0.4767	0.6364	4.3198
1	0.1	-1	6.8019	6.8650	4.5783
5	0.1	-1	1.3174	1.3226	4.8633
10	0.1	-1	0.6564	0.6582	4.9018
1	1	-1	3.2916	3.5305	4.6247
0.1	1	-1	6.1218	6.8332	4.4609
0.1	5	-1	1.0627	1.3165	4.4400
0.1	10	-1	0.4879	0.6552	4.2591

Table 4.3: Comparison of the nonlinear and linear critical Rayleigh numbers Ra_E and Ra_L

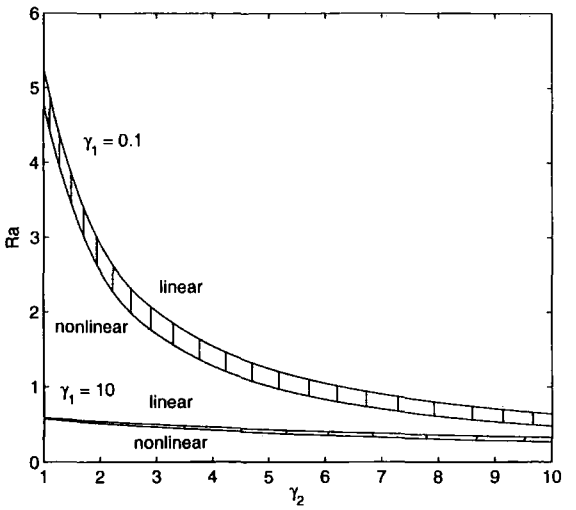

Figure 4.3: Linear and nonlinear critical Rayleigh numbers R_a plotted against γ_2 for γ_1 fixed at 0.1 and 10. The regions of potential subcritical instabilities are the shaded areas on the graph

when $\gamma_1 = 0.1$ and γ_2 again ranges from 1 to 10, the region of potential subcritical instabilities is significant.

4.5 Conclusions

Both the Darcy and Forchheimer equations are used to analytically and numerically study convection induced by the selective absorption of radiation, where the internal heat source is modelled quadratically with respect to concentration, which is an adaption from the models used in Chapters 2 and 3.

The linear results are identical for both models, and are based around the unknown parameters γ_1 and γ_2, as presented in Figures 4.1 and 4.2. It is observed that an increase in either γ_1 or γ_2 causes the Rayleigh number to decrease. More interestingly though is the observation that γ_1 and γ_2 have an almost identical effect on the Rayleigh number in relation to each other. This demonstrates that a variation change in γ_2 will be as equally significant to a change in the Rayleigh number as a variational change to γ_1.

Tables 4.2 and 4.3 present the conditional and unconditional nonlinear stability

and corresponding linear instability results for various γ_1 and γ_2. Both the conditional and unconditional nonlinear analyses show that when γ_1 is the dominant term over γ_2 the thresholds of the linear and nonlinear theory are close, so that potential region of subcritical instabilities is small, implying that the linear theory approximately captures the onset of convective motion.

In contrast, as the magnitude of γ_2 exceeds that of γ_1 and beyond, the potential region of subcritical instabilities increases greatly, for a given accuracy. These results indicate that linear theory may fail to accurately capture the physics of the onset of convection.

Chapter 5

Double-diffusive convection in a porous medium with a concentration based internal heat source

An interesting and significant aspect of the Krishnamurti model, unexamined in Chapters 2 to 4, is the effect of the concentration of the thymol blue on the density of the model. Each of these bodies of work define the state equation to be linear in temperature, with the effect of concentration on density assumed negligible. This chapter explores the use of a double-diffusive convection model in a porous medium, with fixed boundary conditions employed throughout.

Research exploring double-diffusive convection in a fluid-saturated porous layer has been an active area for many years, making this particular chapter considerably relevant to the wider literature. These phenomena of combined heat and mass transfer appear in numerous physical problems such as contaminant transport in saturated soil, food processing, underground disposal of nuclear wastes, and the spreading of pollutants. Comprehensive reviews of the literature concerning double-diffusive natural convection in a fluid-saturated porous medium can be found in the review article by Trevisan & Bejan [95], in the book by Nield & Bejan [77], and in Chapter 14 of the book by Straughan [90]. Recent novel contributions include

Mamou *et al.* [61] for a vertical porous enclosure, Mahidjiba *et al.* [62] for mixed boundary conditions, and Guo & Kaloni [33] with the introduction of the Brinkman effect.

In addition to establishing a linear theory for the double-diffusive convection model, we develop a complementary energy theory. The energy method has been employed with much success in double-diffusive flows, with examples including Carr [11], Guo & Kaloni [33] and Mulone & Rionero [75].

The linear and nonlinear results are derived using Chebyshev tau and compound matrix numerical techniques (see Appendices A.2 and A.1). Similarly to Chapter 3, the Chebyshev tau technique was found to be restrictive due to the heavy computational cost in solving full matrix eigenvalue problems required over several parameter ranges.

The results in this chapter were published in the article Hill [40].

5.1 Governing Equations

Let us consider a fluid saturated porous layer occupying the three dimensional layer $\{(x,y) \in \mathbb{R}^2\} \times \{z \in (0,d_z)\}$, where $Oxyz$ is a cartesian frame of reference with unit vectors $\mathbf{i}$, $\mathbf{j}$, $\mathbf{k}$ respectively. Adopting the same boundaries as in Chapter 2 the upper and lower planes are held fixed at temperatures T_U and T_L, and concentrations 0 and c_L respectively.

We assume the Oberbeck-Boussinesq approximation is valid and that Darcy's law governs the fluid motion in the porous layer. If the layer is parallel to the plane $z = 0$ we have the governing equation

$$\frac{\mu}{k} v_i = -p_{,i} - b_i g \rho(T,c),$$

where v_i, p, are velocity, and pressure, $\mathbf{b} = (0,0,1)$, g is the acceleration due to gravity, μ is the dynamic viscosity of the fluid, and k is the permeability of the porous medium. Denoting T to be the temperature and c to be the concentration of the dissolved species (e.g. the conjugated form of the thymol blue in Krishnamurti [55]), the density $\rho(T,c)$ is given by

$$\rho(T,c) = \rho_0(1 - \alpha(T - T_0) + \alpha_c(c - c_0)),$$

where ρ_0, T_0, and c_0 are reference values of density, temperature and concentration respectively, and α and α_c are the coefficients for thermal and solutal expansion.

In addition to Darcy's law, the governing equations consist of the equations of conservation of energy and mass. The internal heat source is modelled linearly with respect to concentration, which is represented by the introduction of the βc term in the heat equation, where β is some constant of proportionality. Combining these equations with Darcy's law the governing system of equations is as follows:

$$\begin{aligned}
&\frac{\mu}{k}v_i = -p_{,i} - b_i g\rho_0(1 - \alpha(T - T_0) + \alpha_c(c - c_0)),\\
&v_{i,i} = 0,\\
&\frac{1}{M}T_{,t} + v_i T_{,i} = \kappa\triangle T + \beta c,\\
&\epsilon c_{,t} + v_i c_{,i} = \kappa_c \triangle c,
\end{aligned} \tag{5.1}$$

where κ_c and κ_m are the solute and thermal diffusivities respectively, ϵ is the porosity, with

$$(\rho_0 h)_m = (1 - \epsilon)(\rho_0 h)_s + \epsilon(\rho_0 h_p)_f$$

where h_p is the specific heat of the fluid, and h is the specific heat of the solid, with the subscripts f, s, and m referring to the fluid, solid and porous components of the medium respectively. The remaining terms of system (5.1) are defined as $\kappa = \kappa_m/(\rho_0 h_p)_f$ and $M = (\rho_0 h_p)_f/(\rho_0 h)_m$.

Let us now consider the basic steady state solution $(\overline{v}_i, \overline{p}, \overline{T}, \overline{c})$ of (5.1), where, as there is no fluid flow, $\overline{v}_i = 0$. Utilising the boundary conditions, equations $(5.1)_3$ and $(5.1)_4$ show that

$$\begin{aligned}
\overline{T}(z) &= T_L + z\left(-\frac{H\delta T}{d_z} + \frac{\tau d_z}{3}\right) - \frac{\tau z^2}{2} + \frac{\tau z^3}{6d_z},\\
\overline{c}(z) &= \frac{c_L}{d_z}(d_z - z),
\end{aligned}$$

where $H = sign(T_L - T_U)$, $\delta T = |T_L - T_U|$, and $\tau = \beta c_L/\kappa$. A derivation of the hydrostatic pressure $\overline{p}$ may be found from $(5.1)_1$, but is not included as it is eliminated in subsequent analyses. A crucial aspect in the interpretation of the physical system is the value H, which refers to heating from below ($H = +1$) and above ($H = -1$) respectively. The more interesting case is when we heat from below

as this leads to two competing factors, namely the stabilising effect of the species and the destabilising effect of the heating, which is a highly researched phenomena (e.g. see Mulone [74]; Lombardo *et al.* [59]).

To assess the stability of the steady solution a perturbation $(u_i,\ \theta,\ \pi,\ \phi)$ is introduced to this steady state, such that

$$v_i = \overline{v}_i + u_i, \qquad p = \overline{p} + \pi, \qquad T = \overline{T} + \theta, \qquad c = \overline{c} + \phi,$$

with a non-dimensionalisation with scalings of

$$u_i = \frac{\kappa}{d_z} u_i^*, \quad \pi_i = \frac{\mu\kappa}{k}\pi_i^*, \quad \theta = \sqrt{\frac{\mu\kappa(\delta T)}{g\alpha d_z k\rho_0}}\theta^*, \quad \phi = c_L\phi^*, \quad x_i = d_z x_i^*,$$

$$t = \frac{d_z^2}{M\kappa}t^*, \quad \eta = \frac{\kappa_c}{\kappa}, \quad R = \sqrt{\frac{g\alpha d_z k\rho_0(\delta T)}{\mu\kappa}}, \quad R_c = \frac{g\alpha_c c_L d_z k\rho_0}{\mu\kappa}$$

where $R_a = R^2$ and R_c are the thermal and solute Rayleigh numbers respectively.

Dropping all the stars, the governing equations from system (5.1) for the non-dimensionalised quantities now take the following form:

$$\begin{aligned} u_i &= -\pi_{,i} + b_i R\theta - b_i R_c\phi, \\ u_{i,i} &= 0, \\ \theta_{,t} + u_i\theta_{,i} &= wRF(z) + \triangle\theta + \gamma R\phi, \\ \hat{\phi}\phi_{,t} + u_i\phi_{,i} &= w + \eta\triangle\phi. \end{aligned} \tag{5.2}$$

In these equations, $w = u_3$, $\hat{\phi} = \epsilon M$, and $\gamma = d_z^2\tau/\delta T$. An important feature in subsequent analyses is the non-dimensionalised temperature gradient F which is given by

$$F(z) = H - \gamma/3 + \gamma(z - z^2/2).$$

The boundary conditions for the perturbed quantities are

$$w = 0,\ \theta = 0,\ \phi = 0, \qquad z = 0,\ 1,$$

where $(u_i,\ \theta,\ \phi)$ have a periodic plan-form tiling the (x, y) plane.

5.2 Linear Instability Analysis

To proceed with a linear analysis the nonlinear terms from (5.2) are discarded, and a temporal growth rate like $e^{\sigma t}$ is assumed where $u_i = e^{\sigma t}u_i(\mathbf{x})$, $\theta = e^{\sigma t}\theta(\mathbf{x})$, and $\phi = e^{\sigma t}\phi(\mathbf{x})$. The double *curl* of $(5.2)_1$ is taken to remove the pressure term, where the third component is chosen, and the preceding substitutions to system (5.2) are made. The resulting linearised governing set of equations are

$$\begin{aligned} \triangle w &= R\triangle^*\theta - R_c\triangle^*\phi, \\ \sigma\theta &= RF(z)w + \triangle\theta + \gamma R\phi, \\ \hat{\phi}\sigma\phi &= w + \eta\triangle\phi, \end{aligned} \tag{5.3}$$

where $\triangle^* = \partial^2/\partial x^2 + \partial^2/\partial y^2$.

By using normal mode representations of the form $w = W(z)f(x,y)$, $\theta = S(z)f(x,y)$, and $\phi = \Phi(z)f(x,y)$ where $f(x,y)$ is a horizontal plan-form tiling the plane (x,y) periodically which satisfies $\triangle^* f = -a^2 f$ with wavenumber a^2 (see Christopherson [16]), letting $D^2 = \partial^2/\partial z^2$, (5.3) becomes

$$\begin{aligned} &(D^2 - a^2)W + a^2RS - a^2R_c\Phi = 0, \\ &(D^2 - a^2)S + RWF(z) + \gamma R\Phi = \sigma S, \\ &(D^2 - a^2)\Phi + \frac{1}{\eta}W = \frac{\hat{\phi}\sigma}{\eta}\Phi. \end{aligned} \tag{5.4}$$

The eighth order system (5.4) was solved using the Chebyshev-tau method (see Appendix A.2 and Chapter 1 for references). This technique, however, was found to be restrictive due to the heavy computational cost in solving full matrix eigenvalue problems required over three parameter ranges (namely γ, R_c and a^2). The natural progression was to develop the techniques in Chapters 7 and 8 to overcome these difficulties.

Numerical results are presented for a range of γ values, with R_c varying between 0 and 30. Variations in the η and $\hat{\phi}$ values produce only slight universal shifts in the critical thermal Rayleigh number, so we fix η and $\hat{\phi}$ at 0.01 and 0.2 respectively. Figure 5.1 shows the results for heating from above ($H = -1$) with γ increasing in increments of 1 from 1 to 10, where we expect σ to be real at criticality.

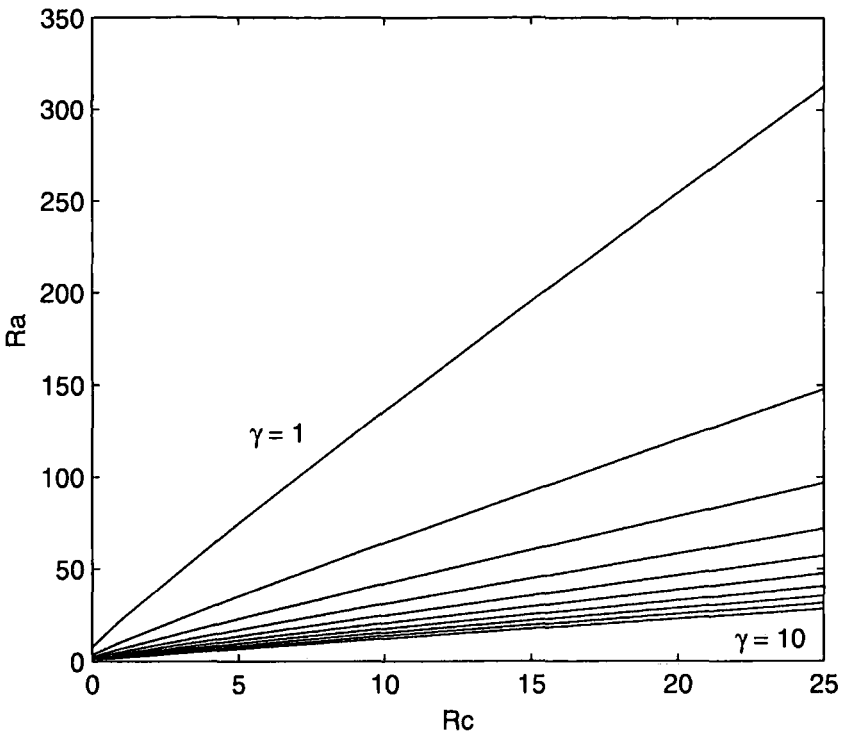

Figure 5.1: Critical thermal Rayleigh number R_a plotted against R_c, with γ increasing in increments of 1 from 1 to 10. These graphs correspond to heating from above ($H = -1$) with η fixed at 0.01.

A linear relationship between R_c and R_a is apparent from Figure 5.1, where, as expected, the spectrum of σ is always found to be real. Positive increments in γ cause a reduction in the critical thermal Rayleigh number, which intuitively makes sense as γ is in essence a measure of the internal heat source, so an increase in γ would cause more instability in the system, allowing the onset of convection to occur early.

When the system is heated from below ($H = +1$) and there is no internal heat source (i.e. $\gamma = 0$) the system can be solved after extensive analysis (see e.g. Straughan [90] pgs 238-247). Figures 5.2 to 5.4 show the results for heating from below ($H = +1$), with the inclusion in each figure of the analytical $\gamma = 0$ criticality values to place these numerical results in context. Figure 5.2 presents results when γ is increased in increments of 10^{-1} from 0.1 to 0.5, with Figure 5.3 showing the results when γ is increased in increments of 10^{-1} from 0.6 to 1.

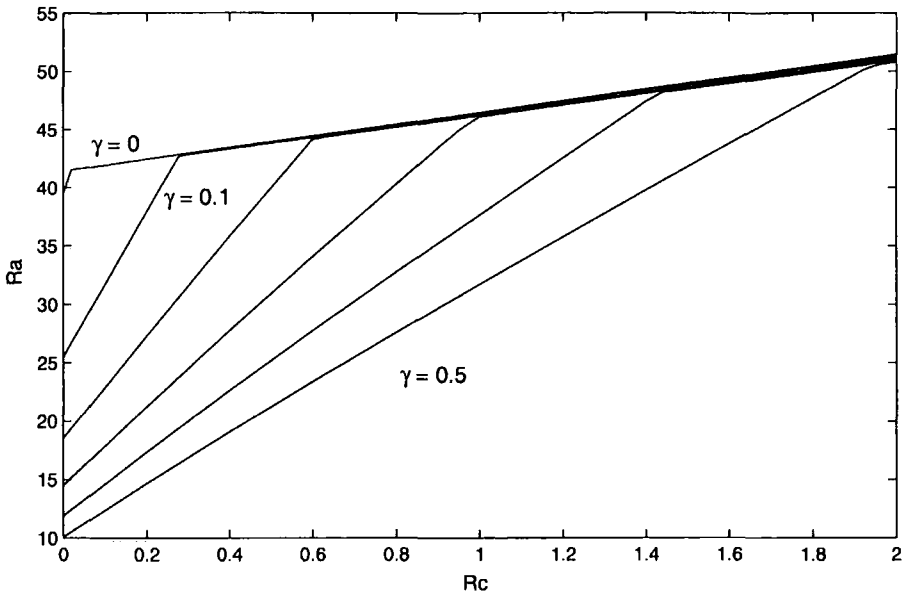

Figure 5.2: Critical thermal Rayleigh number R_a plotted against R_c, with γ varying between 0 and 0.5 in steps of 10^{-1}. These graphs correspond to heating from below ($H = +1$) with η fixed at 0.01.

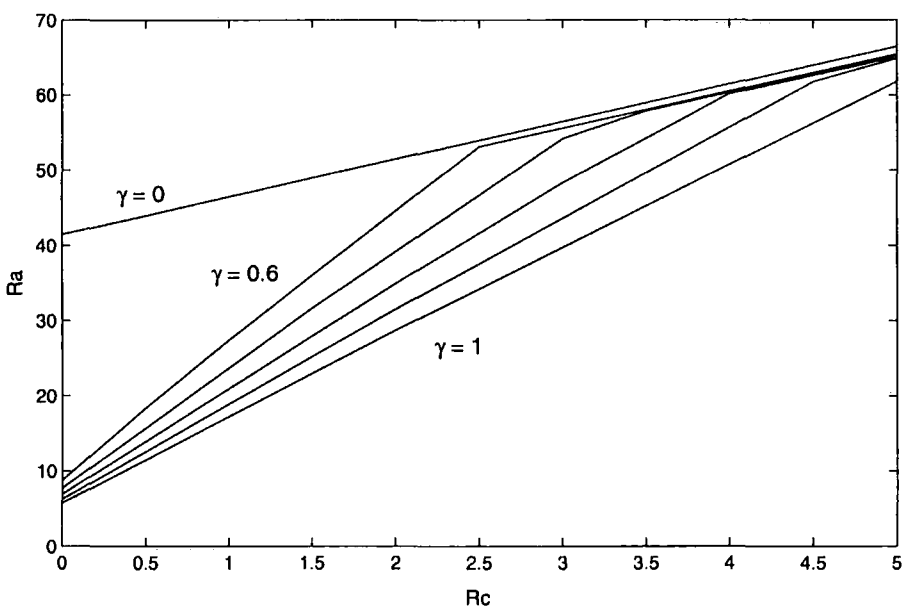

Figure 5.3: Critical thermal Rayleigh number R_a plotted against R_c, with γ including the value 0 and varying between 0.6 and 1 in steps of 10^{-1}. These graphs correspond to heating from below ($H = +1$) with η fixed at 0.01.

In Figures 5.2 and 5.3 the kinks in the graphs represent the point at which convection switches from steady convection ($\sigma = 0$) to oscillatory convection ($Re(\sigma) = 0$, $Im(\sigma) \neq 0$). The onset of both types of convection appear to follow a linear relationship between R_c and R_a. As γ increases the onset of convection is more likely to be via steady convection. It is important to note that small increments in γ appears to cause the magnitude of the steady convection linear relationship to decrease more rapidly than that of oscillatory convection.

To explore this phenomenon further Figure 5.4 shows the extended γ range between 1 and 10. It is possible to extract oscillatory results numerically, so in Figure 5.4 along with the critical thermal Rayleigh number graphs corresponding to $H = +1$, dotted lines are introduced which represent the onset of oscillatory convection for $\gamma = 2$ and 3. The γ terms on the left refer to the critical thermal Rayleigh curves, whilst those on the right refer to the relevant onsets of oscillatory convection.

When $\gamma = 3$ the oscillatory neutral line has a larger gradient than that of the corresponding steady convection line, which implies they do not intersect, i.e. only stationary convection occurs. Using results obtained via the Chebyshev tau method to calculate both steady and oscillatory neutral lines, it is possible to extract a critical value γ_c, above which the lines do not intersect based on their gradients within the calculated R_c range, so that no oscillatory convection should occur. The range in which this critical value was found is $\gamma_c \in [2.2091625, 2.209175]$. The existence of a critical parameter value determining the presence of oscillatory convection is, in the present literature, a new phenomenon.

To further analyse the existence of this critical γ_c term, an analytical truncated series approach is developed.

Corollary 5.2.1 The functions $W(z)$, $S(z)$ and $\Phi(z)$ satisfying system (5.4) belong to the space $\{G(z) \in C[0,1] : G^{(2n)}(0) = G^{(2n)}(1) = 0, n \in \mathbb{N}\}$

Proof: Extending the function $F(z)$ to be even over the interval $[-1, 1]$ leads to the Fourier series expansion

$$F(z) = 1 - \frac{2\gamma}{\pi^2} \sum_{n=1}^{\infty} \frac{cos\ (n\pi z)}{n^2},$$

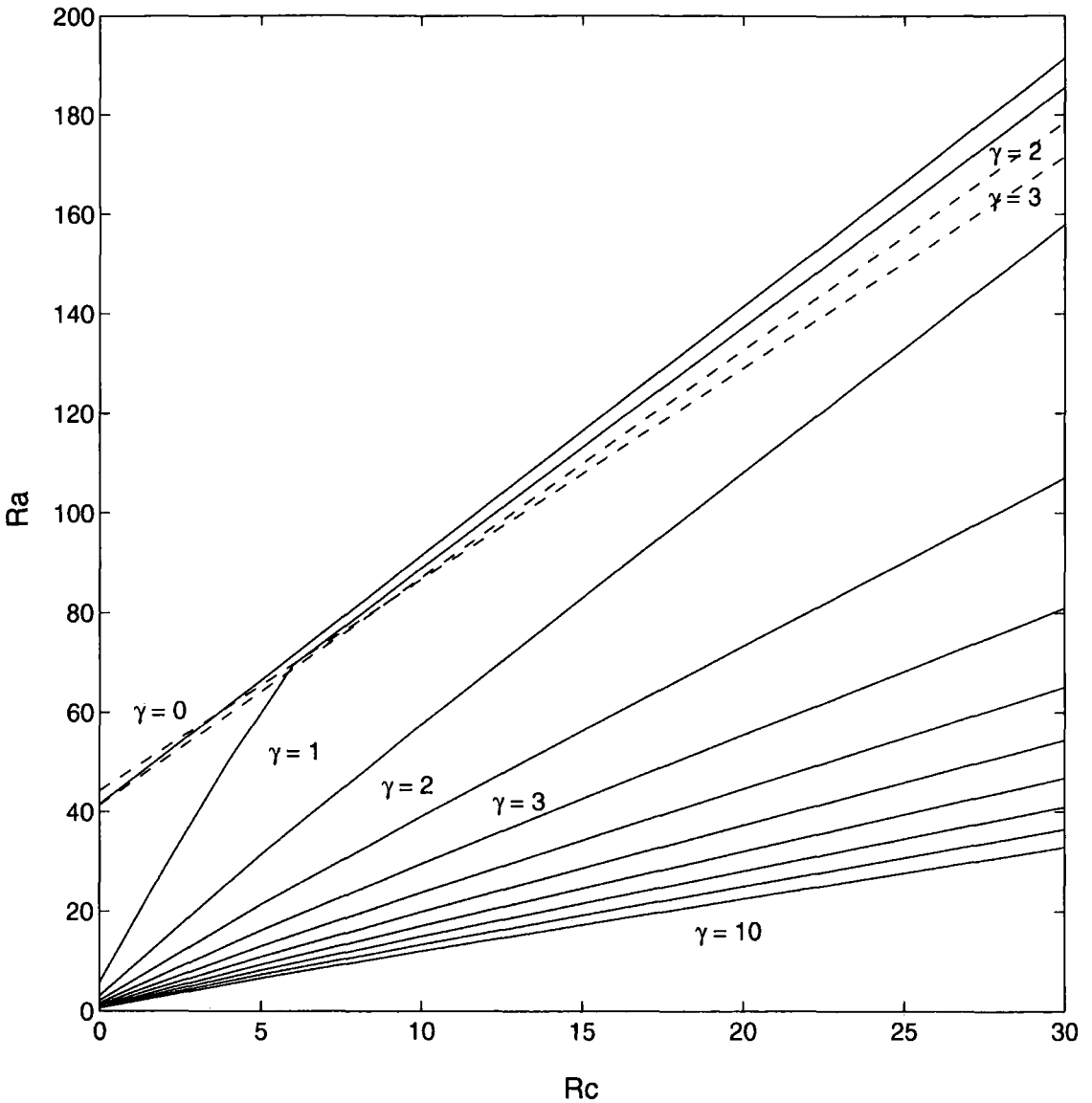

Figure 5.4: Critical thermal Rayleigh number R_a plotted against R_c, with γ including the value 0 and varying between 0 and 10. The graph corresponds to heating from below ($H = +1$) with η fixed at 0.01. The dotted lines represent the extrapolated onset of oscillatory convection for $\gamma = 2$ and 3

such that $F^{(2n+1)}(z) = 0$ for $n \in \mathbb{N}$, $z = 0, 1$.

The proof is by induction. Let the operator $d^{2k}/dz^{2k} - a^2$ be denoted by $L^{(k)}$, for some $k \in \mathbb{N}$, with $L^{(0)}$ being the identity. By definition

$$L^{(0)}W = L^{(1)}W = L^{(0)}S = L^{(1)}S = L^{(0)}\Phi = L^{(1)}\Phi = 0 \quad z = 0, 1,$$

using system (5.4) and the non-dimensionalised boundary conditions. Assume $L^{(p)}W = L^{(p)}S = L^{(p)}\Phi = 0$ for $z = 0,\ 1$ where $p = 0,\ 1,\ 2,\ \ldots,\ n$. To show that it is true for $n+1$ we apply L again and use system (5.4) to give

$$\begin{aligned}
L^{(n+1)}W &= -a^2RL^{(n)}S + a^2R_cL^{(n)}\Phi = 0 \qquad z = 0,\ 1,\\
L^{(n+1)}\Phi &= -\frac{1}{\eta}L^{(n)}W + \frac{\hat{\phi}\sigma}{\eta}L^{(n)}\Phi = 0 \qquad z = 0,\ 1,\\
L^{(n+1)}S &= -\gamma RL^{(n)}\Phi + \sigma L^{(n)}S - RL^{(n)}(F(z)W)
\end{aligned}$$

By assumption $L^{(n)}\Phi = L^{(n)}S = 0$ on $z = 0,\ 1$, and if we let $n = 2m$, using a binomial expansion yields

$$L^{(n)}(FW) = \binom{2m}{0}F^{(2m)}W + \binom{2m}{1}F^{(2m-1)}W^{(1)} + \ldots + \binom{2m}{2m}FW^{(2m)}.$$

By assumption each W term differentiated to an even power from 0 to $2m$ $(=n)$ is 0 for $z = 0,\ 1$. The only remaining terms contain $F(z)$ differentiated to an odd power which, by the definition of the Fourier series, is zero for $z = 0,\ 1$. □

The functions $\sin(p\pi z)$, $p \in \mathbb{N}$, span the space $\{G(z) \in C[0,1] : G^{(2n)}(0) = G^{(2n)}(1) = 0,\ n \in \mathbb{N}\}$ so we may define

$$\begin{aligned}
W(z) &= \sum_{n=1}^{\infty} W_n \sin(n\pi z), \quad S(z) = \sum_{n=1}^{\infty} S_n \sin(n\pi z),\\
\Phi(z) &= \sum_{n=1}^{\infty} \Phi_n \sin(n\pi z),
\end{aligned}$$

for constants W_p, S_p, Φ_p, $p \in \mathbb{N}$. Since $\sin(p\pi z)$, $p \in \mathbb{N}$, form a basis, they can not be written as a linear combination of each other, so after substituting the definitions into $(5.4)_1$ and $(5.4)_3$ we evaluate at $\sin(p\pi z)$, for some $p \in \mathbb{N}$, to find

$$\begin{aligned}
\Lambda_pW_p &= a^2RS_p - a^2R_c\Phi_p,\\
(\eta\Lambda_p + \hat{\phi}\sigma)\Phi_p &= W_p,
\end{aligned} \tag{5.5}$$

where $\Lambda_p = (p\pi)^2 + a^2$.

Applying the substitutions to $(5.4)_2$ with the Fourier expansion of $F(z)$, and making use of some trigonometry identities yields

$$\begin{aligned}
&\sum_{n=1}^{\infty} S_n(\Lambda_n + \sigma)\sin(n\pi z) = \gamma R\sum_{n=1}^{\infty}\Phi_n\sin(n\pi z) + R\sum_{n=1}^{\infty}W_n\sin(n\pi z)\\
&-\frac{R\gamma}{\pi^2}\left(\sum_{n=1}^{\infty}\sum_{m=1}^{\infty}W_n\frac{\sin(m+n)\pi z - \sin(m-n)\pi z}{m^2}\right).
\end{aligned} \tag{5.6}$$

An evaluation at $\sin(p\pi z)$ of (5.6) can now be made. In the double sum term $\sin(p\pi z)$ is produced when $m+n=p$, $m-n=p$, and $m-n=-p$. This yields an infinite sum which must be truncated to extract a usable equation. Truncating the first $p-1$ terms with respect to n in the double sum term, removes the possibility of $m+n=p$. (It is important to note that in subsequent analysis, however, we must take $p=1$). The subsequent infinite sum must again be truncated to extract the Φ_p term to give the following expression:

$$(\Lambda_p+\sigma)S_p = R(1+\frac{\gamma}{4\pi^2p^2})W_p + \gamma R\Phi_p. \tag{5.7}$$

Using (5.5) and (5.7) to eliminate W_p and S_p, and noting that $\Phi_p \neq 0$ for an arbitrarily chosen p, the following identity can be derived:

$$\begin{aligned}\sigma^2(\Lambda_p\hat{\phi}) \;+\; & \sigma\left(\eta\Lambda_p^2 + a^2R_c + \hat{\phi}\Lambda_p^2 - a^2R^2\hat{\phi}(1+\frac{\gamma}{4\pi^2p^2})\right) \\ +\; & \eta\Lambda_p^3 + a^2R_c\Lambda_p - a^2R^2\eta\Lambda_p(1+\frac{\gamma}{4\pi^2p^2}) - \gamma R^2a^2 = 0.\end{aligned} \tag{5.8}$$

We define $\sigma = Re(\sigma) + iIm(\sigma)$, and study the threshold case $Re(\sigma)=0$. To study the onset of oscillatory convection we allow $Im(\sigma)\neq 0$ and take the imaginary part of (5.8), which can be re-written with respect to R^2. It is simple to show that $\partial R^2/\partial p^2 > 0$, so that $p=1$ can be taken. Differentiating with respect to a^2 a global minimum can be found at $a^2=\pi^2$. Hence the analytical form for the oscillatory neutral line yielded by (5.8) is:

$$R^2 = \frac{4\pi^2(\hat{\phi}+\eta)}{\hat{\phi}(1+\frac{\gamma}{4\pi^2})} + \frac{R_c}{\hat{\phi}(1+\frac{\gamma}{4\pi^2})}. \tag{5.9}$$

This is a relatively good approximation to the exact numerical results for smaller γ values and underlines the actual linear behaviour numerically observed between R_c and R_a.

To study the onset of stationary convection we let $Im(\sigma)=0$ and take the real part of (5.8), which can be re-written with respect to R^2. In a similar fashion to the previous derivation it can be shown that $\partial R^2/\partial p^2 > 0$, so that $p=1$ can be taken. Thus, letting $\Lambda=\Lambda_1$, the analytical form for the steady neutral curve is:

$$R^2 = \frac{\eta\Lambda^3}{a^2(\eta\Lambda(1+\frac{\gamma}{4\pi^2})+\gamma)} + \frac{\Lambda R_c}{\eta\Lambda(1+\frac{\gamma}{4\pi^2})+\gamma}. \tag{5.10}$$

Viewing this result geometrically, an a^2 (wavelength number) dependence of the gradient with respect to R_c is observed. Studying $\partial R^2/\partial a^2$ it is possible to show that, for fixed γ, $a^2 \to 0$ as $R_c \to \infty$. The actual numerical results also show an inversely proportional relationship between R_c and a^2. Due to the changing gradient of the steady neutral curve, the critical γ value for which the steady neutral curve's gradient falls below that of the oscillatory neutral curve must be established as $R_c \to \infty$, (which coincides with $a^2 \to 0$). Hence, using the gradients of the oscillatory and steady neutral curves, namely (5.9) and (5.10)

$$\frac{4\pi^2}{\eta(4\pi^2+\gamma)+4\gamma} < \frac{4\pi^2}{\hat{\phi}(4\pi^2+\gamma)} \tag{5.11}$$

is the condition for the existence of only stationary convection. Rearranging (5.11) yields a critical value of $\gamma_c = 1.968739985$. Although all γ values above the numerical γ_c would result in steady convection, the heuristic analysis does therefore imply that this value is not optimal, due to the non-linearity of the stationary neutral curve.

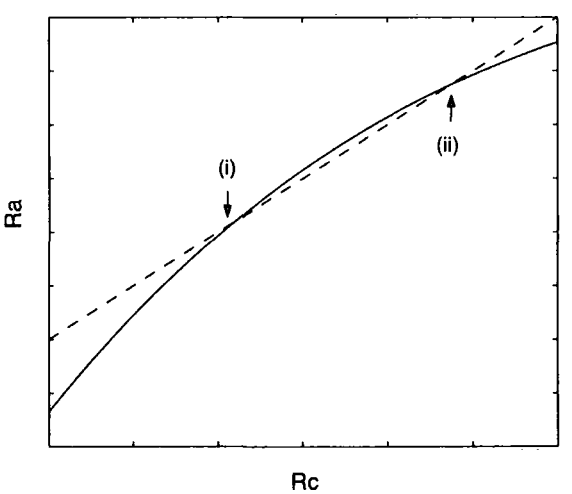

Figure 5.5: Visual representation of a finite oscillatory convection interval, with critical thermal Rayleigh number R_a plotted against R_c. (i) marks the shift from stationary to oscillatory convection; (ii) marks the shift from oscillatory to stationary convection.

If the constantly changing gradient of stationary neutral curve presented by the analysis is actually present in the physical system, this also allows for the possibility

of a range of γ values which have only a finite interval of oscillatory convection. Figure 5.5 is a visual representation of this potential phenomenon, where the steady and oscillatory neutral curves are represented by solid and dashed lines respectively.

To explore the impact of these potential features on the actual physical system a more extensive range of R_c values could be explored numerically, but it must be underlined that in this chapter the actual numerical data and the approximate analysis do strongly indicate the existence of a critical γ_c value, with no oscillatory convection occurring for $\gamma \geq \gamma_c$.

5.3 Nonlinear Stability Analysis

Due to the potential regions of subcritical instabilities, where the onset of convection occurs prior to the thresholds predicted by the linear theory being reached, a nonlinear energy analysis is developed to provide thresholds for global stability.

To obtain global nonlinear stability bounds in the stability measure $L^2(V)$, where V is the period cell for the perturbations, we multiply equations $(5.2)_1$, $(5.2)_3$ and $(5.2)_4$ by u_i, θ and ϕ respectively and integrate over V to obtain

$$\begin{aligned} \|\mathbf{u}\|^2 &= R\langle\theta, w\rangle - R_c\langle\phi, w\rangle, \\ \frac{1}{2}\frac{d}{dt}\|\theta\|^2 &= R\langle wF, \theta\rangle - \|\nabla\theta\|^2 + \gamma R\langle\phi, \theta\rangle, \\ \frac{\hat{\phi}}{2}\frac{d}{dt}\|\phi\|^2 &= \langle w, \phi\rangle - \eta\|\nabla\phi\|^2. \end{aligned} \tag{5.12}$$

where $\|\cdot\|$ and $\langle\cdot\rangle$ denote the norm and inner product on $L^2(V)$.

Letting λ_1 and λ_2 be positive coupling parameters to be selected at our discretion, and defining an energy

$$E(t) = \frac{1}{2}\|\theta\|^2 + \frac{\lambda_1\hat{\phi}}{2}\|\phi\|^2,$$

we have the following identity:

$$\frac{dE}{dt} = \mathcal{I} - \mathcal{D}, \tag{5.13}$$

where

$$\begin{aligned} \mathcal{I} &= R\langle wF, \theta\rangle + \gamma R\langle\phi, \theta\rangle + \lambda_1\langle w, \phi\rangle + \lambda_2 R\langle\theta, w\rangle - \lambda_2 R_c\langle\phi, w\rangle, \\ \mathcal{D} &= \|\nabla\theta\|^2 + \eta\lambda_1\|\nabla\phi\|^2 + \lambda_2\|\mathbf{u}\|^2. \end{aligned}$$

Let $1/R_E = \max_{\mathcal{H}}(\mathcal{I}/\mathcal{D})$, where $\mathcal{H}$ is the space of admissible functions. Using the Poincaré inequality to deduce that $\mathcal{D} \geq cE$ for some constant c, if $R_E > 1$ then using (5.13) yields

$$\frac{dE}{dt} \leq -\left(\frac{R_E - 1}{R_E}\right) cE.$$

Integrating we have $E(t) \leq E(0)e^{-at} \to 0$ as $t \to \infty$, where $a = c(R_E - 1)/R_E$. By the definition of $E(t)$ the decay of θ and ϕ clearly follows. However, for global nonlinear stability the decay of $\mathbf{u}$ must be shown.

Let $\alpha, \beta > 0$ be some constants, then using the arithmetic-geometric mean inequality in $(5.12)_1$ yields

$$\|\mathbf{u}\|^2 \leq \frac{R\alpha}{2}\|\theta\|^2 + \frac{R}{2\alpha}\|\mathbf{u}\|^2 + \frac{R_c\beta}{2}\|\phi\|^2 + \frac{R_c}{2\beta}\|\mathbf{u}\|^2.$$

Letting $\alpha = R$ and $\beta = 2R_c$, as $\theta, \phi \to 0$ in the stability measure $L^2(V)$ as $t \to \infty$, the decay of $\mathbf{u}$ clearly follows.

Assuming the sharpest boundary condition $R_E = 1$, the Euler-Lagrange equations (see Section 2.3 for an explicit example of the derivation of Euler Lagrange equations) for the maximisation problem $1/R_E = \max_{\mathcal{H}}(\mathcal{I}/\mathcal{D})$ are

$$\begin{aligned} &R(F + \lambda_2)\theta + (\lambda_1 - R_c\lambda_2)\phi - 2\lambda_2 u_i = \omega_{,i}, \\ &R(F + \lambda_2)w + \gamma R\phi + 2\triangle\theta = 0, \\ &\gamma R\theta + (\lambda_1 - R_c\lambda_2)w + 2\eta\lambda_1\triangle\phi = 0, \end{aligned} \tag{5.14}$$

where ω is the Lagrange multiplier. To eliminate ω from $(5.14)_1$ the double *curl* can be taken to find

$$2\lambda_2\triangle w - R(F + \lambda_2)\triangle^*\theta - (\lambda_1 - R_c\lambda_2)\triangle^*\phi = 0. \tag{5.15}$$

The critical nonlinear Rayleigh number Ra_E, which is given by

$$Ra_E = \max_{\lambda_1,\lambda_2} \min_{a^2} R^2(a^2, \lambda_1, \lambda_2). \tag{5.16}$$

can now be derived from the sixth-order eigenvalue problem consisting of equations $(5.14)_2$, $(5.14)_3$, and (5.15).

This system was solved using the compound matrix method and the Chebyshev-tau technique. Both methods are explained in detail in Appendices A.1 and A.2,

although brief descriptions are given in this chapter to clarify the use of the methods in the context of the system of the second order coupled equations being explored. Similarly to Section 7.2, the Chebyshev-tau technique was found to be restrictive due to the heavy computational cost in solving full matrix eigenvalue problems. This problem was more acute as five parameter ranges were required (namely γ, R_c, a^2, λ_1 and λ_2). The natural progression was to develop the techniques in Chapters 7 and 8 to overcome these difficulties.

Due to a significantly large number of local maxima, the optimisation problem (5.16) is very difficult to solve due to the high sensitivity of the solution. To overcome this problem (5.14) can solved analytically, by averaging $F(z)$ over the $z \in [0, 1]$ range, to provide an estimate of the coupling parameters near the global maximum. After deriving that $F_{av} = 1$, and following a similar argument to the analysis derived in Section 5.2, one can show that

$$R^2 = \frac{4\eta\lambda_1\lambda_2\Lambda^3 - a^2\Lambda(\lambda_1 - R_c\lambda_2)^2}{a^2\gamma(\lambda_2+1)(\lambda_1 - R_c\lambda_2) + \lambda_2\Lambda\gamma^2 + \Lambda a^2(\lambda_2+1)^2\eta\lambda_1}.$$

With this guide it is possible to assess the optimisation problem, although one must always be careful to minimise over a^2 as the local minima can be difficult to recognise.

Figure 5.6 presents the linear and nonlinear results in graphical form to visually demonstrate the potential regions of subcritical instabilities, with the solid and dashed lines representing the linear and nonlinear results respectively. The top and bottom graphs correspond to heating from below ($H = +1$) and above ($H = -1$) respectively. The parameter η remains fixed at 0.01 and R_c ranges from 0 to 10.

5.4 Conclusions

The onset of convection in a fluid saturated porous layer with a temperature and concentration based density has been examined.

Figures 5.1 to 5.4 present the critical thermal Rayleigh numbers relating to the corresponding linear theory for a fixed range of solute Rayleigh numbers and γ values. The γ term is, in essence, a measure of the internal heat source. Both the actual numerical and approximate analytical results strongly suggest the existence of a critical γ_c value, where no oscillatory convection occurs for $\gamma_c \leq \gamma$. With the

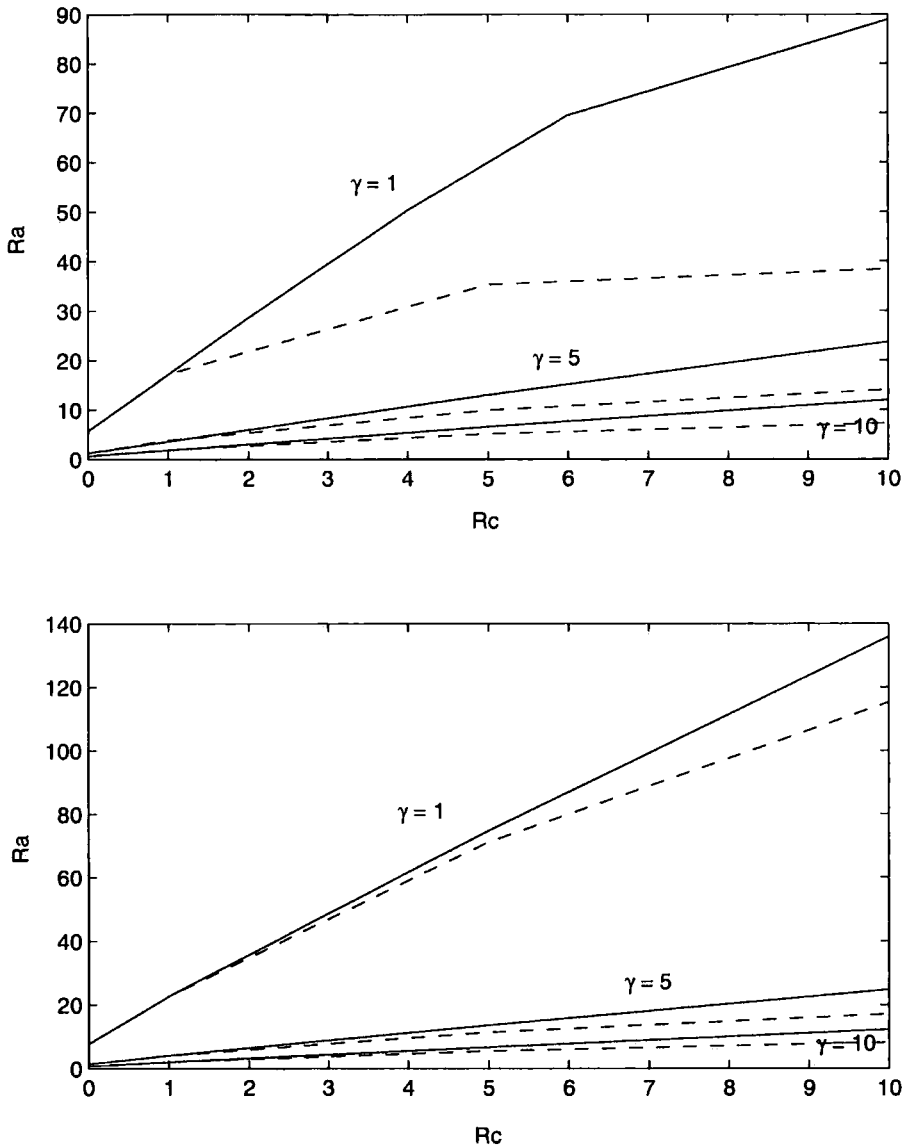

Figure 5.6: Visual representation of linear (solid line) and nonlinear (dashed line) results, with critical thermal Rayleigh number R_a plotted against R_c. The top and bottom graphs correspond to heating from below ($H = +1$) and above ($H = -1$) respectively.

extrapolation of oscillatory results from the numerical analysis, a fixed range for γ_c can be derived by direct comparison between the stationary and oscillatory neutral lines. However, the analysis does suggest a nonlinear relationship between the critical thermal and solute Rayleigh numbers such that this range is not optimal. The suggested nonlinear behaviour also potentially yields finite intervals of oscillatory convection, as demonstrated by Figure 5.5. This behaviour, in the present literature, is an apparently unobserved phenomenon.

The thresholds of both the numerical linear instability and nonlinear stability results are presented in Figure 5.6. More comparable linear and nonlinear thresholds are apparent as the onset of convection predicted by the linear theory becomes fully stationary. However, irrespective of γ, their agreement does deteriorate as the solute Rayleigh number becomes large, indicating that the linear theory may fail to suitably emulate the physics of the onset of convection. The continual degradation of the agreement between the two thresholds is a phenomenon common to many systems with similar graphical examples as demonstrated by Joseph [47] and Mulone [74].

Chapter 6

Linear and nonlinear stability thresholds for thermal convection in a box

In this chapter we derive linear instability and nonlinear energy stability thresholds for thermal convection in a linearly viscous fluid contained in a finite box. A vertical gravity field acts and the vertical walls are maintained at different temperatures. The analysis contained herein is timely because convection problems driven by periodic temperature gradients, gravity gradients, and inclined temperature gradients have been the topic of much recent attention, see Capone & Rionero [10], Sarawanan & Kandaswamy [84], Alex & Patil [1] [2], Kaloni & Lon [50] - [52]. The work here is for convection in a three-dimensional box. This is another area, namely three-dimensional hydrodynamic stability calculations, which has formed the subject of much recent attention, Crisciani [17], Holzbecher [45], Theofilis [92], Mercier *et al.* [70], Mahidjiba *et al.* [63].

In fact, the precise problem we investigate was previously studied by Georgescu & Mansutti [25]. They claim that the linear instability thresholds are the same as the nonlinear stability ones found by using an energy method. We refute this assertion as our results are completely different, due to the employment of the correct governing equations.

The results in this chapter are also presented in the article Hill & Straughan [43].

A further manuscript, Hill [42], studies a porous (as opposed to a fluid) medium. This lends much credence to the results of the original paper (Hill & Straughan [43]) over those of Georgescu & Mansutti [25], as the linear and nonlinear boundaries do not coincide.

6.1 Formation of the problem

Let $Oxyz$ be a cartesian frame of reference with unit vectors **i**, **j**, **k** respectively, and consider a fluid filled rectangular box Ω where the $Oy-$axis is in the vertical direction and the bottom face of the box is on the $(x,z)-$ plane, with the origin located at the corner of this face. The bounded dimensions of the box are denoted by B_x, B_y and B_z in the x, y and z directions respectively.

The governing equations for the fluid can be expressed by the Navier-Stokes equations, with a Boussinesq approximation, yielding

$$v_{i,t} + v_j v_{i,j} = -\frac{1}{\rho_0} p_{,i} + \nu \triangle v_i - \frac{b_i g}{\rho_0} \rho, \tag{6.1}$$

$$v_{i,i} = 0 \tag{6.2}$$

$$T_{,t} + v_i T_{,j} = \kappa \triangle T \tag{6.3}$$

where (6.2) and (6.3) are the incompressibility condition and balance of energy respectively. In these equations v_i, t, x_i, p, and T are velocity, time, displacement, pressure and temperature, and ν, g and κ are the kinematic viscosity, acceleration due to gravity and thermal diffusivity, with $\mathbf{b} = (0,1,0)^T$. The density is assumed to have a linear temperature dependence of the form $\rho = \rho_0(1 - \alpha(T - T_r))$ where ρ and α are density and the thermal expansion coefficient and ρ_0 and T_r are constant reference values.

The boundary conditions for the problem on the boundary $\partial\Omega$ of Ω are taken from Georgescu & Mansutti [25], namely $u_i = 0$, $T = T_0, T_1$ at $x = 0, B_x$ and $T = T_0 + (T_1 - T_0)x/B_x$ at $y = 0, B_y$.

A basic steady state, in whose stability we are interested in, is taken following the same proposition of no fluid flow as adopted in Georgescu & Mansutti [25]. This

yields the steady state temperature field

$$\overline{T} = T_0 + \frac{(T_1 - T_0)}{B_x} x.$$

To assess the stability of the steady solution we introduce a perturbation (u_i, θ, π) to the steady state solution, such that $v_i = \overline{v}_i + u_i$, $T = \overline{T} + \theta$, $p = \overline{p} + \pi$, and non-dimensionalise with scalings of

$$u_i = \frac{\nu}{B_y} u_i^*, \quad \pi_i = \frac{\rho_0 \nu^2}{B_y^2} \pi_i^*, \quad \theta = \theta^* \sqrt{\frac{\delta T \nu^3}{g \alpha \kappa B_y^3}}, \quad x_i = B_y x_i^*,$$
$$t = \frac{B_y^2}{\nu} t^*, \quad d_x = \frac{B_x}{B_y}, \quad R = \sqrt{\frac{g \alpha B_y^3 (\delta T)}{\nu \kappa}}$$

where $\delta T = T_1 - T_0$, $Pr = \nu/\kappa$ is the Prandtl number and $R_a = R^2$ is the Rayleigh number.

Substituting the perturbations and non-dimensionalised variables into equations (6.1) - (6.3), and dropping the stars we derive the system

$$u_{i,t} + u_j u_{i,j} = -\pi_{,i} + b_i R\theta + \triangle u_i, \tag{6.4}$$

$$u_{i,i} = 0, \tag{6.5}$$

$$Pr(\theta_{,t} + u_i \theta_{,i}) + \frac{f_i R u_i}{d_x} = \triangle \theta, \tag{6.6}$$

where $\mathbf{f} = (1, 0, 0)$. The perturbed boundary conditions are now $u_i = \theta = 0$ on $\partial\Omega$. Equation (6.4) - (6.6) now model the same physical problem as proposed in Georgescu & Mansutti [25], although our equations are different.

6.2 Linear Instability Analysis

The linearised equations are derived from equations (6.4) - (6.6) by discarding the nonlinear terms, and then the double *curl* of (6.4) is taken to remove the pressure term. Assuming a temporal growth rate like $e^{(\sigma t)}$, we may then write $u_i = e^{(\sigma t)} u_i(\mathbf{x})$ and $\theta = e^{(\sigma t)} \theta(\mathbf{x})$. Normal mode representations are also assumed for u_i, and θ. This is the assumption that any unknown function $g(x, y, z)$ is of the form

$$g(x, y, z) = \hat{g}(y) \exp\left(i \left(2\pi m' \frac{x}{d_x} + 2\pi k' \frac{z}{d_z} \right) \right)$$

where $i = \sqrt{-1}$ and d_z is B_z/B_y, (such that d_x and d_z are the aspect ratios along the x and z directions). The m' and k' are integers as they refer to the number of cells in the x and z direction respectively. Letting $m = 2\pi m'/d_x$, $k = 2\pi k'/d_z$, and $a^2 = m^2 + k^2$, equations (6.4)) - (6.6)) yield

$$\begin{aligned}
\sigma(D^2 - a^2)\hat{u} &= -RimD\hat{\theta} + (D^2 - a^2)^2\hat{u} \\
\sigma(D^2 - a^2)\hat{v} &= -a^2R\hat{\theta} + (D^2 - a^2)^2\hat{v} \\
\sigma(D^2 - a^2)\hat{w} &= -RikD\hat{\theta} + (D^2 - a^2)^2\hat{u} \\
\sigma Pr\hat{\theta} &= (D^2 - a^2)\hat{\theta} - \frac{R\hat{u}}{d_x}
\end{aligned} \tag{6.7}$$

where $D = d/dy$, $\hat{\mathbf{u}} = (\hat{u}, \hat{v}, \hat{w})$, and the boundary conditions are

$$\hat{u} = 0, \quad \hat{v} = D\hat{v} = 0, \quad \hat{w} = 0, \quad \hat{\theta} = 0, \qquad y = 0,\ 1. \tag{6.8}$$

We take *curl* (6.4) and the first and third components of the resulting equations yield

$$\left.\begin{aligned}
(D^3 - a^2D)\hat{w} - ikD^2\hat{v} &= \sigma D\hat{w} \\
(D^3 - a^2D)\hat{u} - imD^2\hat{v} &= \sigma D\hat{u}
\end{aligned}\right\} \qquad y = 0,\ 1. \tag{6.9}$$

These boundary conditions exclude the use of the methods in Chapters 7 and 8 as, in their current form, they are designed for homogeneous boundary conditions.

System (6.7) and boundary conditions (6.8) and (6.9) constitute a fourteenth order eigenvalue system. To solve this we employ the Chebyshev tau method.

Although comprehensive details are given in Dongarra *et al.* [20] and Appendix A.2, a brief overview of the implementation of the Chebyshev tau technique to system (6.7) is given in this section, with particular reference to the implementation of the boundary conditions.

Defining T_i, $i \in \mathbb{N}$, be the ith Chebyshev polynomial, system (6.7) is transformed to the domain (-1, 1) and then $\hat{u}$, $\hat{v}$, $\hat{w}$ and $\hat{\theta}$ are written as a finite series of Chebyshev polynomials such that

$$\hat{u} = \sum_{n=0}^{N+2} U_nT_n \qquad \hat{v} = \sum_{n=0}^{N+2} V_nT_n \qquad \hat{w} = \sum_{n=0}^{N+2} W_nT_n \qquad \hat{\theta} = \sum_{n=0}^{N+2} S_nT_n.$$

The inner product with T_k, $k = 0, \ldots, N+2$, is taken on the weighted Chebyshev space to form a generalised eigenvalue problem.

It is important to note that under the transformation to (-1, 1) the boundary conditions defined in (6.9) become

$$\left.\begin{aligned}(4D^3 - a^2D)\hat{w} - 2ikD^2\hat{v} &= \sigma D\hat{w} \\ (4D^3 - a^2D)\hat{u} - 2imD^2\hat{v} &= \sigma D\hat{u}\end{aligned}\right\} \quad y = -1,\ 1,$$

which can be evaluated using the idenities

$$\begin{aligned}T_n'(\pm 1) &= (\pm 1)^{n-1}n^2 \\ T_n''(\pm 1) &= \frac{(\pm 1)^n}{3}n(n-1)(n^2+n+12) \\ T_n'''(\pm 1) &= \frac{(\pm 1)^{n-1}}{15}n(n-1)(n^4-9n^3+101n^2-39n+210)\end{aligned}$$

Table 6.1 presents the linear results for the aspect ratios 0.5, 0.8, 1, 2, 3 and 4 for d_x and d_z, where the values of m' and k' which minimise the critical Rayleigh number are both 1 unless stated otherwise, such that $*^a$, $*^b$ and $*^c$ refer to $m' = 2,\ 3,\ 4$ respectively with $k' = 1$ in each case.

Table 6.1: Linear results for the critical Rayleigh number, where d_x and d_z are the aspect ratios in the x and z directions respectively.

d_x	d_z=0.5	d_z=0.8	d_z=1	d_z=2	d_z=3	d_z=4
0.5	553.010	358.792	316.470	261.745	251.845	248.964
0.8	574.067	294.158	235.374	161.489	148.464	143.960
1	632.939	294.217	224.275	137.823	122.870	117.729
2	895.111^a	403.720	275.646	125.001	100.740	92.6019
3	1096.28^b	477.540^a	338.068^a	151.111	117.020	105.684
4	1265.88^c	553.1^b	389.822^b	176.778^a	140.912^a	126.234^a

The spectrum of σ is found numerically to be real to a given accuracy for the parameter ranges explored, which is an interesting result considering the lack of symmetry of the linearised system. The critical Rayleigh numbers numerically derived are not in accordance with those presented in Georgescu & Mansutti [25].

6.3 Nonlinear Stability Analysis

To obtain global nonlinear stability bounds in the stability measure $L^2(\Omega)$ we multiply equations (6.4) and (6.6) by u_i and θ, respectively, and integrate over Ω to obtain

$$\frac{1}{2}\frac{d}{dt}\|\mathbf{u}\|^2 = R\langle\theta, v\rangle - \|\nabla\mathbf{u}\|^2 \tag{6.10}$$

$$\frac{Pr}{2}\frac{d}{dt}\|\theta\|^2 = -\frac{R}{d_x}\langle u, \theta\rangle - \|\nabla\theta\|^2 \tag{6.11}$$

where again $\mathbf{u} = (u, v, w)$, and $\|\cdot\|$ and $\langle\cdot\rangle$ denote the norm and inner product on $L^2(\Omega)$.

Multiplying (6.11) by a coupling parameter $\lambda > 0$ we can define

$$E(t) = \frac{1}{2}\|\mathbf{u}\|^2 + \frac{\lambda Pr}{2}\|\theta\|^2,$$
$$\mathcal{I} = \langle\theta, v\rangle - \frac{\lambda}{d_x}\langle u, \theta\rangle,$$
$$\mathcal{D} = \|\nabla\mathbf{u}\|^2 + \lambda\|\nabla\theta\|^2.$$

Thus

$$\begin{aligned}\frac{dE}{dt} &= R\mathcal{I} - \mathcal{D} \\ &\leq -\mathcal{D}\left(1 - \frac{R}{R_E}\right)\end{aligned}$$

where $1/R_E = \max_{\mathcal{H}}(\mathcal{I}/\mathcal{D})$ and $\mathcal{H}$ is the space of admissible functions for solutions to equations (6.4) - (6.6).

Utilising the Poincaré inequality it follows that $\mathcal{D} \geq cE$ for some constant c. Hence, letting $a = c(R_E - R)/R_E > 0$, $E(t) \leq E(0)e^{-at}$ which tends to 0 as $t \to \infty$, showing the decay of $\mathbf{u}$ and θ.

The Euler Lagrange equations (see Section 2.3 for an explicit example of the derivation of Euler Lagrange equations) which arise for R_E are

$$\left(b_i R_E - \frac{f_i R_E \lambda}{d_x}\right)\theta + 2\triangle u_i = \omega_{,i} \tag{6.12}$$

$$R_E v - \frac{R_E\lambda}{d_x}u + 2\lambda\triangle\theta = 0, \tag{6.13}$$

where ω is a Lagrange multiplier. We stress that equations (6.12) and (6.13) are not the same as equations (24) and (25) of Georgescu & Mansutti [25] who claim the equations arising from a nonlinear stability analysis are the same as those of the linear instability theory. To eliminate ω from equation (6.12) the double *curl* is taken, and the same normal mode representations are adopted as in Section 6.2 to yield the system

$$
\begin{aligned}
2(D^2-a^2)^2\hat{u} &= imRD\hat{\theta} + \frac{R\lambda}{d_x}(D^2-k^2)\hat{\theta},\\
2(D^2-a^2)^2\hat{v} &= a^2R\hat{\theta} - \frac{imR\lambda}{d_x}D\hat{\theta},\\
2(D^2-a^2)^2\hat{w} &= ikRD\hat{\theta} + \frac{R\lambda mk}{d_x}\hat{\theta},\\
2(D^2-a^2)\hat{\theta} &= \frac{R}{d_x}\hat{u} - \frac{R}{\lambda}\hat{v},
\end{aligned}
$$

where $D = d/dy$. The boundary conditions are

$$\hat{u} = 0, \quad \hat{v} = D\hat{v} = 0, \quad \hat{w} = 0, \quad \hat{\theta} = 0, \qquad y = 0, 1.$$

To derive the remaining boundary conditions the *curl* of (6.12) with respect to u and w is taken to yield

$$
\left.
\begin{aligned}
2(D^3-a^2D)\hat{u} - 2imD^2\hat{v} &= \frac{R\lambda}{d_x}D\hat{\theta}\\
(D^3-a^2D)\hat{w} - ikD^2\hat{v} &= 0
\end{aligned}
\right\} \qquad y = 0, 1.
$$

This is a fourteenth-order eigenvalue problem for the critical nonlinear Rayleigh number Ra_N, which is given by

$$Ra_N = \max_{\lambda}\min_{a^2} R^2(a^2, \lambda).$$

As in Section 6.2 this eigenvalue problem is solved utilising the Chebyshev tau method.

Table 6.2 presents the nonlinear results for the aspect ratios 0.5, 0.8, 1, 2, 3 and 4 for d_x and d_z. The values of m' and k' which minimise the critical Rayleigh number are all 1.

Table 6.2: Nonlinear results for the critical Rayleigh number, where d_x and d_z are the aspect ratios in the x and z directions respectively.

d_x	d_z=0.5	d_z=0.8	d_z=1	d_z=2	d_z=3	d_z=4
0.5	373.009	285.633	267.447	245.855	242.320	241.124
0.8	314.160	196.710	171.138	140.888	136.404	134.977
1	311.717	178.790	149.343	113.810	108.618	107.034
2	367.659	177.650	134.820	81.4641	73.4232	71.0530
3	433.934	201.040	148.515	83.4573	74.3344	72.0738
4	494.477	225.514	164.866	90.1527	80.4592	78.7357

Figure 6.1 gives a visual representation of the linear instability and nonlinear stability boundaries.

It is clearly demonstrated in Figure 6.1 that the linear and non-linear results do no coincide. This leaves open a large region of potential subcritical instabilities.

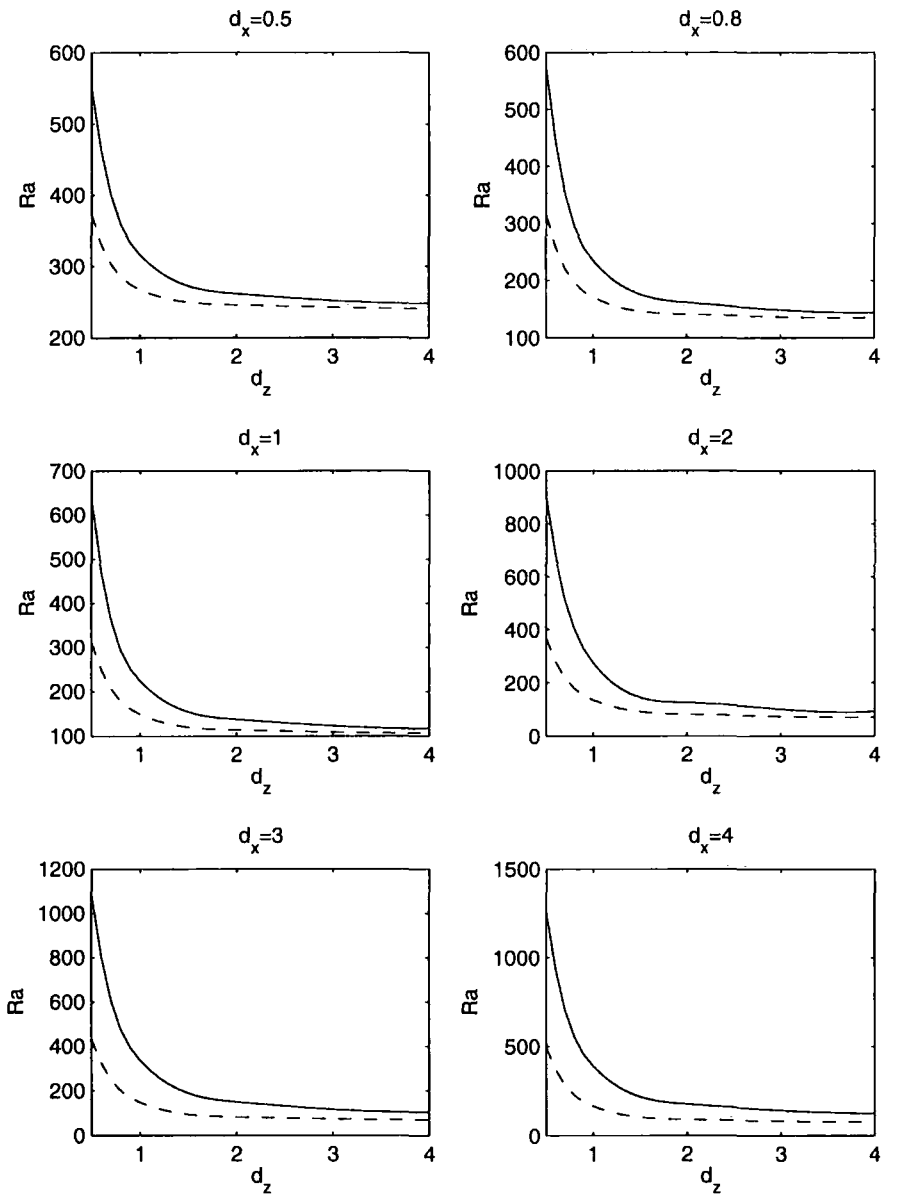

Figure 6.1: Visual representation of linear (solid line) and nonlinear (dashed line) results, with critical thermal Rayleigh number R_a plotted against d_z.

Chapter 7

A Legendre polynomial based spectral method for eigenvalue problems in hydrodynamic stability

7.1 Introduction

In each of the previous chapters the established methods used, although powerful, produced a variety of computational and storage problems, as highlighted in each instance of their utilisation. Chapters 2 to 4 have typical characteristics of the stability analysis of fluid motion in porous media with homogeneous standard boundary conditions, so it is a natural progression to develop more efficient techniques based on the experience of employing the well established routines.

An illustrative example in the text of the drawbacks of the Chebyshev tau technique is in Chapter 5. The Chebyshev tau-QZ approach reduces the differential equations into a generalised eigenvalue problem, which contains full matrices. Of course this is highly computational taxing considering that the matrices are over 100×100 to guarantee accuracy. Couple this with the spurious eigenvalues which have been linked to superimposing boundary conditions (see Dongarra *et al.* [20]) and the problems when varying over the several parameter ranges (γ, R_c, a^2, λ_1, λ_2

for example) required in this chapter become apparent.

Utilising the compound matrix approach yields a different set of complications. The chief difficulty of the compound matrix method is in the calculation of the compound matrix equations (i.e. the differentials of each of the minors of the solution matrix) which expand in size dramatically as the number of differential equations increase. Since these equations must be calculated before any numerical analysis is attempted, differential equations of sixth order and above (which are the basis of most the numerical analysis in this body of work) become far too problematic, as mentioned specifically in Section 3.3.

It was concluded through the experience of the numerical analysis of Chapters 2 to 5 that the polynomial based structure adopted by the Chebyshev tau technique was the optimal approach, if the dual problems of matrix fullness and boundary conditions could be addressed.

In this chapter a Legendre polynomial based spectral method is developed. This generates sparse matrices, where the standard homogeneous boundary conditions for porous media problems are contained within the method, negating the need for their superimposition onto the matrices as is necessary with the Chebyshev tau method. Several different examples of its application to porous media are presented to demonstrate its adaptability, accuracy and relevant ease in implementation (these examples are different to the systems presented in Chapters 2 to 6 to highlight the wide reaching potential of the method). In each example this method is compared to the Chebyshev tau technique to assess accuracy and speed of convergence. The results clearly demonstrate that the Legendre method coupled with the Arnoldi technique of finding matrix eigenvalues leads to substantial computational advantages. This lends the technique to a considerable number of extremely useful applications. The determining of a neutral curve in hydrodynamic stability often involves hundreds of eigenvalue calculations to accommodate different parameter values within the model (as highlighted in Chapters 3 and 5), making the sparsity of the Legendre polynomial based spectral method a crucial advantage. While the exponentially fast convergence of a spectral method usually means that traditional techniques which yield full matrices do not present an issue because very few polynomials are required,

some practical eigenvalue problems do need many polynomials. Such cases are parallel flow situations, see e.g. Dongarra *et al.* [20], where one may need upward of 200 polynomials and high precision arithmetic. Another motivation for the spectral technique employed here is its ability to extend in a natural way to two and three dimensional stability problems for which the matrices are large and then their sparse structure is a major advantage. If one tries to use a technique such as the Chebyshev tau method in higher dimensions it is not so clear how one incorporates the boundary conditions, in addition to the matrices being full. The spectral technique advocated here extends naturally to two and three space dimensions by using tensor products of the basis elements in x, y and z.

The Legendre idea employed here was introduced for the solution of differential equations by Shen [85]. No eigenvalue calculations were considered. Kirchner [54] developed a method for solving eigenvalues for the Orr - Sommerfeld equation which essentially uses the technique of Shen [85]. The Orr - Sommerfeld equation is fourth order and not characteristic of the Darcy flow governing model in porous media. The main contribution here is to show how to adapt the Shen method naturally to eigenvalue problems for porous convection. Since the Orr - Sommerfeld equation is fourth order, the version of the Shen method adopted by Krichner [54] is different from that given here where we concentrate on writing the equations as a system of coupled second order equations. For completeness, we show how other problems in fluid mechanics which involve coupled second and fourth order equations may be solved by a combination of the ideas described in Kirchner [54] and those given here.

The layout of the chapter now follows. In Section 7.2 we illustrate the technique by application to a simple problem, the simple harmonic motion equation. Then in Sections 7.3 and 7.4 we illustrate the method by application to two different convection problems in porous media. Section 7.3 treats the problem of Hadley flow where convection is driven by vertical and horizontal temperature gradients. Section 7.4 deals with multi-component convection in a porous medium where oscillatory instabilities may arise due to competition between a temperature field and two different salt fields. From the mathematical viewpoint Section 7.3 effectively treats a fourth order equation with complex coefficients, written as two second order equations,

whereas Section 7.4 analyses an eighth order system, expressed as 4 interconnected second order equations. To illustrate the versatility of the Legendre polynomial - Galerkin method we show how Benard convection in a fluid may be treated in Section 7.5. This is different from convection in a porous medium because it involves a fourth order equation coupled with a second order one. In this way one sees how the Legendre polynomial method may be applied to a variety of problems in hydrodynamic stability. The chapter is completed in Section 7.6 by analysing the benefits of the technique described here as compared with competing methods. It must be stressed that this method is highly applicable to Chapters 2 to 6, although these examples are used to highlight the wide reaching potential of the method.

The results in this chapter are also presented in the article Hill & Straughan [41].

7.2 Structure of the technique for second order equations

Consider the domain $\Omega = (-1, 1)$, with the Hilbert space

$$H_0^1(\Omega) = \{v : v, v' \in L_2(\Omega),\ v(-1) = v(1) = 0\},$$

where

$$L^2(\Omega) = \{v : v(\Omega) \to \mathbb{C},\ \int_\Omega |v|^2 dx < \infty\}.$$

Let $\langle \cdot \rangle$ be the inner product on $L^2(\Omega)$, e.g. $\langle f, g\rangle = \int_\Omega f\bar{g}dx$, $\bar{g}$ being complex conjugate, and $\|\cdot\|$ the associated norm. If the setting is real the space L^2 employed will involve real functions rather than complex ones. To motivate the Legendre polynomial based spectral technique we begin with the equation

$$u'' + \lambda u = 0, \tag{7.1}$$

where $u \in H_0^1(\Omega)$, and $u = 0$ at $z = \pm 1$.

Equation (7.1) can be solve numerically by replacing the infinite dimensional space $H_0^1(\Omega)$ by a finite dimensional space $S_N \subset H_0^1(\Omega)$ of dimension $N \in \mathbb{N}$. Assuming that a basis $\phi_1, \ldots, \phi_N$ of S_N can be constructed, the solution u to (7.1)

may be approximated by $u = \sum_{k=1}^{N} u_k \phi_k$ and then (7.1) replaced by

$$\sum_{k=1}^{N} u_k \phi_k'' + \lambda \sum_{k=1}^{N} u_k \phi_k = 0, \tag{7.2}$$

where the u_k are the Fourier coefficients.

Let L_i, $i \in \mathbb{N}$, be the ith Legendre polynomial on $(-1, 1)$ with $S_N = \mathcal{P}^{N+1}(\Omega) \cap H_0^1(\Omega)$, where $\mathcal{P}^p(\Omega)$ denotes the polynomials of degree p on Ω. Using the identity

$$(2i+1)L_i(z) = L_{i+1}'(z) - L_{i-1}'(z), \tag{7.3}$$

cf. Sneddon [87], p. 69, for $p \geq 2$, we define the basis function

$$\phi_i(z) = \int_{-1}^{z} L_i(s)\, ds = \frac{L_{i+1} - L_{i-1}}{2i+1}, \quad i = 1, \ldots, p-1, \tag{7.4}$$

cf. Shen [85], p. 1492. By the definition of Legendre polynomials the basis functions ϕ_i are linearly independent, such that $S_N = span\{\phi_i\}$ $i = 1, \ldots, N$ with $N = dim\,(S_N)$. A crucial aspect of these basis functions is their inclusion in the space $H_0^1(\Omega)$ or, more specifically in this context, that $\phi_i(-1) = \phi_i(1) = 0$. This follows when utilising the relation $L_i(\pm 1) = (\pm 1)^i$. This inherent structure clearly avoids the need for the superimposition of the standard homogeneous boundary conditions in the resulting matrix - a fact frequently needed with e.g. the Chebyshev tau analysis. This inherent structure is highly significant in the method's applicability to two and three dimensional porous problems as discussed in Section 7.1.

To solve (7.2) we multiply by ϕ_i and integrate over Ω to find

$$\left\langle \sum_{k=1}^{N} u_k \phi_k'',\ \phi_i \right\rangle + \lambda \left\langle \sum_{k=1}^{N} u_k \phi_k,\ \phi_i \right\rangle = 0 \qquad i = 1, \ldots, N. \tag{7.5}$$

By making use of the divergence theorem and utilising (7.4) we can observe that

$$\left\langle \sum_{k=1}^{N} u_k \phi_k'',\ \phi_i \right\rangle = -\sum_{k=1}^{N} u_k \langle \phi_k', \phi_i' \rangle = -\left\langle \sum_{k=1}^{N} u_k L_k,\ L_i \right\rangle. \tag{7.6}$$

System (7.5), with the rearrangement of (7.6), may be solved by utilising the inherent orthogonality of Legendre polynomials within the specified inner product, where

$$(L_i,\ L_j) = \int_{\Omega} L_i(z) L_j(z)\, dz = \begin{cases} \dfrac{2}{2i+1}, & i = j \\ 0, & i \neq j \end{cases}. \tag{7.7}$$

This procedure leads to a generalised eigenvalue problem of the form

$$A\mathbf{u} = \lambda B\mathbf{u} \tag{7.8}$$

where $\mathbf{u} = (u_1, \ldots, u_N)^T$. By using the orthogonal behaviour shown in (7.7) the matrix A can derived from (7.6) yielding diagonal elements $A_{i,i} = 2/(2i+1)$, where $i = 1, \ldots, N$. This desirable feature that the matrix A is diagonal is due to the fact that ϕ_i is selected so that $\phi_i' = L_i$.

Similarly

$$\left\langle \sum_{k=1}^{N} u_k \phi_k,\ \phi_i \right\rangle = \left\langle \sum_{k=1}^{N} u_k \left(\frac{L_{k+1} - L_{k-1}}{2k+1} \right),\ \frac{L_{i+1} - L_{i-1}}{2i+1} \right\rangle,$$

which, utilising (7.7), yields the symmetric banded matrix B with elements

$$B_{i,j} = \begin{cases} \dfrac{4}{(2j-1)(2j+1)(2j+3)} & j = i, \qquad i = 1, \ldots, N \\ \dfrac{-2}{(2j-3)(2j-1)(2j+1)} & j = i+2, \qquad i = 1, \ldots, N-2 \end{cases}$$

which is of bandwidth 4. The equivalent procedure with the Chebyshev tau approach yields (full) matrices A and B which are not of banded structure as they are here.

System (7.8) is a sparse eigenvalue problem making it ideal for specific sparse iterative solvers such as the implicitly restarted Arnoldi method (IRAM) as presented in the ARPACK package (see Lehoucq *et al.* [58]). This reduces computational and storage requirements needed by the QZ algorithm (see e.g. Golub & Van Loan, [28]), which is necessary for a technique like the Chebyshev tau method, since A and B are full with B frequently singular. The speed up achieved with the Arnoldi technique is a notable feature presented here.

We now begin with application to porous convection and convection in a fluid. While we study three distinct but representative problems we stress that the techniques are easily adaptable to many other hydrodynamic stability problems (with special reference to Chapters 2 to 6, as they provided the motivation behind developing this method), and even stability problems in other areas of Continuum Mechanics. For example, we have investigated stability problems in some viscoelastic flows and also a stability problem for a thermoelastic plate.

7.3 Hadley Flow

Hadley flow refers to convection in a layer of porous medium where the basic temperature field varies in the vertical (i.e. $z-$direction) as well as along one of the horizontal directions, which we will define as the $x-$direction. This system is presented in more detail by Nield [76] and is also used as a test case for the Chebyshev tau technique in Straughan & Walker [91]. It is a useful example as the equations have complex coefficients dependent on the z variable, and can be very sensitive to small variations in the parameters, making it beneficial as a test of the method's accuracy.

Defining the porous medium to be contained in the layer $z \in (-H/2, H/2)$ we adopt the temperature field boundary conditions

$$T = T_0 \mp \frac{1}{2}\triangle T - \beta_T x, \qquad z = \pm\frac{1}{2}H,$$

where $\triangle T$ is the temperature differential in the z direction and β_T is some constant of proportionality. Employing a non-dimensionalised form of the temperature field boundary conditions, the steady state solution has the form:

$$\begin{aligned} \overline{U} &= R_H z, \\ \overline{T} &= -R_V z + \tfrac{1}{24}R_H^2(z - 4z^3) - R_H x, \end{aligned} \tag{7.9}$$

where $z \in (-1/2,\ 1/2)$, R_H and R_V are the vertical and horizontal Rayleigh numbers, respectively, and $\bar{U}(z)$ is the $x-$component of velocity. Defining $a^2 = k^2 + m^2$ with k and m being the x and y wavenumber, the non-dimensionalised perturbation equations from (7.9) are

$$\begin{aligned} &(D^2 - a^2)W + a^2 S = 0, \\ &(D^2 - a^2 - i\sigma - ik\overline{U}(z))S + ika^{-2}R_H DW - (D\overline{T})W = 0, \end{aligned} \tag{7.10}$$

where $D = d/dz$. System (7.10) is subject to the boundary conditions

$$W = S = 0 \qquad z = \pm\frac{1}{2}.$$

In (7.10), $W(z)$ and $S(z)$ are the third component of velocity and temperature field perturbation, respectively. Adopting the Legendre-based spectral technique, (7.10) reduces to the generalised matrix eigenvalue problem,

$$A\mathbf{x} = \sigma B\mathbf{x}$$

where here $\mathbf{x} = (w_1, \ldots, w_N, s_1, \ldots, s_N)$, and the matrices are given by

$$A = \begin{pmatrix} D_2 - a^2 D_0 & a^2 D_0 \\ \frac{ik}{a^2} R_H D_1 + (R_v - \frac{R_H^2}{24}) D_0 + \frac{R_H^2}{8} z^2 D_0 & D_2 - a^2 D_0 - \frac{ik}{2} R_H z D_0 \end{pmatrix},$$

$$B = \begin{pmatrix} 0 & 0 \\ 0 & iD_0 \end{pmatrix},$$

recalling that in deriving A and B we switch $(-1/2, 1/2)$ to the domain $(-1, 1)$ of the Legendre polynomials. Here $z^m D_n = \langle \sum_{k=1}^N z^m \phi_k^{(n)}, \phi_i \rangle$, where $\phi_k^{(n)} = d^n \phi_k / dz^n$. The matrix representations D_2 and D_0 were derived in Section 7.2 when demonstrating the simplest case, whereas the remaining matrices are given in Appendices C.1 to C.3. All the matrix representations are banded in structure.

An important aspect of this method is its behaviour when the coefficients of the porous equations are functions of z. Using the recurrence formula, (see e.g. Sneddon [87], pg. 68)

$$zL_n = \frac{n+1}{2n+1} L_{n+1} + \frac{n}{2n+1} L_{n-1} \tag{7.11}$$

each $z^n \phi_k$, $n \in \mathbb{N}$ term can be expressed as a combination of Legendre polynomials. This in turn allows the relevant inner product to be evaluated using the orthogonality conditions (7.7), as shown in Appendices C.2 and C.3 for z and z^2, although this becomes computationally taxing for large n, which is addressed in Chapter 8. Due to the inherent nature of the recurrence formula, as the powers of z become larger the bandwidth of the corresponding matrix also grows.

Proposition 7.3.1 If $U(z) \in \mathcal{P}^k(\Omega)$ for some $k \in \mathbb{N}$ then $\langle U(z) D_0, \phi_i \rangle$, $i = 1, \ldots, N$ has bandwidth $2k + 2$.

Proof: Assuming that $m \geq k+1$, by repeated application of recurrence relation (7.11) it clearly follows that

$$U(z) L_{m+1} = a_1 L_{m+k+1} + a_2 L_{m+k} + \ldots + a_{2k} L_{m-k+1},$$

$$U(z) L_{m-1} = b_1 L_{m+k-1} + b_2 L_{m+k-2} + \ldots + b_{2k} L_{m-k-1},$$

for some constants a_i, b_i, $i = 1, \ldots, 2k$. The function $U(z)\phi_m$ can now be represented as

$$\frac{U(z) L_{m+1} - U(z) L_{m-1}}{2m+1} = \sum_{s=0}^{2k+2} c_i L_{m+k+1-s} \tag{7.12}$$

for some constants c_i. Consider row i in the matrix representation of the inner product $\langle UD_0, \phi_i \rangle$. The only terms that are non-zero in the inner product of $U(z)D_0$ and ϕ_i are the $(i+1)^{th}$ or $(i-1)^{th}$ Legendre polynomials. If we consider this using (7.12) we have indices $i+1$ and $i-1$ when $m = i-k+s$ and $m = i-k-2+s$ respectively for $s = 0, \ldots, 2k+2$, for those m which are greater than or equal to 1. At its maximum this yields $2k+3$ distinct values of m, each of which represents an entry into the i^{th} row of the matrix. Hence, as the diagonal term is included in every row, the matrix has bandwidth $2k+2$. □

Table 7.1 presents the leading eigenvalue in the spectrum as obtained using both the Legendre based spectral technique and the Chebyshev tau method with the x - wavenumber $k = 0$, and the y - wavenumber $m = 10$, $R_H = 114.2$ and $R_V = 100$ fixed such that the method determines the value of σ. While we only present one eigenvalue, similar behaviour is observed for other eigenvalues.

N	σ_L	σ_C
14	−0.2934315592	−0.2912641416
16	−0.2934328110	−0.2934658698
18	−0.2934327663	−0.2934479056
20	−0.2934327661	−0.2934319875
22	−0.2934327661	−0.2934327166
24	−0.2934327661	−0.2934327711
26	−0.2934327661	−0.2934327661

Table 7.1: Comparison of the Legendre and Chebyshev tau techniques with the results denoted by σ_L and σ_C respectively, with N being the number of polynomials.

Convergence of both methods is evident from Table 7.1, where the Legendre method clearly requires fewer polynomials to converge to the required accuracy. In fact, the better convergence rate of the Legendre polynomial method is striking since the Chebyshev tau method requires approximately 30% more polynomials to achieve the same accuracy. The results are also in accordance with those published by Straughan & Walker [91].

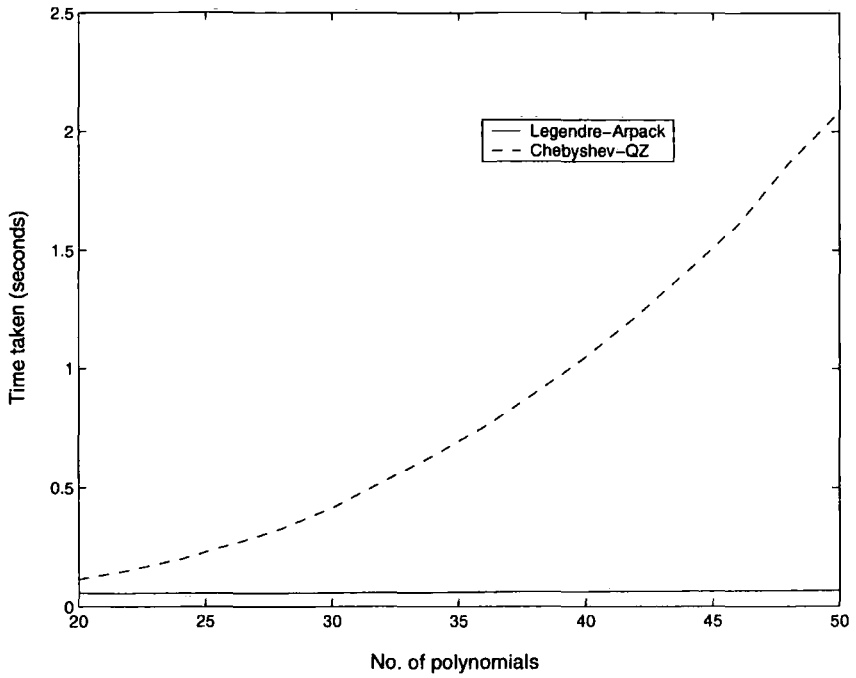

Figure 7.1: Number of polynomials used against computational time

Figure 7.1 provides a visual representation of the computational time required to converge to the first eigenvalue of the spectrum as the number of polynomials is increased. The Legendre-Arpack line refers to the solutions obtained via the Legendre polynomial based spectral method utilising the Arnoldi method obtained from the ARPACK system (see Lehoucq *et al.* [58]), whilst the Chebyshev-QZ line refers to the Chebyshev tau method coupled with the QZ algorithm (see e.g. Golub & Van Loan [28]).

It is clear from Figure 7.1 that as the matrices associated with the generalised eigenvalue problem grow in size the Legendre-Arnoldi method is substantially more computationally efficient than the Chebyshev tau-QZ technique.

7.4 Multi-component convection-diffusion

Here we study another representative porous convection eigenvalue problem. In this case we solve an eighth order system which models multi-component diffusion in a porous medium as presented in Tracey [94]. The size of the system is the

same as that of Chapter 3, which rendered the use of the compound matrix method unuseable.

Consider a porous medium contained in the layer $z \in (0, d)$ with constant boundary temperatures $T = 0°\text{C}$ $(z = 0)$ and $T = T_U \geq 4°\text{C}$ $(z = d)$, respectively. The fluid saturating the porous medium is water and so if $T_U > 4°\text{C}$ the physical picture models a layer of gravitationally unstable water lying beneath a layer which is gravitationally stable (since water has a density maximum at approximately 4°C). This results in convection in the lower layer which may penetrate into the upper layer.

The fluid is assumed to have 2 different species dissolved in it, where we will denote C^β, $\beta = 1, 2$, to be the the concentration of component β. The density is assumed quadratic in the temperature field and linear with respect to these concentrations such that

$$\rho = \rho_0 \left(1 - \alpha(T - 4)^2 + \sum_{\beta=1}^{2} \alpha_\beta (C^\beta - C_0^\beta) \right),$$

where ρ_0 and C_0^β are density and salt references respectively and α and α_β are the thermal and solute coefficients.

Employing Darcy's law to model fluid flow along with the incompressibility condition and the equations of conservation of temperature and solute yields the system

$$\begin{aligned} p_{,i} &= -\frac{\mu}{k} v_i - g\rho_0 \left(1 - \alpha(T - 4)^2 + \sum_{\beta=1}^{2} \alpha_\beta (C^\beta - C_0^\beta) \right) b_i, \\ T_{,t} + v_i T_{,i} &= \kappa \triangle T, \\ C^\beta_{,t} + v_i C^\beta_{,i} &= \kappa_\beta \triangle C^\beta, \end{aligned} \tag{7.13}$$

where the variables p, μ, k, v_i and g represent pressure, dynamic viscosity, permeability, velocity and gravitational acceleration respectively and $\mathbf{b} = (0,0,1)$. The variables κ and κ_β $(\beta = 1, 2)$ represent thermal and solute diffusivities respectively.

Defining a^2 to be the wavenumber, the non-dimensionalised linear perturbation equations arising from (7.13) are

$$\begin{aligned} &(D^2 - a^2)W - 2(\zeta - z)a^2 S - a^2\Psi^1 - a^2\Psi^2 = 0, \\ &(D^2 - a^2)S - RW = \sigma S \\ &(D^2 - a^2)\Psi^1 - R_1 W = P_1 \sigma \Psi^1 \\ &(D^2 - a^2)\Psi^2 - R_2 W = P_2 \sigma \Psi^2 \end{aligned} \tag{7.14}$$

where $D = d/dz$, $\zeta = 4/T_U$, R and R_β are the thermal and solute Rayleigh numbers respectively and the P_β are salt Prandtl numbers. Here W, S, Ψ^1, Ψ^2 are the $z-$dependent parts of the perturbations of velocity, temperature, solute 1, and solute 2. The appropriate boundary conditions are

$$W = S = \Psi^1 = \Psi^2 = 0, \qquad z = 0,\ 1.$$

The Legendre polynomial scheme advocated here applied to (7.14) reduces to solving the generalised matrix eigenvalue problem

$$A\mathbf{x} = \sigma B\mathbf{x},$$

where $\mathbf{x} = (w_1, \ldots, w_N, s_1, \ldots, s_N, \psi_1^1, \ldots, \psi_N^1, \psi_1^2, \ldots, \psi_N^2)$, with ψ_i^α being the coefficients in the expansion of Ψ^α, $\alpha = 1, 2$, in terms of the basis ϕ_i. The matrices A and B given by

$$A = \begin{pmatrix} D_2 - a^2 D_0 & a^2 z D_0 - a^2 b D_0 & -a^2 D_0 & -a^2 D_0 \\ -RD - 0 & D_2 - a^2 D_0 & 0 & 0 \\ -R_1 D_0 & 0 & D_2 - a^2 D_0 & 0 \\ -R_2 D_0 & 0 & 0 & D_2 - a^2 D_0 \end{pmatrix},$$

$$B = \begin{pmatrix} 0 & 0 & 0 & 0 \\ 0 & D_0 & 0 & 0 \\ 0 & 0 & P_1 D_0 & 0 \\ 0 & 0 & 0 & P_2 D_0 \end{pmatrix},$$

where $b = 2\zeta - 1$ with the matrix representations $z^m D_n$ as presented in Section 7.3.

The leading eigenvalue of the spectrum are shown in Table 7.2 for fixed variables $a^2 = 21.344$, $\zeta = 0.14286$, $R = 228.009$, $R_1 = -291.066$, $R_2 = 261$, $P_1 = 4.5454$ and $P_2 = 4.7619$.

Again, the convergence rate of the Legendre polynomial method is striking and requires fewer polynomials to converge to the required accuracy than the Chebyshev tau method. We observe that the Chebyshev tau method requires approximately 75% more polynomials to achieve the same accuracy. Figure 7.2 provides a visual representation of the computational time required to converge to the required

N	σ_L	σ_C
6	−5.60913318	−5.61227689
8	−5.60913183	−5.60921498
10	−5.60913183	−5.60913147
12	−5.60913183	−5.60913180
14	−5.60913183	−5.60913183

Table 7.2: Comparison of the Legendre and Chebyshev tau techniques with the results denoted by σ_L and σ_C respectively, with N being the number of polynomials.

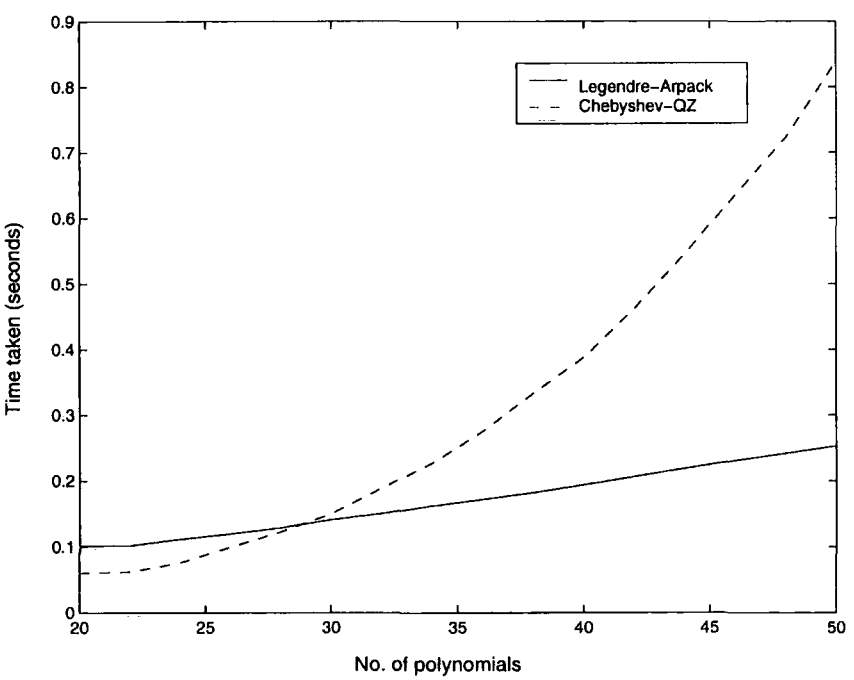

Figure 7.2: Number of polynomials used against computational time

eigenvalue as the number of polynomials is increased. Similarly to Figure 7.1 the Legendre-Arpack line refers to the solutions obtained via the Legendre polynomial based spectral method coupled with the Arnoldi algorithm, whilst the Chebyshev-QZ line refers to the Chebyshev tau method.

Figure 7.2 again demonstrates a high level computational efficiency of the Legendre-Arnoldi method when compared with the Chebyshev tau-QZ technique.

7.5 Structure of the technique for fourth order equations

As shown in Chapter 6, the Navier-Stokes equation is naturally 4th order as opposed to 2nd order from Darcy's law in porous media. When one deals with convection problems in fluid mechanics one is, therefore, usually faced with solving a system comprised of a 4th order equation combined with one or more second order equations. The basis ϕ_i defined in (7.4) is inadequate to cope with the 4th order equation (unless the fluid layer is subject to artificial stress free boundary conditions). Therefore, we now combine the Kirchner [54] technique (which is also used by Shen [85], but not for eigenvalue problems) with the basis in (7.4). To illustrate the idea we restrict attention to the classical Bénard problem, cf. Straughan [90], p. 49.

If a fluid layer is heated from below, once the gravitational effect has been overcome the fluid rises creating convective motion, which is known to as Bénard convection. If we suppose the fluid is contained in the infinite layer $\mathbb{R}^2 \times \{z \in (0, 1)\}$, with fixed upper and lower boundary temperatures, the perturbation equations to the steady state solution are found to be, cf. Straughan [90], p. 50,

$$\begin{aligned} &u_{i,t} + u_j u_{i,j} = -p_{,i} + \triangle u_i + b_i R\theta, \\ &u_{i,i} = 0, \\ &Pr(\theta_{,t} + u_i \theta_{,i}) = Rw + \triangle\theta, \end{aligned} \tag{7.15}$$

where u_i, p and θ are the non-dimensionalised velocity, pressure and temperature respectively, Pr and R are the Prandtl and Rayleigh numbers respectively and $w = u_3$. The boundary conditions are that $u_i = \theta = 0$ on $z = 0, 1$ and u_i, θ satisfy

a plane tiling planform. Note that θ represents a perturbation to the steady state temperature field so the zero boundary conditions on $z = 0, 1$ are consistent. The plan-forms represent the horizontal shape of the convection cells formed at the onset of instablity. These cells form a regular horizontal pattern tiling the (x, y) plane, e.g. hexagons, where the wavenumber a (cf. Straughan [90], p. 51) is a measure of the width (to depth) of the convection cell. Defining $a^2 = k^2 + m^2$ with k and m being the x and y wavenumber, the linearised equations governing instability from (7.15) are

$$\begin{aligned} (D^2 - a^2)^2 W - a^2 RS &= \sigma(D^2 - a^2)W, \\ (D^2 - a^2)S + RW &= \sigma PrS, \end{aligned} \tag{7.16}$$

with boundary conditions

$$W = DW = S = 0, \qquad z = 0,\ 1.$$

Here $W(z)$ and $S(z)$ are the vertical component of velocity and temperature field as functions of z.

For the W part we follow the method of Kirchner [54]. Thus, consider the Hilbert space

$$H_0^2(\Omega) = \{v : v, v', v'' \in L_2(\Omega),\ v(\pm 1) = v'(\pm 1) = 0\}.$$

Here $W \in H_0^2(\Omega)$ and $S \in H_0^1(\Omega)$. The basis functions for the finite dimensional space $S_N \subset H_0^1(\Omega)$ are chosen as in (7.4) and we turn our attention to building a basis for some finite dimensional space $T_N \subset H_0^2(\Omega)$ of dimension $N \in \mathbb{N}$. Defining $T_N = \mathcal{P}^{N+3} \cap H_0^2(\Omega)$ we introduce the set of basis functions for $i = 1, \ldots, N$ as in Kirchner [54], (see also Shen [85], p. 1496), and so define β_i by

$$\begin{aligned} \beta_i(z) &= \int_{-1}^{z}\int_{-1}^{s} L_{i+1}(t)\,dt\,ds \\ &= \int_{-1}^{z}\int_{-1}^{s} \frac{L'_{i+2}(t) - L'_i(t)}{2i+3}\,dt\,ds \\ &= \frac{1}{(2i+3)}\int_{-1}^{z}\left[L_{i+2}(s) - L_i(s)\right]ds \\ &= \frac{L_{i+3} - L_{i+1}}{(2i+3)(2i+5)} - \frac{L_{i+1} - L_{i-1}}{(2i+1)(2i+3)}. \end{aligned} \tag{7.17}$$

By the definition of Legendre polynomials the basis functions β_i are linearly independent, such that $T_N = span\{\beta_i\}$ $i = 1, \ldots, N$ with $N = dim\,(T_N)$, cf. Kirchner [54].

The system (7.16) may now be written in terms of the basis functions, such that

$$\sum_{k=1}^{N} w_k(D^4 - 2a^2D^2 + a^4)\beta_k - a^2R\sum_{k=1}^{N} s_k\phi_k = \sigma\sum_{k=1}^{N}(D^2 - a^2)w_k\beta_k, \quad (7.18)$$

$$\sum_{k=1}^{N} s_k(D^2 - a^2)\phi_k + R\sum_{k=1}^{N} w_k\beta_k = \sigma Pr\sum_{k=1}^{N} s_k\phi_k. \quad (7.19)$$

The method is now to take the inner product of (7.18) with β_i and the inner product of (7.19) with ϕ_i and derive a finite dimensional generalised eigenvalue problem for σ.

The key to the method is that $\beta_i'' = L_{i+1}$ which leads to a diagonal matrix associated with D^4. Since $\beta_i' = (L_{i+2} - L_i)/(2i+3)$ the D^2 operator also leads to a banded matrix. To see this note that

$$\begin{aligned}\langle D^4W, \beta_i\rangle &= -\langle D^3W, \beta_i'\rangle + \beta_i D^3W|_{-1}^{1} \\ &= \langle D^2W, \beta_i''\rangle - \beta_i' D^2W|_{-1}^{1} \\ &= \sum_{k=1}^{N} w_k\langle \beta_k'', \beta_i''\rangle \\ &= \sum_{k=1}^{N} w_k\langle L_{k+1}, L_{i+1}\rangle = \frac{2w_i}{2i+3},\end{aligned}$$

where we have used the forms for β_i, β_i' and the fact that $L_i(\pm 1) = (\pm 1)^i$.

A similar calculation shows that

$$\langle D^2W, \beta_i\rangle = -\left\langle \sum_{k=1}^{N} w_k\frac{L_{k+2} - L_k}{2k+3}, \frac{L_{i+2} - L_i}{2i+3}\right\rangle,$$

which is the $(i+1)^{th}$ row of the matrix representation $-D_0$ as presented Section 7.3.

After some calculations we can show equations (7.18), (7.19) reduce to the generalised eigenvalue problem

$$A\mathbf{x} = \sigma B\mathbf{x}$$

where $\mathbf{x}$=$(w_1, \ldots, w_N, s_1, \ldots, s_N)$, and the matrices A and B are now given by

$$A = \begin{pmatrix} D_4^{\beta}(\beta) - 2a^2D_2^{\beta}(\beta) + a^4D_0^{\beta}(\beta) & -Ra^2D_0^{\beta}(\phi) \\ RD_0^{\phi}(\beta) & D_2^{\phi}(\phi) - a^2D_0^{\phi}(\phi) \end{pmatrix},$$

$$B = \begin{pmatrix} D_2^{\beta}(\beta) - a^2D_0^{\beta}(\beta) & 0 \\ 0 & PrD_0^{\phi}(\phi) \end{pmatrix}.$$

The notation $D_n^a(b)$ is the matrix representation of $\langle \sum_{k=1}^{N} d^n b_k/(dy)^n,\ a_i \rangle$, where a and b are the relevant basis functions. Those matrix representations not defined in both Section 7.3 and this section are presented in Appendices C.4 to C.6.

Table 7.3 presents results for the leading eigenvalue of the spectrum for both the Legendre and D^2 Chebyshev tau techniques, with variables fixed at $a^2 = 5$, $R = 111.3$ and $Pr = 6$. The D^2 Chebyshev technique is used as it is desirable to reduce the order of the differential equations whenever possible when using this spectral technique Dongarra *et al.* [20].

N	σ_L	σ_C
6	9.978751578	9.770168425
8	9.978787315	9.982167291
10	9.978787485	9.978681120
12	9.978787486	9.97878353
14	9.978787486	9.978787384
16	9.978787486	9.978787484
18	9.978787486	9.978787486

Table 7.3: Comparison of the Legendre and Chebyshev tau techniques with the results denoted by σ_L and σ_C respectively, with N being the number of polynomials.

Again both methods converge to the required accuracy, with the Legendre spectral method requiring less polynomials. In fact, the Chebyshev tau method requires approximately 50% more polynomials to achieve the same accuracy. Figure 7.3 provides a visual representation of the computational time required to locate the full spectrum of eigenvalues as the number of polynomials is increased. Similarly to Figure 7.1 the Legendre-Arpack line refers to the solutions obtained via the Legendre polynomial based spectral method coupled with the Arnoldi algorithm, whilst the Chebyshev-QZ line refers to the Chebyshev tau method coupled with the QZ algorithm.

Figure 7.3 again demonstrates a high level computational efficiency even when the full eigenvalue spectrum is calculated.

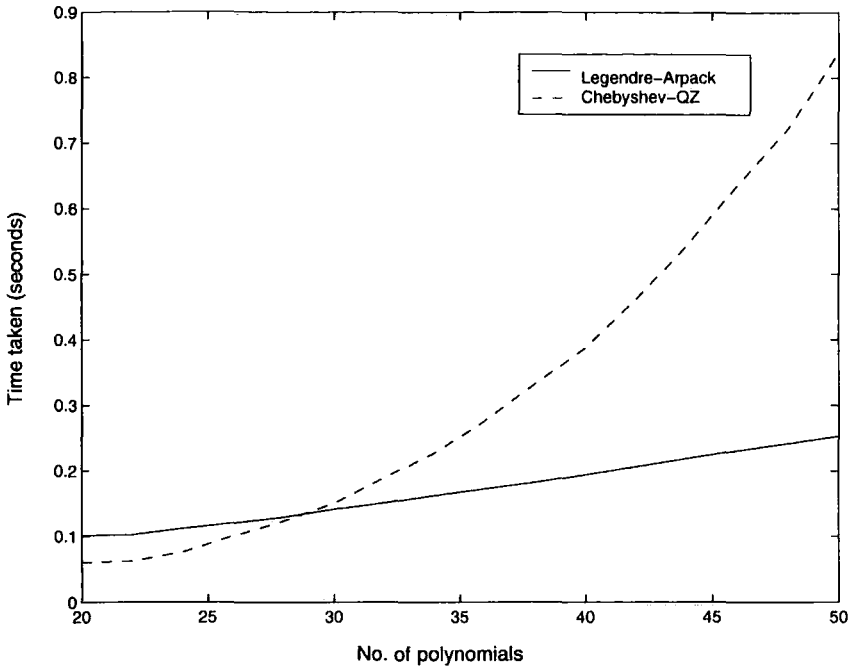

Figure 7.3: Number of polynomials used against computational time

It is worth noting that the generalised eigenvalue problem for the Legendre method employs matrices of order $2N$ compared to matrices of order $3N$ for the D^2 Chebyshev tau technique. There is, therefore, an advantage in using the Legendre method in that smaller matrices are employed. This is a major consideration when employing the basis functions β_i. In a similar manner to the basis functions ϕ_i, $z^n\beta_i$ can be expressed as Legendre polynomials using identity (7.11), which inherently increases the bandwidth of the matrix to as the powers of z increase. In fact, we may now show

Proposition 7.5.1 If $U(z) \in \mathcal{P}^k(\Omega)$ for some $k \in \mathbb{N}$ then $\langle UD_0, \beta_i \rangle$, $i = 1, \ldots, N$ has bandwidth $2k + 8$.

Proof: The proof of Proposition 7.5.1 is analogous to the proof of Proposition 7.3.1. □

7.6 Conclusions

A Legendre polynomial based spectral method is presented for solving stability problems associated with the analysis of porous media, building on the experience gained from employing the well established methods in previous chapters. The specific choice of basis functions leads to sparse matrices, with banded sub-matrices of size $N \times N$, where N is the number of Legendre polynomials used. To capitalise on this inherent structure we make use of a parallel sparse matrix iterative solver. In this chapter we use the implicitly restarted Arnoldi method (IRAM) as presented in the ARPACK package (see Lehoucq *et al.*, [58]). This is seen to substantially reduce the computational and storage requirements as opposed to those needed by the QZ algorithm (see e.g. Golub & Van Loan [28]). Thus, the sparsity of the matrices in the Legendre technique described here is a significant advantage. In Figures 7.1 and 7.3 the Chebyshev tau-QZ technique is seen to be approximately as fast as the Legendre-Arnoldi technique when the number of polynomials is less than 30 or so. In Figure 7.2 when the number of equations is greater, and consequently, the matrices are larger, the Legendre-Arnoldi technique is faster even for a small number of polynomials. Thus, for 2 or 3-D stability problems when a large number of polynomials are required we expect the Legendre-Arnoldi method to be worthy of employment.

The current method is particularly advantageous in that it extends naturally to two and three dimensional eigenvalue problems. This is easily achieved by using tensor products of basis elements in x, y and z.

Sections 7.3 to 7.4 analyse different examples of hydrodynamic systems, which are convection in a porous medium with an inclined temperature gradient (Hadley flow), multi-component convection-diffusion in a porous medium, and Bénard convection in a fluid. The resulting eigenvalue problems are solved using both the Legendre polynomial based and Chebyshev tau spectral techniques. In each of these cases the Legendre polynomial based spectral technique converges to the required eigenvalue utilising less polynomials than the Chebyshev tau method, and with substantially greater computational efficiency, especially since the Legendre technique allows us to employ the Arnoldi algorithm.

Chapter 8

A Chebyshev polynomial based spectral method for eigenvalue problems in hydrodynamic stability

8.1 Introduction

The Legendre polynomial based spectral method developed in Chapter 7 was shown to overcome the dual problems of matrix fullness and boundary conditions, providing a viable, more efficient, alternative to the Chebyshev tau technique. However, (as discussed in Section 7.3) the recurrence formula, (see e.g. Sneddon [87], pg. 68)

$$zL_n = \frac{n+1}{2n+1}L_{n+1} + \frac{n}{2n+1}L_{n-1}$$

must be utilised to express each $z^n l_k$, $n \in \mathbb{N}$ term as a combination of Legendre polynomials, (where l_k a basis function built from Legendre polynomials). The complications this formula generates are twofold. Firstly, the actual evaluation of $z^n l_k$ for any $n \in \mathbb{N}$ and calculation of the inner product $\langle z^n l_k, l_i \rangle$ is a difficult process using this formula, which becomes highly problematic (and therefore prone to human error unless automated) due to its inherent recurrent nature. Couple this with the expanding bandwidth of the corresponding matrix as the powers of z become larger

and the advantages gained by using Legendre based methods become diluted.

The Chebyshev tau technique partially overcomes the problems presented by powers of z due to the formula

$$T_n T_m = \frac{T_{n+m} + T_{|n-m|}}{2} \qquad \forall\, n, m \in \mathbb{N}.$$

When evaluating $z^n T_k$ the polynomial in z can be re-written in terms of Chebyshev polynomials, which, when using this formula, leads to a relatively straightforward evaluation. Thus, the motivation behind developing another polynomial based spectral method based on Chebyshev polynomials is apparent.

Although other research has been conducted on developing Chebyshev spectral methods (see e.g. Shen [86]; Gottlieb & Orszag [29]), the method developed in this chapter is the first technique which combines both sparsity of the matrices in the generalised eigenvalue problem and the inclusion of the standard homogeneous boundary conditions within the method utilising Chebyshev polynomials. The same examples utilised in Chapter 7 are employed due to their use at demonstrating the adaptability, accuracy and relevant ease in implementation of the method. In each example this method is compared to the Chebyshev tau technique to assess accuracy and speed of convergence. In each case the results clearly demonstrate that the Chebyshev spectral method coupled with the Arnoldi technique of finding matrix eigenvalues (see e.g. Lehoucq *et al.* [58]) leads to substantial computational advantages. In a direct comparison between the Chebyshev-Arnoldi and Legendre-Arnoldi methods, the difference in computationally efficiency was found to be proportionally small, although the Legendre method did perform marginally better due to the slightly smaller bandwidth for specific problems. This chapter is constructed in a similar fashion to Chapter 7.

The results in this chapter are also presented in the manuscript Hill [42].

8.2 Structure of the technique for second order equations

Consider the domain $\Omega = (-1, 1)$, with the Hilbert space

$$L^2(\Omega) = \left\{ v : \Omega \to \mathbb{C} \,\middle|\, \int_\Omega |v|^2 dx < \infty \right\}.$$

To motivate the Chebyshev polynomial based spectral technique we begin by demonstrating its application to the equation

$$u'' + \lambda u = 0, \tag{8.1}$$

where $u \in L^2(\Omega)$, and $u|_{\partial\Omega} = 0$.

Denote T_i, $i \in \mathbb{N}$ to be the i^{th} Chebyshev polynomial on $(-1, 1)$ with

$$S_N = \{u \in span\{T_0(z), \ldots, T_{N+1}(z)\} : u|_{\partial\Omega} = 0\}.$$

The numerical approach to the solution of (8.1) is to find $u_N \in S_N$ such that

$$\langle u_N'', v\rangle_\omega + \lambda\langle u_N, v\rangle_\omega = 0 \qquad \forall\, v \in S_N, \tag{8.2}$$

where $\omega(z) = (1-z^2)^{-\frac{1}{2}}$ and $\langle u, v\rangle_\omega = \int_\Omega uv\omega\, dz$ is the inner product in the weighted space $L^2_\omega(\Omega)$, with $\|\cdot\|_\omega$ being the associated norm.

The key aspect in the development of the numerical method is in the choice of basis functions for S_N. In the present literature (see e.g. Shen [86]) the use of a basis function of the form

$$\phi_i(z) = 2(z^2 - 1)T_{i-1}, \quad i = 1, \ldots, N, \tag{8.3}$$

is assumed to lead to full matrices in the relevant linear system, making its use virtually prohibited in practice. Alternate bases are used, such as in Shen [86], although these lead to non-sparse upper triangular matrices. In this paper it is shown that by utilising the properties of the commonly used Chebyshev weight in the inner product, the basis function (8.3) yields a sparse linear system.

The inherent structure of these bases also clearly avoids the need for the superimposition of the standard homogeneous boundary conditions in the resulting matrix, which causes complications in Chebyshev tau analysis.

The following proposition demonstrates the key aspects of the technical implementation of the Chebyshev spectral element method, where we have introduced the notation $\phi_{ij} = \langle \phi_i, \phi_j \rangle_\omega$ and $\phi_{ij}^{(2)} = \langle \phi_i'', \phi_j \rangle_\omega$.

Proposition 8.2.1 Let $\phi_k(z) = 2(z^2-1)T_{k-1}$ where $S_N = span\{\phi_1, \ldots, \phi_N\}$, then

$$\langle \phi_k'', \phi_j \rangle_\omega = \begin{cases} -\frac{\pi}{2}(i^2 - 2i + 3) & j = k,\ k > 1 \\ \frac{\pi}{2} i(i-1) & j = k-2,\ k > 2 \\ \frac{\pi}{2}(i-1)(i-2) & j = k+2,\ k > 1 \end{cases}$$

where $\phi_{11}^{(2)} = -4\pi$, $\phi_{13}^{(2)} = 2\pi$, and

$$\langle \phi_k, \phi_j \rangle_\omega = \begin{cases} \frac{3\pi}{4} & j = k,\ k > 3 \\ -\frac{\pi}{2} & j = k-2,\ k > 4, \quad j = k+2,\ k > 2 \\ \frac{\pi}{8} & j = k-4,\ k > 5, \quad j = k+4,\ k > 1 \end{cases}$$

where $\phi_{11} = 4\pi/2$, $\phi_{22} = \pi/4$, $\phi_{33} = 7\pi/8$, $\phi_{31} = \phi_{13} = -\pi$, $\phi_{42} = \phi_{24} = -3\pi/8$, and $\phi_{15} = \phi_{51} = \pi/4$.

Proof: As the basis functions ϕ_k are linearly independent, their spanning of the space S_N is clear.

The key aspect of this method is in the interpretation of the differential terms. By making use of the divergence theorem, utilising the $z^2 - 1$ term in the basis ϕ_i, and employing the identity $(z^2-1)T_{i-1}' = (i-1)(T_i - T_{i-2})/2$,

$$\begin{aligned} \langle \phi_k'', \phi_i \rangle_\omega &= -\int_\Omega \frac{\phi_k'}{\sqrt{1-z^2}} \left(\phi_i' + \frac{z\phi_i}{1-z^2} \right) dz \\ &= -\int_\Omega \frac{\phi_k'}{\sqrt{1-z^2}} \left(\phi_i' - 2zT_{i-1} \right) dz \\ &= -\int_\Omega \frac{4zT_{k-1} + 2(z^2-1)T_{k-1}'}{\sqrt{1-z^2}} \left(4zT_{i-1} + 2(z^2-1)T_{i-1}' - 2zT_{i-1} \right) dz \\ &= -\langle (k+1)T_k - (k-3)T_{|k-2|}, iT_i - (i-2)T_{|i-2|} \rangle_\omega. \end{aligned}$$

Similarly

$$\langle \phi_k, \phi_i \rangle_\omega = \left\langle \frac{T_{k+1}}{2} - T_{k-1} + \frac{T_{|k-3|}}{2},\ \frac{T_{i+1}}{2} - T_{i-1} + \frac{T_{|i-3|}}{2} \right\rangle_\omega.$$

Employing the inherent orthogonality of Chebyshev polynomials where

$$\langle T_i(z), T_j(z) \rangle_\omega = c_i \frac{\pi}{2} \delta_{ij} \ \forall i, j \geq 0, \tag{8.4}$$

with $c_0 = 2$ and $c_i = 1$ for $i \geq 1$, the results clearly follow. □

Defining the space S_N in terms of the basis functions (8.3), equation (8.2) may be written

$$\left\langle \sum_{k=1}^{N} u_k \phi_k'', \ \phi_i \right\rangle_\omega + \lambda \left\langle \sum_{k=1}^{N} u_k \phi_k, \ \phi_i \right\rangle_\omega = 0 \qquad i = 1, \ldots, N. \tag{8.5}$$

Applying the results in Proposition 8.2.1, (8.5) yields a generalised eigenvalue problem of the form

$$A\mathbf{u} = \lambda B\mathbf{u} \tag{8.6}$$

where $\mathbf{u} = (u_1, \ldots, u_N)^T$.

The sparsity of system (8.6) makes it ideal for specific sparse iterative solvers such as the implicitly restarted Arnoldi method (IRAM) as presented in the ARPACK package (see Lehoucq *et al.* [58]), also used in Chapter 7. As increasing the efficiency of numerical solvers is a key aspect in their development, the notable features of reduced computational and storage requirements compared with the more widely used QZ algorithm (see e.g. Golub & Van Loan [28]) are presented throughout the chapter.

Although the focus of the examples of applying the Chebyshev spectral element method in the paper are based in hydrodynamics, the method easily leads itself to other other areas of Continuum Mechanics such as thermoelastic and viscoelastic flows.

8.3 Hadley Flow

As discussed in Section 7.3, Hadley flow is a useful example as the equations have complex coefficients dependent on the z variable, and can be very sensitive to small variations in the parameters, making it beneficial as a test of the method's accuracy. Following the same derivation and notations as in Section 7.3 we derive the system

$$\begin{aligned} &(D^2 - a^2)W + a^2 S = 0, \\ &(D^2 - a^2 - i\sigma - ik\overline{U}(z))S + ika^{-2}R_H DW - (D\overline{T})W = 0, \end{aligned} \tag{8.7}$$

where $D = d/dz$, subject to the boundary conditions

$$W = S = 0 \qquad z = \pm\frac{1}{2}.$$

The Chebyshev polynomial scheme advocated here applied to (8.7) reduces to solving the generalised matrix eigenvalue problem,

$$A\mathbf{x} = \sigma B\mathbf{x}$$

where $\mathbf{x} = (w_1, \ldots, w_N, s_1, \ldots, s_N)$, and the matrices are given by

$$A = \begin{pmatrix} D_2 - a^2 D_0 & a^2 D_0 \\ \frac{ik}{a^2} R_H D_1 + (R_v - \frac{R_H^2}{24}) D_0 + \frac{R_H^2}{8} z^2 D_0 & D_2 - a^2 D_0 - \frac{ikR_H}{2} z D_0 \end{pmatrix}$$

$$B = \begin{pmatrix} 0 & 0 \\ 0 & iD_0 \end{pmatrix}.$$

Here $z^m D_n = \langle \sum_{k=1}^{N} z^m \phi_k^{(n)}, \phi_i \rangle_\omega$, where $\phi_k^{(n)} = d^n \phi_k / dz^n$. Those not defined in Proposition 8.2.1, are defined in the subsequent proposition, where we have introduced the notation $\phi_{ij}^{(1)} = \langle \phi_i', \phi_j \rangle_\omega$ and $z^k \phi_{ij} = \langle z^k \phi_i, \phi_j \rangle_\omega$.

Proposition 8.3.1 The non-zero elements of D_1, and $z^j D_0$ for $j = 1, \ldots, 2$ are given by

$$\langle \phi_k', \phi_j \rangle_\omega = \begin{cases} -\frac{\pi}{4}(3i - 4) & j = k + 1,\ k > 2 \\ \frac{\pi}{4}(3i - 2) & j = k - 1,\ k > 2 \\ \frac{\pi}{4}(i - 2) & j = k + 3,\ k > 1 \\ -\frac{\pi}{4}(i) & j = k - 3,\ k > 4 \end{cases}$$

where $\phi_{21}^{(1)} = \pi/2$, $\phi_{41}^{(1)} = -\pi/2$, $\phi_{12}^{(1)} = \phi_{23}^{(1)} = -\pi$, $\phi_{41}^{(1)} = -\pi/2$, and $\phi_{14}^{(1)} = \pi$,

$$\langle z\phi_k, \phi_j \rangle_\omega = \begin{cases} \frac{\pi}{8} & j = k + 1,\ k > 3, \quad j = k - 1,\ k > 4 \\ -\frac{3\pi}{16} & j = k + 3,\ k > 2, \quad j = k - 3,\ k > 5 \\ \frac{\pi}{16} & j = k + 5,\ k > 1, \quad j = k - 5,\ k > 6 \end{cases}$$

where $z\phi_{12} = z\phi_{21} = \pi/4$, $z\phi_{23} = z\phi_{32} = -\pi/16$, $z\phi_{34} = z\phi_{43} = 3\pi/16$, $z\phi_{14} =$

$z\phi_{41} = -3\pi/8$, $z\phi_{25} = z\phi_{52} = \pi/8$, and $z\phi_{16} = z\phi_{61} = \pi/8$,

$$\langle z^2\phi_k, \phi_j\rangle_\omega = \begin{cases} \frac{\pi}{8} & j = k,\ k > 4, \\ -\frac{\pi}{32} & j = k+2,\ k > 3, \quad j = k-2,\ k > 5 \\ -\frac{\pi}{16} & j = k+4,\ k > 2, \quad j = k-4,\ k > 6 \\ \frac{\pi}{32} & j = k+6,\ k > 1, \quad j = k-6,\ k > 7 \end{cases}$$

where $z^2\phi_{11} = \pi/4$, $z^2\phi_{22} = 3\pi/32$, $z^2\phi_{33} = \pi/16$, $z^2\phi_{44} = 5\pi/32$, $z^2\phi_{13} = z^2\phi_{31} = \pi/16$, $z^2\phi_{24} = z^2\phi_{42} = -3\pi/32$, $z^2\phi_{15} = z^2\phi_{51} = -\pi/8$, $z^2\phi_{26} = z^2\phi_{62} = -\pi/32$, and $z^2\phi_{17} = z^2\phi_{71} = \pi/16$.

Proof: The term $\langle\phi_k', \phi_i\rangle$ is derived by differentiating the basis function yielding

$$\langle\phi_k', \phi_i\rangle_\omega = \left\langle (k+1)T_k - (k-3)T_{|k-2|}, \frac{T_{i+1}}{2} - T_{|i-1|} + \frac{T_{|i-3|}}{2} \right\rangle_\omega .$$

Evaluating the inner product using (8.4) yields the desired result.

The other two inner products can be easily derived using the identity

$$T_nT_m = \frac{T_{n+m} + T_{|n-m|}}{2} \qquad \forall\ n, m \in \mathbb{N}. \tag{8.8}$$

□

The motivation behind developing this Chebyshev spectral technique was to address the problems generated with the introduction of high order polynomials when employing the Legendre polynomial based spectral method developed in Chapter 7. As discussed in Section 7.3, the recurrence formula (see e.g. Sneddon [87], pg. 68)

$$zL_n = \frac{n+1}{2n+1}L_{n+1} + \frac{n}{2n+1}L_{n-1}$$

must be utilised to express each $z^n l_k$, $n \in \mathbb{N}$ term as a combination of Legendre polynomials, (where l_k a basis function built from Legendre polynomials). The highly problematic (and therefore prone to human error unless automated) evaluation of $z^n l_k$ for any $n \in \mathbb{N}$, calculation of the inner product $\langle z^n l_k, l_i\rangle$ and the expanding bandwidth of the corresponding matrix as the powers of z become larger, make the advantages gained by using Legendre based methods become diluted.

The Chebyshev technique in this chapter partially overcomes the problems presented by powers of z due to the formula (8.8). When evaluating z^nT_k the polynomial

in z can be re-written in terms of Chebyshev polynomials, which, when using this formula, leads to a relatively straightforward evaluation. It is important to note though, that if a function such as e^z is introduced, the bandwidth growth can not be reduced by employing this method over the Legendre variant .

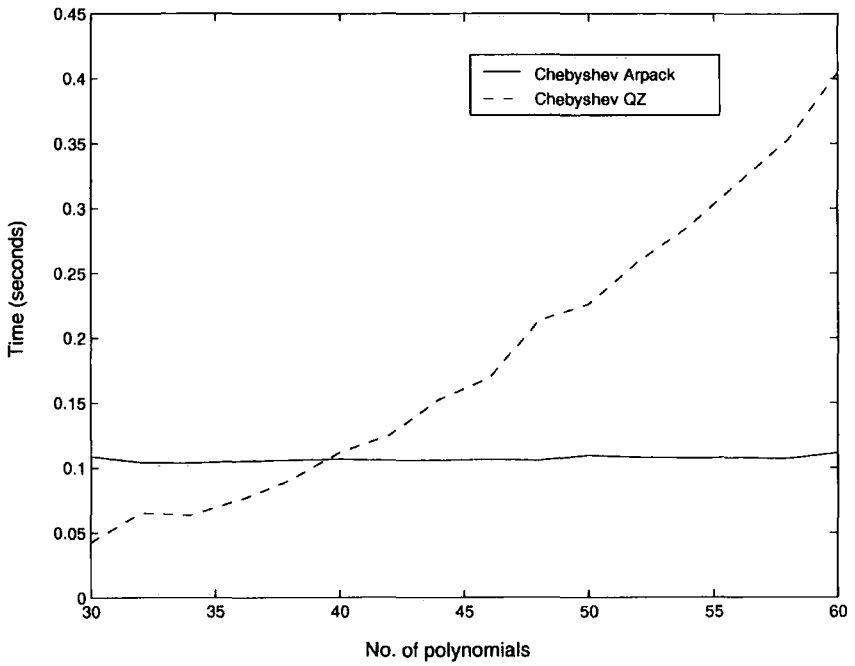

Figure 8.1: Number of polynomials used against computational time

To place the efficiency of the Chebyshev spectral method in context Figure 8.1 provides a visual representation of the computational time required to converge to the first eigenvalue of the spectrum as the number of polynomials is increased. The solutions obtained via the Chebyshev polynomial based spectral method utilising the Arnoldi method obtained from the ARPACK system (see Lehoucq *et al.* [58]) are represented by the Chebyshev-Arpack line, whilst the Chebyshev-QZ line refers to the Chebyshev tau method coupled with the QZ algorithm (see e.g. Golub & Van Loan [28]).

Each method determines the value of σ. where the x - wavenumber $k = 0$, the y - wavenumber $m = 10$, $R_H = 114.2$ and $R_V = 100$ are fixed. The results obtained are also in agreement with those published by Straughan & Walker [91].

Figure 8.1 clearly demonstrates that as the matrices associated with the gener-

alised eigenvalue problem grow in size the Chebyshev-Arnoldi method is substantially more computationally efficient than the Chebyshev tau-QZ technique. In a direct comparison between both the Chebyshev-Arnoldi and Legendre-Arnoldi methods, the Legendre variant was found to be marginally more computationally efficient. The difference is to be expected, as the bandwidth for this specific problem is slightly larger for the Chebyshev variant, although the results are sufficiently close to make any visual representation unnecessary.

8.4 Multi-component convection-diffusion

Here we study another representative porous convection eigenvalue problem. In this case we solve an eighth order system which models multi-component diffusion in a porous medium as presented in Tracey [94] which has been explored in Section 7.4.

Adopting the notation of Section 7.4 the non-dimensionalised linear perturbation equations of the system are

$$\begin{aligned}
&(D^2 - a^2)W - 2(\zeta - z)a^2 S - a^2\Psi^1 - a^2\Psi^2 = 0,\\
&(D^2 - a^2)S - RW = \sigma S\\
&(D^2 - a^2)\Psi^1 - R_1 W = P_1\sigma\Psi^1\\
&(D^2 - a^2)\Psi^2 - R_2 W = P_2\sigma\Psi^2
\end{aligned} \tag{8.9}$$

where $D = d/dz$, $\zeta = 4/T_U$, R and R_β are the thermal and solute Rayleigh numbers respectively and the P_β are salt Prandtl numbers. Here W, S, Ψ^1, Ψ^2 are the $z-$dependent parts of the perturbations of velocity, temperature, solute 1, and solute 2. The appropriate boundary conditions are

$$W = S = \Psi^1 = \Psi^2 = 0, \qquad z = 0,\ 1.$$

The Chebyshev polynomial scheme advocated here applied to (8.9) reduces to solving the generalised matrix eigenvalue problem

$$A\mathbf{x} = \sigma B\mathbf{x},$$

where $\mathbf{x} = (w_1, \ldots, w_N, s_1, \ldots, s_N, \psi_1^1, \ldots, \psi_N^1, \psi_1^2, \ldots, \psi_N^2)$, with ψ_i^α being the coefficients in the expansion of Ψ^α, $\alpha = 1, 2$, in terms of the basis ϕ_i. The matrices A

and B are given by

$$A = \begin{pmatrix} D_2 - a^2 D_0 & a^2 z D_0 - a^2 b D_0 & -a^2 D_0 & -a^2 D_0 \\ -R D_0 & D_2 - a^2 D_0 & 0 & 0 \\ -R_1 D_0 & 0 & D_2 - a^2 D_0 & 0 \\ -R_2 D_0 & 0 & 0 & D_2 - a^2 D_0 \end{pmatrix},$$

$$B = \begin{pmatrix} 0 & 0 & 0 & 0 \\ 0 & D_0 & 0 & 0 \\ 0 & 0 & P_1 D_0 & 0 \\ 0 & 0 & 0 & P_2 D_0 \end{pmatrix},$$

where $b = 2\zeta - 1$. The matrix representations D_2, D_0, and zD_0 are given in Propositions 8.2.1 and 8.3.1.

To place the efficiency of the Chebyshev spectral method in context Figure 8.2 provides a visual representation of the computational time required to converge to the first eigenvalue of the spectrum as the number of polynomials is increased. The solutions obtained via the Chebyshev polynomial based spectral method utilising the Arnoldi method are represented by the Chebyshev-Arpack line, whilst the Chebyshev-QZ line refers to the Chebyshev tau method coupled with the QZ algorithm.

Each method determines the value of σ. where $a^2 = 21.344$, $\zeta = 0.14286$, $R = 228.009$, $R_1 = -291.066$, $R_2 = 261$, $P_1 = 4.5454$ and $P_2 = 4.7619$ are fixed.

Figure 8.2 demonstrates the high level of computational efficiency of the Chebyshev -Arnoldi method when compared with the Chebyshev tau-QZ technique, where no significant difference was found between the Chebyshev-Arnoldi and Legendre-Arnoldi methods.

8.5 Structure of the technique for fourth order equations

To demonstrate the Chebyshev spectral method's further adaptability to coupled second and fourth order equations we turn our attention to the classical Bénard

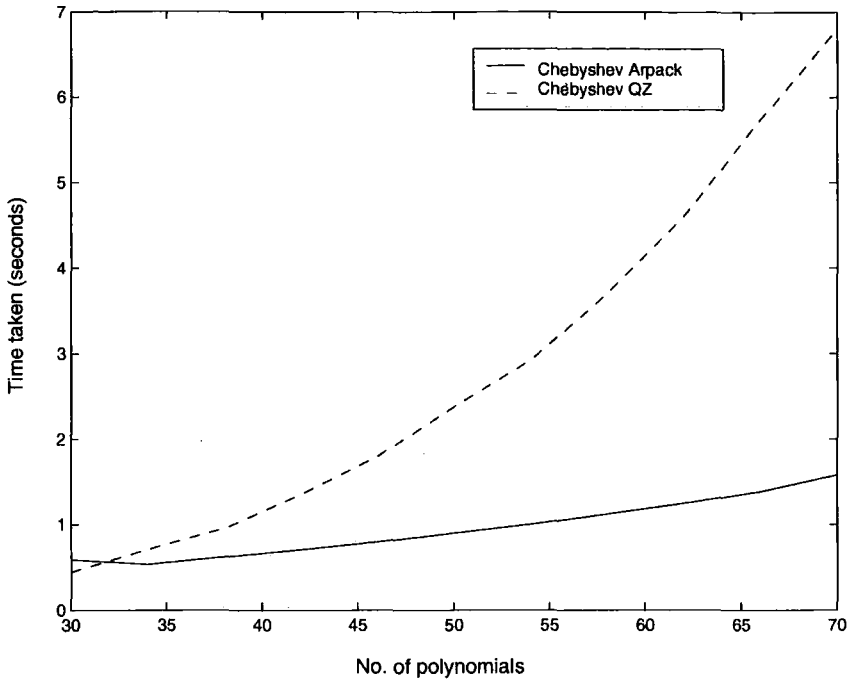

Figure 8.2: Number of polynomials used against computational time

problem in a similar vein to Section 7.5 for the Legendre polynomial based spectral method.

Defining the infinite layer $\mathbb{R}^2 \times \{z \in (0,\ 1)\}$, with fixed upper and lower boundary temperatures, the perturbation equations to the steady state solution are found to be, cf. Straughan [90], p. 50,

$$\begin{aligned} u_{i,t} + u_j u_{i,j} &= -p_{,i} + \triangle u_i + k_i R\theta, \\ u_{i,i} &= 0, \\ Pr(\theta_{,t} + u_i \theta_{,i}) &= Rw + \triangle\theta, \end{aligned} \tag{8.10}$$

where u_i, p and θ are the non-dimensionalised velocity, pressure and temperature respectively, Pr and R are the Prandtl and Rayleigh numbers respectively and $w = u_3$. The boundary conditions are that $u_i = \theta = 0$ on $z = 0, 1$ and u_i, θ satisfy a plane tiling planform. Defining $a^2 = k^2 + m^2$ with k and m being the x and y wavenumber, the linearised equations governing instability from (8.10) are

$$\begin{aligned} (D^2 - a^2)^2 W - a^2 RS &= \sigma(D^2 - a^2)W, \\ (D^2 - a^2)S + RW &= \sigma PrS, \end{aligned} \tag{8.11}$$

with boundary conditions

$$W = DW = S = 0, \qquad z = 0,\ 1.$$

Here $W(z)$ and $S(z)$ are the vertical component of velocity and temperature field as functions of z.

The basis ϕ_i defined in (8.3) is inadequate to cope with the 4th order equation, so a new basis function must be defined that produces sparse matrices and maintains the boundary conditions.

As stated in Section 8.2 the key aspect in the development of the numerical method is in the choice of basis functions for S_N. In the present literature (see e.g. Shen [86]) bases are constructed which lead to non-sparse upper triangular matrices. By observing the behaviour of the basis when differentiated, with special reference to the $(z^2-1)^2$ term which is explained more fully in the proof of Proposition 8.5.1, a basis function of the form

$$\phi_i(z) = (z^2-1)^2 T_{i-1}, \quad i = 1, \ldots, N, \tag{8.12}$$

yields a sparse linear system.

Due to the $(z^2-1)^2$ term in (8.12) the superimposition of the boundary conditions in the resulting matrix is clearly not needed, as both the basis and its first differential satisfy the relevant requirements.

The following proposition demonstrates the key aspects of the technical implementation of the Chebyshev spectral element method to fourth order equations, where we have introduced the notation $\beta_{ij}^{(4)} = \langle \beta_i'''', \beta_j \rangle_\omega$ and $\beta_{ij}^{(2)} = \langle \beta_i'', \beta_j \rangle_\omega$.

Proposition 8.5.1 Let $\beta_k(z) = (z^2-1)^2 T_{k-1}$ where $S_N = span\{\beta_1, \ldots, \beta_{N-2}\}$, then

$$\langle \beta_k'''', \beta_j \rangle_\omega = \begin{cases} \frac{3\pi}{16}(i^4 - 4i^3 + 21i^2 - 34i + 40) & j = k,\ k > 2 \\ -\frac{\pi}{8}(i-1)(i-2)(i^2 - 4i + 15) & j = k+2,\ k > 1 \\ -\frac{\pi}{8} i(i-1)(i^2+11) & j = k-2,\ k > 2 \\ \frac{\pi}{32}(i-4)(i-3)(i-2)(i-1) & j = k+4,\ k > 1 \\ \frac{\pi}{32}(i-1)i(i+1)(i+2) & j = k-4,\ k > 4 \end{cases}$$

where $\beta_{11}^{(4)} = 9\pi$, $\beta_{22}^{(4)} = 15\pi/2$, $\beta_{13}^{(4)} = -6\pi$, $\beta^{(4)}15 = 3\pi/2$, and

$$\langle \beta_k'', \beta_j \rangle_\omega = \begin{cases} -\frac{\pi}{32}(5i^2 - 10i + 17) & j = k,\ k > 3 \\ \frac{\pi}{128}(15i^2 - 55i + 82) & j = k+2,\ k > 3 \\ \frac{\pi}{128}(15i^2 - 5i + 32) & j = k-2,\ k > 4 \\ -\frac{\pi}{64}(3i^2 - 16i + 25) & j = k+4,\ k > 2 \\ -\frac{\pi}{64}(3i^2 + 4i + 5) & j = k-4,\ k > 6 \\ \frac{\pi}{128}(i-4)(i-3) & j = k+6,\ k > 1 \\ \frac{\pi}{128}(i+1)(i+2) & j = k-6,\ k > 7 \end{cases}$$

where $\beta_{11}^{(2)} = -3\pi/4$, $\beta_{22}^{(2)} = -9\pi/32$, $\beta_{33}^{(2)} = -17\pi/16$, $\beta_{13}^{(2)} = 21\pi/32$, $\beta_{24}^{(2)} = 9\pi/16$, $\beta_{31}^{(2)} = 13\pi/16$, $\beta_{24}^{(2)} = 21\pi/32$, $\beta_{35}^{(2)} = 23\pi/16$, $\beta_{15}^{(2)} = -5\pi/8$, $\beta_{26}^{(2)} = -17\pi/32$, $\beta_{51}^{(2)} = -3\pi/8$, $\beta_{62}^{(2)} = -3\pi/8$, $\beta_{17}^{(2)} = 3\pi/16$ and $\beta_{71}^{(2)}) = 3\pi/32$.

Proof: As the basis functions β_k are linearly independent their span of the space S_N is clear.

The key aspect of this method is in the interpretation of the differential terms. Let $\beta_i(z) = (z^2 - 1)\delta_i$ and $\beta_i'(z) = (z^2 - 1)\gamma_i$. By making use of the divergence theorem, and utilising the $z^2 - 1$ term in the basis ϕ_i

$$\begin{aligned} \langle \beta_k'''', \beta_i \rangle_\omega &= \int_\Omega \frac{\beta_k'''}{\sqrt{1-z^2}} \left(-\beta_i' - \frac{z}{1-z^2}\beta_i \right) dz \\ &= \int_\Omega \frac{\beta_k'''}{\sqrt{1-z^2}} (-\beta_i' + z\delta_i)\ dz \\ &= \int_\Omega \frac{\beta_k''}{\sqrt{1-z^2}} \left(\beta_i'' - z\gamma_i - \delta_i - z\delta_i' + z^2 T_{i-1} \right) dz \\ &= \frac{1}{16}\langle (k+3)(k+2)T_{k+1} - 2(k-3)(k+1)T_{k-1} \\ &\quad -(k-5)(k-4)T_{|k-3|}, \\ &\quad (i+2)(i+1)T_{i+1} - 2(i-1)^2 T_{i-1} + (i-4)(i-3)T_{|i-3|} \rangle_\omega. \end{aligned}$$

Similarly

$$\begin{aligned} \langle \beta_k'', \beta_i \rangle_\omega &= \frac{1}{64}\langle (k+3)(k+2)T_{k+1} - 2(k-3)(k+1)T_{k-1} \\ &\quad -(k-5)(k-4)T_{|k-3|}, \\ &\quad T_{i+3} - 4T_{i+1} + 6T_{i-1} - 4T_{|i-3|} + T_{|i-5|} \rangle_\omega. \end{aligned}$$

Employing the inherent orthogonality of Chebyshev polynomials defined in (8.4) the results clearly follow. □

After some calculations we can show equations (8.11) reduce to the generalised eigenvalue problem

$$A\mathbf{x} = \sigma B\mathbf{x}$$

where $\mathbf{x}=(w_1, \ldots, w_N, s_1, \ldots, s_N)$, and the matrices A and B are now given by

$$A = \begin{pmatrix} D_4(\beta) - 2a^2 D_2(\beta) + a^4 D_0(\beta) & -Ra^2 D_0^{\phi}(\beta) \\ RD_0^{\beta} & D_2 - a^2 D_0 \end{pmatrix},$$

$$B = \begin{pmatrix} D_2(\beta) - a^2 D_0(\beta) & 0 \\ 0 & PrD_0 \end{pmatrix}.$$

Here D_2 and D_0 are the matrix representations defined for the basis function ϕ_i in Propositions 8.2.1 and 8.3.1, whereas $D_4(\beta)$ and $D_2(\beta)$ are the matrix versions of the inner products $\langle \beta_k'''', \beta_j \rangle_\omega$ and $\langle \beta_k'', \beta_j \rangle_\omega$, as presented in Proposition 8.5.1. The matrices $D_0(\beta)$, D_0^{β} and $D_0^{\phi}(\beta)$, corresponding to $\langle \beta_k, \beta_i \rangle_\omega$, $\langle \beta_k, \phi_i \rangle_\omega$, and $\langle \phi_k, \beta_i \rangle_\omega$ respectively, can be trivially derived by utilising (8.8).

Figure 8.3 provides a visual representation of the computational time required to locate the full spectrum of eigenvalues as the number of polynomials is increased. Similarly to previous figures the Chebyshev-Arpack line refers to the solutions obtained via the Chebyshev spectral method coupled with the Arnoldi algorithm, whilst the Chebyshev-QZ line refers to the Chebyshev tau method coupled with the QZ algorithm.

The results in Figure 8.3 again clearly demonstrate a high level computational efficiency even when the full eigenvalue spectrum is calculated. In a direct comparison between both the Chebyshev-Arnoldi and Legendre-Arnoldi methods, the Legendre variant was found to be marginally more computationally efficient. The minute difference is to be expected, as the bandwidth for this specific problem is slightly larger for the Chebyshev variant, although the results are sufficiently close to make any visual representation unnecessary. There is another advantage in using the Chebyshev spectral method in that matrices of order $2N$ compared to matri-

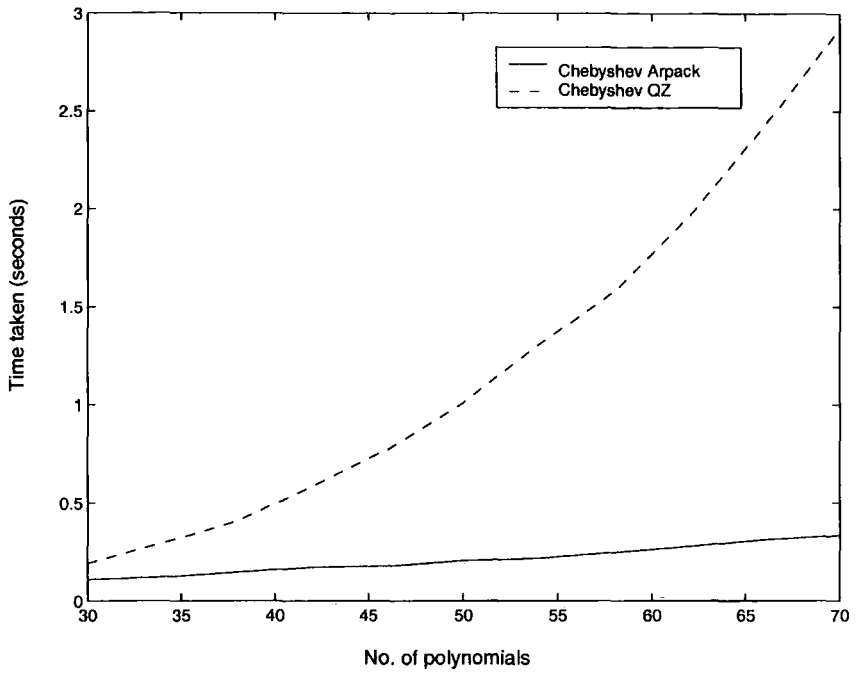

Figure 8.3: Number of polynomials used against computational time

ces of order $3N$ for the D^2 Chebyshev tau technique are utilised, again reduces computational costs.

8.6 Comparison of the Chebyshev and Legendre-Arnoldi techniques

The conclusions of this chapter with regards to the comparison between the Chebyshev polynomial based spectral method and the Chebyshev tau technique are analogous to those of Chapter 7. In essence the method is more computationally efficient than the Chebyshev tau technique for standard homogeneous boundary condition problems, and it is demonstrated that it is a viable technique to employ.

Both the Legendre polynomial based method of Chapter 7 and the Chebyshev variant of this chapter have the advantages of sparsity and inclusion of the standard homogeneous boundary conditions. However, understanding the differences between the methods is key to deciding which is best to employ for a specific problem.

As highlighted in Sections 8.1 and 8.3 the primary difference between the meth-

ods is their ability to absorb high order polynomials into the basis functions the methods are based on. Due to the Legendre recurrence formula, high order polynomials are difficult to evaluate when combined with Legendre basis functions, and lead to bandwidth growth of the corresponding matrix. In the Chebyshev case, these high order polynomials can be easily written in terms of Chebyshev polynomials and evaluated.

However, if polynomials of low order (the evaluation of those below z^4 required acceptable time consumption to evaluate) are employed, the Legendre method does perform marginally better as the corresponding matrices have lower bandwidths. It is also important to note that if a function such as e^z is introduced, the bandwidth growth can not be reduced by employing the Chebyshev over the Legendre variant .

Although these methods have been shown to perform competently in comparison with the Chebyshev tau technique, it must be pointed out that they are, in their current form, only applicable to homogeneous boundary conditions. The Chebyshev tau technique can be adapted to any boundary conditions, see e.g. Chapter 6. However, it is possible to use different combinations of the polynomials to tailor to the boundary conditions of the particular problem. For example, a Chebyshev polynomial based method was developed for a problem which was homogeneous for the function, first and third derivatives, which was certainly not a trivial extension of the method presented in this chapter.

Although we have concentrated on hydrodynamic problems, the methods presented in Chapters 7 and 8 can be adapted to many other classes of stability problem in Continuum Mechanics. For example, stability in porous media with different governing laws such as that of Brinkman, viscoelastic flows, and stability problems in elasticity or thermoelasticity.

Chapter 9

Conclusions

The main aims of the thesis have been to investigate thermal convection in fluid and porous media, and to develop efficient spectral finite element methods to improve on the more commonly used techniques for these types of problems. Linear instability and nonlinear stability analyses have been employed to assess critical thresholds for the onset and type of convection involved, where a variety of numerical methods have been utilised including those developed in the thesis.

Chapters 2 to 5 thoroughly explored convection induced by the selective absorption of radiation in a porous medium, which is a modification of the system modelled by Krishnamurti [55]. This model has not been particularly explored in the current literature even though it provides a closer model of cumulus convection as it occurs in the atmosphere.

In Chapter 2 a standard Darcy model for fluid flow in porous media was adopted, with a linear temperature dependent density. The thresholds of the nonlinear theory, which guarantee stability when the Rayleigh number is below them, were shown to be extremely close to the thresholds of the linear energy theory which guarantee instability. As the region of potential subcritical instabilities were extremely small it can be concluded that linear theory is accurate enough to predict the onset of convective motion for this model within the restrictions of the parameter ranges.

However, Amahmid *et al.* [4] proposed that for sparsely packed porous media (more appropriate to this model as potential refraction is decreased) the Brinkman model, which accounts for friction due to macroscopic shear, is more appropriate

to describe fluid flows in a porous matrix. This model was employed in Chapter 3. Again it was demonstrated that linear and nonlinear thresholds were extremely close. Employing the compound matrix method in both the linear and nonlinear numerical analysis became problematic due to the high order of the equations, with the Chebyshev tau technique also being restrictive due to the heavy computational cost in solving full matrix eigenvalue problems required over several parameter ranges. This lead to the development of the methods in Chapters 7 and 8 to overcome these difficulties.

In Chapters 2 and 3 the assumption was made that the internal heat source was linear with respect to concentration. However, it is stated in Krishnamurti [55] that 'This linear relationship is a first order approximation and may need modification for high concentrations of [thymol] blue'. Thus Chapter 4 was motivated by the exploration of the validity of an alternative quadratic model. Both the Darcy and Forchheimer equations were used. It is observed that an increase in either γ_1 or γ_2 causes the Rayleigh number to decrease, where γ_1 and γ_2 contain the constants of proportionality relating the linear and quadratic elements of the internal heat source respectively. More interestingly though is the observation that γ_1 and γ_2 have an almost identical effect on the Rayleigh number in relation to each other. This demonstrates that a variation change in γ_2 will be as equally significant to a change in the Rayleigh number as a variational change to γ_1.

Both the conditional and unconditional nonlinear analyses showed that when γ_1 was the dominant term over γ_2 the thresholds of the linear and nonlinear theory are extremely close, so that potential region of subcritical instabilities is small, implying that the linear theory effectively captures the onset of convective motion. In contrast, as the magnitude of γ_2 approached that of γ_1 and beyond, the potential region of subcritical instabilities increased greatly, for a given accuracy. These results indicate that linear theory may fail to accurately capture the physics of the onset of convection.

The final avenue of interesting exploration was in the density term. Although it had been assumed neglible previously, a natural progression was to due to introduce the concentration of the species into the density, as presented in Chapter 5. The

γ term, in essence, was defined to be a measure of the internal heat source, such that both the actual numerical and approximate analytical results strongly suggested the existence of a critical γ_c value, where no oscillatory convection occured for $\gamma_c \leq \gamma$. With the extrapolation of oscillatory results from the numerical analysis, a fixed range for γ_c was derived by direct comparison between the stationary and oscillatory neutral lines. However, the analysis did suggest a nonlinear relationship between the critical thermal and solute Rayleigh numbers such that this range is not optimal. The suggested nonlinear behaviour also potentially yielded finite intervals of oscillatory convection, as demonstrated by Figure 5.5. This behaviour, in the present literature, is an apparently unobserved phenomenon. Further work could extend the regions of parameters to assess more accuarately some of the features of the γ_c term. Similarly to Chapter 3, the Chebyshev tau technique was found to be restrictive due to the heavy computational cost in solving full matrix eigenvalue problems required over several parameter ranges.

Chapter 6 presented the problem of thermal convection in a linearly viscous fluid in a finite box. The linear instability threshold was found to be well above the global stability boundary found through the energy method, as visually demonstrated by Figure 6.1. This contradicts previous work by Georgescu and Mansutti [25] who claim that the thresholds coincide.

Chapters 7 and 8 presented Legendre and Chebyshev polynomial based spectral methods, respectively, for the evaluation of generalised eigenvalue problems, developed on the experience of the numerical analysis of Chapters 2 to 6. A polynomial based structure adopted by the Chebyshev tau technique was decided to be the best approach, if the dual problems of matrix fullness and spurious eigenvalues linked to boundary conditions inherent in this method could be addressed. The methods developed generate sparse matrices, where the standard homogeneous boundary conditions for porous media problems are contained within the method, negating the need for their superimposition onto the matrices as is necessary with the Chebyshev tau method. Examples in comparison to the widely used Chebyshev tau method clearly demonstrate that both Legendre/Chebyshev methods coupled with the Arnoldi technique of finding matrix eigenvalues leads to substantial com-

putational advantages.

The Legendre idea employed was introduced for the solution of differential equations by Shen [85], where no eigenvalue calculations were considered. Kirchner [54] developed a method for solving eigenvalues for the Orr - Sommerfeld equation which essentially uses the technique of Shen [85]. By contrast a Chebyshev variation with the sparsity and inclusion of boundary conditions is not present in the literature.

Although the Legendre technique shares the sparsity and boundary condition advantages of the Chebyshev spectral method, due to Legendre polynomials' recurrence formula (see Sneddon [87]) the inclusion of high order polynomials in the targeted problem results in complicated evaluation and growth in the bandwidth of the corresponding generalised matrix eigenvalue problem (see Chapter 8). These disadvantages can be eased by utilising Chebyshev polynomials.

Further work could assess the practicality of developing techniques for non-homogeneous boundary conditions utilising Chebyshev and Legendre techniques.

Although the thesis has concentrated on convection problems, the new methods presented can be adapted to many other classes of stability problem in Continuum Mechanics. For example, stability in porous media with a different governing law such as that of Brinkman, viscoelastic flows, and stability problems in elasticity or thermoelasticity.

Appendix A

Numerical Methods

A.1 The Compound Matrix Method

To demonstrate the implementation of the compound matrix method we consider a general linear system

$$\begin{aligned} \psi'' &= a_1\psi' + a_2\psi + a_3\rho' + a_4\rho, \\ \rho'' &= b_1\rho' + b_2\rho + b_3\psi' + b_4\psi, \end{aligned} \tag{A.1.1}$$

where a prime denotes differentiation with respect to x, $a_1, \ldots, a_4$ and $b_1, \ldots, b_4$ are real and/or complex coefficients which contain the generalised eigenvalue of the system σ, and $x \in (0, 1)$. The boundary conditions

$$\psi = \rho = 0 \qquad z = 0, 1 \tag{A.1.2}$$

are assumed.

To solve (A.1.1) subject to (A.1.2) the compound matrix method is applied as follows.

Let $\boldsymbol{\psi} = (\psi, \psi', \rho, \rho')^T$ and suppose $\boldsymbol{\psi_1}$ and $\boldsymbol{\psi_2}$ are independent solutions to (A.1.1) with values at $z = 0$ of (0,1,0,0) and (0,0,0,1) respectively. The two initial value problems can be integrated numerically between 0 and 1, and the solution found by writing it as a linear combination of the two solutions obtained i.e.

$$\psi = c_1\psi_1 + c_2\psi_2, \qquad \rho = c_1\rho_1 + c_2\rho_2,$$

for some constants c_1 and c_2. Then, the correct boundary conditions $\psi = \rho = 0$ at $z = 1$ are imposed which require

$$det \begin{pmatrix} \psi_1 & \psi_2 \\ \omega_1 & \omega_2 \end{pmatrix} = 0.$$

Due to the potentially large values involved, the calculation of the determinant can lead to large round off errors which can significantly alter the results. To overcome this problem we define the variables $y_1, \ldots, y_6$ to be the 2×2 minors of the 4×2 solution matrix whose columns are $\boldsymbol{\psi_1}$ and $\boldsymbol{\psi_2}$. Thus,

$$\begin{aligned} y_1 &= \psi_1\psi_2' - \psi_2\psi_1', & y_2 &= \psi_1\rho_2 - \psi_2\rho_1, \\ y_3 &= \psi_1\rho_2' - \psi_2\rho_1', & y_4 &= \psi_1'\rho_2 - \psi_2'\rho_1, \\ y_5 &= \psi_1'\rho_2' - \psi_2'\rho_1', & y_6 &= \rho_1\rho_2' - \rho_2\rho_1'. \end{aligned}$$

Differentiating the $y's$ and using the governing system (A.1.1), the initial value problem for the compound matrix variables are found to be

$$\begin{aligned} y_1' &= a_1y_1 + a_4y_2 + a_3y_3, \\ y_2' &= y_3 + y_4, \\ y_3' &= b_1y_1 + b_4y_2 + b_3y_3, \\ y_4' &= a_2y_2 + a_4y_1 + y_5 - a_3y_6, \\ y_5' &= -b_2y_1 + a_2y_3 + b_4y_4 + (a_1 + b_3)y_5 + a_4y_6, \\ y_6' &= -b_2y_2 - b_1y_4 + b_3y_6. \end{aligned}$$

This system can now be numerically integrated subject to the initial condition

$$y_5(0) = 1$$

and the final condition

$$y_2(1) = 0$$

to derive σ to some pre-defined degree of accuracy.

More details and a through discussion of the compound matrix method can be found in Brown & Marletta [9], Davies [18], Drazin & Reid [21], Gardner *et al.* [24], Greenberg & Marletta [30] [31] [32], Ivansson [46] and Straughan & Walker [91].

A.2 The Chebyshev Tau Method

To demonstrate the implementation of the Chebyshev tau algorithm we consider a similar system as introduced in Dongarra *et al.* [20] where

$$\begin{aligned} u'' + \lambda u &= 0, \quad x \in (-1,1), \\ u(-1) &= u(1) = 0. \end{aligned} \tag{A.2.3}$$

The notation $\langle u, v\rangle_\omega = \int_{-1}^{1} uv\omega\, dz$ refers to the inner product in the weighted space $L^2_\omega(-1,1)$, where $\omega(z) = (1-z^2)^{-\frac{1}{2}}$ with $\|\cdot\|_\omega$ being the associated norm.

The underlying principle is to write u as a finite series of Chebyshev polynomials such that

$$u(x) = \sum_{k=0}^{N+2} u_k T_k(x). \tag{A.2.4}$$

Due to the truncation of the infinite series the problem may be re-written

$$u'' + \lambda u = \tau_1 T_{N+1} + \tau_2 T_{N+2}, \tag{A.2.5}$$

where τ_1 and τ_2 are parameters which may be used to quantify the error associated with the truncation in (A.2.4). The use of these tau coefficients as error bounds can be found in Fox [23], although the approach is for ordinary differential equations as opposed the eigenvalue problems.

In the weighted space $L^2_\omega(-1,1)$ the Chebyshev polynomials are orthogonal, so taking the weighted inner product of (A.2.5) with T_i yields

$$\begin{aligned} \langle u'' + \lambda u, T_i\rangle_\omega &= 0, \quad i = 0,1,\ldots,N, \\ \langle u'' + \lambda u, T_{N+j}\rangle_\omega &= \tau_j \|T_{N+j}\|^2_\omega, \quad j = 1,2. \end{aligned} \tag{A.2.6}$$

The two remaining conditions are derived from the boundary conditions where, as $T_n(\pm 1) = (\pm 1)^n$,

$$\sum_{k=0}^{N+2} (\pm 1)^k u_k = 0, \qquad \sum_{k=0}^{N+2} u_k = 0. \tag{A.2.7}$$

The $(N+3)$ unknowns u_i, $i = 0,\ldots,N+2$ can now be derived from the $(N+3)$ equations comprising of (A.2.6) and (A.2.7).

The derivative of a Chebyshev polynomial can be expressed as a linear combination of lower order Chebyshev polynomials where

$$T_n' = \begin{cases} 2n(T_1 + T_2 + \cdots + T_{n-1}), & n \text{ even}, \\ nT_0 + 2n(T_2 + T_3 + \cdots + T_{n-1}), & n \text{ odd}. \end{cases} \tag{A.2.8}$$

To evaluate the differential terms in the Chebyshev tau technique we begin by differentiating (A.2.4) to yield

$$u' = \sum_{k=0}^{N+2} u_k T_k'(x) = \sum_{k=0}^{N+2} \sum_{r=0}^{N+2} u_k D_{rk} T_r. \tag{A.2.9}$$

Comparing the coefficients in (A.2.8) and (A.2.9) it can be deduced that the non-zero terms are

$$\begin{aligned} D_{0,2j-1} &= 2j - 1, & j \geq 1, \\ D_{i,i+2j-1} &= 2(i + 2j - 1), & i \geq 1,\ j \geq 1. \end{aligned} \tag{A.2.10}$$

When solving a generalised eigenvalue probelm this is utilised in its matrix form, namely

$$D = \begin{pmatrix} 0 & 1 & 0 & 3 & 0 & 5 & 0 & 7 & \cdots \\ 0 & 0 & 4 & 0 & 8 & 0 & 12 & 0 & \cdots \\ 0 & 0 & 0 & 6 & 0 & 10 & 0 & 14 & \cdots \\ \vdots & & & & \ddots & & & & \cdots \\ 0 & & & & & & & & \end{pmatrix}.$$

Differentiating (A.2.9) yields

$$u'' = \sum_{k=0}^{N+2} \sum_{r=0}^{N+2} u_k D_{rk} T_r' = \sum_{k=0}^{N+2} \sum_{r=0}^{N+2} \sum_{p=0}^{N+2} D_{pr} D_{rk} u_k T_p. \tag{A.2.11}$$

By utilising (A.2.10) and the identity (A.2.8) it can be deduced from (A.2.11) that

$$\begin{aligned} D^2_{0,2j} &= \frac{1}{2}(2j)^3, \quad j \geq 1, \\ D^2_{i,i+2j} &= (i + 2j)4j(i + j), \quad i \geq 1,\ j \geq, 1, \end{aligned}$$

or in matrix form as

$$D^2 = \begin{pmatrix} 0 & 0 & 4 & 0 & 32 & 0 & 108 & \cdots \\ 0 & 0 & 0 & 24 & 0 & 120 & 0 & \cdots \\ 0 & 0 & 0 & 0 & 48 & 0 & 192 & \cdots \\ \vdots & & & & \ddots & & & \cdots \\ 0 & & & & & & & \end{pmatrix}.$$

With these definitions the Chebyshev tau approximation to the orginal problem (A.2.3) would be written as

$$D^2\mathbf{u} = -\lambda I\mathbf{u},$$

where I is the $(N+2)\times(N+2)$ identity matrix and $\mathbf{u} = (u_0, \ldots, u_{N+2})$. To incoporate the boundary conditions the last two rows of D^2 are replaced with

$$\begin{pmatrix} 1 & 0 & 1 & \ldots & 1 & 0 \\ 0 & 1 & 0 & \ldots & 0 & 1 \end{pmatrix},$$

and the last two rows of I are replaced with zeros.

More details and a through discussion of the Chebyshev tau method can be found in Straughan & Walker [91] and Dongarra *et al.* [20].

Appendix B

Inequalities

B.1 Young's Inequality

Let a, b be arbitrary functions and $p, q \geq 1$ such that $1/p + 1/q = 1$, then Young's inequality is

$$ab \leq \frac{a^p}{p} + \frac{b^q}{q}.$$

Further discussion of Young's inequality can be found in Young [98] and Mitrinovic [72].

B.2 Poincaré's Inequality

Let V be a three dimensional cell, where, for simplicity, the cell has dimensions $0 \leq x < 2a_1$, $0 \leq y < 2a_2$, and $0 < z < 1$. Suppose u is a function periodic in x and y of period $2a_1$ and $2a_2$ repectively, and $u = 0$ on $z = 0, 1$. Then the Poincaré inequality may be written

$$\int_V u^2 \, dV \leq \frac{1}{\pi^2} \int_V |\nabla u|^2 \, dV.$$

Further discussion of the Poincaré inequality can be found in Saloff-Coste [83].

B.3 Sobolev Inequality

If Ω is a bounded domain in $\mathbb{R}^3$ with boundary $\partial\Omega$, then for functions with $u = 0$ on $\partial\Omega$,

$$\left(\int_\Omega u^6\, dV\right)^{\frac{1}{3}} \leq C_1 \int_\Omega |\nabla u|^2\, dV,$$

where the constant C_1 is independent of the domain. Furthermore, combining this with Hölder's inequality for u^4,

$$\int_\Omega u^4\, dV \leq C_2 \left(\int_\Omega u^6\, dV\right)^{\frac{2}{3}},$$

we derive the inequality

$$\int_\Omega u^4\, dV \leq C_3 \left(\int_\Omega |\nabla u|^2\right)^2 dV.$$

Further explanation of this Sobolev inequality can be found on pages 388-391 of Straughan [90].

Appendix C

Legendre Spectral Method Identities

Throughout Appendix C the notation $D_n^a(b)$ is defined as the matrix representation of $\langle \sum_{k=1}^{N} d^n b_k/(dy)^n,\ a_i \rangle$, where a and b are the relevant basis functions.

C.1 Calculation of $D_1^{\phi}(\phi)$

Utilising the identity (7.3) $D_1^{\phi}(\phi)$ may be written

$$\left\langle \sum_{k=1}^{N} \phi_k',\ \phi_i \right\rangle = \left\langle \sum_{k=1}^{N} L_k,\ \frac{L_{i+1} - L_{i-1}}{2i+1} \right\rangle.$$

By applying the orthogonality relationship in (7.7), the skew-symmetric matrix representation $D_1^{\phi}(\phi)$ can be derived, where, letting $M = D_1^{\phi}(\phi)$,

$$M_{i,\,i+1} = \frac{2}{(2i+1)(2i+3)}, \qquad i = 1, \ldots, N-1,$$

where M is of bandwidth 2.

C.2 Calculation of $zD_0^{\phi}(\phi)$

Using the basis functions (7.4) and the recurrence relation (7.11) we have

$$\left\langle \sum_{k=1}^{N} z\phi_k,\ \phi_i \right\rangle = \left\langle \sum_{k=1}^{N} \left(\frac{(k+2)L_{k+2}}{(2k+3)(2k+1)} - \frac{L_k}{(2k-1)(2k+3)} - \frac{(k-1)L_{k-2}}{(2k-1)(2k+1)} \right),\ \frac{L_{i+1} - L_{i-1}}{2i+1} \right\rangle.$$

By applying the orthogonality relationship in (7.7), the symmetric matrix representation $zD_0^{\phi}(\phi)$ can be derived, where, letting $M = zD_0^{\phi}(\phi)$,

$$M_{i,j} = \begin{cases} \dfrac{2(i+1)}{(2i-1)(2i+1)(2i+3)(2i+5)} & j = i+1 \\ \dfrac{-2(i+2)}{(2i+1)(2i+3)(2i+5)(2i+7)} & j = i+3 \end{cases}$$

where M is of bandwidth 6.

C.3 Calculation of $z^2 D_0^{\phi}(\phi)$

Using the basis functions (7.4) and repeatedly applying the recurrence relation (7.11) we have

$$\left\langle \sum_{k=1}^{N} z^2 \phi_k,\ \phi_i \right\rangle = \left\langle \sum_{k=1}^{N} \left(\frac{(k+2)(k+3)L_{k+3}}{(2k+3)(2k+5)(2k+1)} + \frac{(k^2+k-3)L_{k+1}}{(2k-1)(2k+5)(2k+1)} - \frac{(k^2+k-3)L_{k-1}}{(2k-3)(2k+3)(2k+1)} - \frac{((k-1)(k-2))L_{k-3}}{(2k-1)(2k-3)(2k+1)} \right), \frac{L_{i+1} - L_{i-1}}{2i+1} \right\rangle.$$

By applying the orthogonality relationship in (7.7)), the symmetric matrix representation $z^2 D_0^{\phi}(\phi)$ can be derived, where, letting $M = z^2 D_0^{\phi}(\phi)$,

$$M_{i,j} = \begin{cases} \dfrac{4(i^2+i-3)}{(2i-3)(2i-1)(2i+1)(2i+3)(2i+5)} & j = i \\ \dfrac{6}{(2i-1)(2i+1)(2i+3)(2i+5)(2i+7)} & j = i+2 \\ \dfrac{-2(i+3)(i+2)}{(2i+1)(2i+3)(2i+5)(2i+7)(2i+9)} & j = i+4 \end{cases},$$

where M is of bandwidth 8.

C.4 Calculation of $D_0^{\beta}(\beta)$

Using the basis functions (7.17)) we have

$$\left\langle \sum_{k=1}^{N} \beta_k,\ \beta_i \right\rangle = \left\langle \sum_{k=1}^{N} \frac{(L_{k+3} - L_{k+1})}{(2k+3)(2k+5)} - \frac{(L_{k+1} - L_{k-1})}{(2k+1)(2k+3)}, \frac{L_{i+3} - L_{i+1}}{(2i+3)(2i+5)} - \frac{L_{i+1} - L_{i-1}}{(2i+1)(2i+3)} \right\rangle.$$

By applying the orthogonality relationship in (7.7), the symmetric matrix representation $D_0^{\beta}(\beta)$ can be derived, where, letting $M = D_0^{\beta}(\beta)$,

$$M_{i,j} = \begin{cases} \dfrac{12}{(2i-1)(2i+1)(2i+3)(2i+5)(2i+7)} & j = i \\ \dfrac{-8}{(2i+1)(2i+3)(2i+5)(2i+7)(2i+9)} & j = i+2 \\ \dfrac{2}{(2i+3)(2i+5)(2i+7)(2i+9)(2i+11)} & j = i+4 \end{cases},$$

where M is of bandwidth 8.

C.5 Calculation of $D_0^{\beta}(\phi)$

Using the basis functions (7.4) and (7.17) we have

$$\left\langle \sum_{k=1}^{N} \phi_k,\ \beta_i \right\rangle = \left\langle \sum_{k=1}^{N} \frac{L_{k+1} - L_{k-1}}{(2k+1)},\ \frac{L_{i+3} - L_{i+1}}{(2i+3)(2i+5)} - \frac{L_{i+1} - L_{i-1}}{(2i+1)(2i+3)} \right\rangle.$$

By applying the orthogonality relationship in (7.7), the matrix representation $D_0^{\beta}(\phi)$ can be derived, where, letting $M = D_0^{\beta}(\phi)$,

$$M_{i,j} = \begin{cases} \dfrac{-6}{(2i-1)(2i+1)(2i+3)(2i+5)} & j = i \\ \dfrac{6}{(2i+1)(2i+3)(2i+5)(2i+7)} & j = i+2 \\ \dfrac{-2}{(2i+3)(2i+5)(2i+7)(2i+9)} & j = i+4 \\ \dfrac{2}{(2i-3)(2i-1)(2i+1)(2i+3)} & j = i-2 \end{cases},$$

where M is of bandwidth 8.

C.6 Calculation of $D_0^{\phi}(\beta)$

Using the basis functions (7.4) and (7.17) we have

$$\left\langle \sum_{k=1}^{N} g_k \beta_k,\ \phi_i \right\rangle = \left\langle \sum_{k=1}^{N} \frac{g_k(L_{k+3} - L_{k+1})}{(2k+3)(2k+5)} - \frac{g_k(L_{k+1} - L_{k-1})}{(2k+1)(2k+3)},\ \frac{L_{i+1} - L_{i-1}}{(2i+1)} \right\rangle.$$

By applying the orthogonality relationship in (7.7), the matrix representation $D_0^{\phi}(\beta$ can be derived, where, letting $M = D_0^{\phi}(\beta)$,

$$M_{i,j} = \begin{cases} \dfrac{-6}{(2i-1)(2i+1)(2i+3)(2i+5)} & j = i \\ \dfrac{2}{(2i+1)(2i+3)(2i+5)(2i+7)} & j = i+4 \\ \dfrac{6}{(2i-3)(2i-1)(2i+1)(2i+3)} & j = i-2 \\ \dfrac{-2}{(2i-5)(2i-3)(2i-1)(2i+1)} & j = i-4 \end{cases},$$

where M is of bandwidth 8.

Bibliography

[1] Alex SM & Patil PR. *Effect of a variable gravity field on convection in an anisotropic porous medium with internal heat source and inclined temperature gradient*, J. Heat Transfer **124** (2002) pp 144–150.

[2] Alex SM & Patil PR. *Effect of variable gravity field on thermal instability in a porous medium with inclined temperature gradient and vertical throughflow*, J. Porous Media **5** (2002) pp 137–147.

[3] Amahmid A, Hasnaoui M & Vasseur P. *Etude analytique et numerique de la convection naturelle dans une couche poreuse de Brinkman doublement diffusive*, Int. J. Heat Mass Transfer **42** (1999) pp 2991–3005.

[4] Amahmid A, Hasnaoui M, Mamou M & Vasseur P. *Double-diffusive parallel flow induced in a horizontal Brinkman porous layer subjected to constant heat and mass fluxes: analytical and numerical studies*, Heat Mass Trans. **35** (1999) pp 409–421.

[5] Amili P & Yortsos YC. *Stability of heat pipes in vapor-dominated systems*, Int. J. Heat Mass Transfer **47** (2004) pp 1223–1246.

[6] Andrade JS, Costa UMS, Almeida MP, Makse HA & Stanley HE. *Inertial effects on fluid flow through disordered porous media*, Phys. Rev. Lett. **82** (1999) pp 5249–5252.

[7] Bhandar AS, Vogel MJ & Steen PH. *Energy landscapes and bistability to finite-amplitude disturbances for the capillary bridge*, Phys. Fluids **16** (2004) pp 3063–3069.

[8] Bourne D. *Hydrodynamic stability, the Chebyshev tau method and spurious eigenvalues*, Continuum Mech. Thermodyn. **15** (2003) pp 571–579.

[9] Brown BM & Marletta M. *Spectral inclusion and spectral exactness for singular non - self - adjoint Hamiltonian systems*, Proc. Roy. Soc. London A **459** (2003) pp. 1987–2009.

[10] Capone F & Rionero S. *Nonlinear stability of a convective motion in a porous layer driven by a horizontally periodic temperature gradient*, Continuum Mech. Thermodyn. **15** (2003) pp 529–538.

[11] Carr M. *A model for convection in the evolution of under-ice melt ponds*, Continuum Mech. Thermodyn. **15** (2003) pp 45–54.

[12] Carr M. *Unconditional nonlinear stability for temperature dependent density flow in a porous medium*, Math. Mod. and Meth. in App. Sci. **13** (2003) pp 207–220.

[13] Carr M & de Putter S. *Penetrative convection in a horizontally isotropic porous layer*, Continuum Mech. Thermodyn. **15** (2003) pp 33–43.

[14] Chandrasekhar S. *Hydrodynamic and Hydromagnetic Stability*, New York: Dover, 1981.

[15] Chasnov JR & Tse KL. *Turbulent penetrative convection with an internal heat source*, Fluid Dyn. Res. **28** (2001) pp 397–421.

[16] Christopherson DG. *Note on the vibration of membranes*, Quart. J. Math. **11** (1940) pp 63–65.

[17] Crisciani F. *Nonlinear stability of the Sverdrup flow against mesoscale disturbances*, Nuovo Cimento C **27** (2004) pp 7-16.

[18] Davies EB. *Pseudospectra: the harmonic oscillator and complex resonances*, Proc. Roy. Soc. London A **455** (1999) pp. 117–139.

[19] Delgado J, Nunez-Yepez HN & Salas-Brito AL. *On the Lagrangian form of the variational equations of Lagrangian dynamical systems*, Chaos Solitions Fractals **20** (2004) pp 925–935.

[20] Dongarra JJ, Straughan B & Walker DW. *Chebyshev tau-QZ algorithm methods for calculating spectra of hydrodynamic stability problems*, App. Num. Math. **22** (1996) pp 399–434.

[21] Drazin PG & Reid WH. *Hydrodynamic Stability*, Cambridge: Cambridge University Press, 1981.

[22] Forchheimer P. *Wasserbewegung durch Boden*, Ver. Deusch. Ing. Z. **50** (1901) pp 1781–1788.

[23] Fox L. *Chebyshev methods for ordinary differential equations*, Comput. J. **4** (1962) pp 318–331.

[24] Gardner DR, Trogdon SA & Douglass RW. *A modified tau spectral method that eliminates spurious eigenvalues*, J. Comput. Phys. **80** (1989) pp 137–167.

[25] Georgescu A & Mansutti D. *Conincidence of the linear and non-linear stability bounds in a horizontal thermal convection problem*, Int. J. Non-linear Mech. **34** (1999) pp 603–613.

[26] Gheorghiu CI & Pop IS. *A modified Chebyshev-tau method for a hydrodynamic stability problem.* In "Proc. Intl. Conf. Approximation and Optimization", vol. II (1996) pp 119–126.

[27] Giorgi T. *Derivation of the Forchheimer law via matched asymptotic exapansions. Transport in porous media*, Trans. Porous Med. **29** (1997) pp 191–206.

[28] Golub GH & Van Loan CF. *Matrix Computations*, 3rd edition. Johns Hopkins Univ Pr, 1996.

[29] Gottlieb D & Orszag SA. *Numerical Analysis of Spectral Methods: Theory and Applications*, Society for Industrial and Applied Mathematics: Philadelphia, 1977.

[30] Greenberg L & Marletta M. *Numerical methods for higher order Sturm - Liouville problems*, J. Comput. App. Math. **125** (2000) pp 367–383.

[31] Greenberg L & Marletta M. *Numerical solution of non self - adjoint Sturm - Liouville problems and related systems*, SIAM J. Numer. Anal. **38** (2001) pp 1800–1845.

[32] Greenberg L & Marletta M. *The Ekman flow and related problems: spectral theory and numerical analysis* , Math. Proc. Camb. Phil. Soc. **136** (2004) pp. 719–764.

[33] Guo J & Kaloni PN. *Double-diffusive convection in a porous medium, nonlinear stability, and the Brinkman effect*, Stud. App. Math. **94** (2005) pp 341–358.

[34] Haidvogel DB & Zang T. *The accurate solution of Poisson's equation by expanding in Chebyshev polynomials*, J. Comput. Phys. **30** (1979) pp 167–180.

[35] Herron IH & Ali HN. *The principle of exchange of stabilities for Couette flow*, Q. Appl. Math. **61** (2003) pp 279–293.

[36] Hill AA. *Convection due to the selective absorption of radiation in a porous medium*, Continuum Mech. Thermodyn. **15** (2003) pp 275–285.

[37] Hill AA. *Convection induced by the selective absorption of radiation for the Brinkman model*, Continuum Mech. Thermodyn. **16** (2004) pp 43–52.

[38] Hill AA. *Conditional and unconditional nonlinear stability for convection induced by absorption of radiation in a porous medium*, Continuum Mech. Thermodyn. **16** (2004) pp 305–318.

[39] Hill AA. *Penetrative convection induced by the absorption of radiation with a nonlinear internal heat source*, Dyn. Atmos. Oceans **38** (2004) pp 57–67.

[40] Hill AA. *Double-diffusive convection in a porous medium with a concentration based internal heat source*, Proc. Roy. Soc. London A **461** (2005) pp 561–574.

[41] Hill AA & Straughan B. *Legendre spectral element method for eigenvalues in hydrodynamic stability* , J. Comput. Appl. Math., in the press (2005).

[42] Hill AA. *A Chebyshev polynomial based spectral method for eigenvalue problems in continuum mechanics*, manuscript (2005).

[43] Hill AA & Straughan B. *Linear and nonlinear bounds in a horizontal thermal convection problem*, manuscript (2005).

[44] Hill AA. *Horizontal thermal convection in a porous medium*, manuscript (2005).

[45] Holzbecher E. *Free convection in open-top enclosures filled with a porous medium heated from below*, Numer. Heat Trans. A - Appl. **46** (2004) pp 241–254.

[46] Ivansson S. *Compound - matrix Riccati method for solving boundary value problems*, Zeit. Angew. Math. Mech. **83** (2004) pp 535–548.

[47] Joseph DD. *Global stability of the conduction-diffusion solution*, Arch. Rational Mech. Anal. **36** (1970) pp 285–292.

[48] Joseph DD. *Stability of Fluid Motions II*, New York: Springer Verlag, 1976.

[49] Kaiser R & Mulone G. *A note on nonlinear stability of plane parallel shear flows*, J. Math. Anal. Appl. **302** (2005) pp 543–556.

[50] Kaloni PN & Lou JX. *On the stability of thermally driven shear flow of an Oldroyd-B fluid heated from below*, J. Non-Newtonian Fluid Mech. **107** (2002) pp 97–110.

[51] Kaloni PN & Lou JX. *Convective instability of magnetic fields*, Phys. Rev. E **70** (2004) art. no. 026313.

[52] Kaloni PN & Lou JX. *Nonlinear convection of a viscoelastic fluid with inclined temperature gradient*, Cont. Mech. Thermodyn. **17** (2005) pp 17–27.

[53] Kim S & Russel WB. *Modelling of porous medium by renormalisation of the Stokes equation*, J. Fluid Mech. **154** (1985) pp 269–286.

[54] Kirchner NP. *Computational aspects of the spectral Galerkin FEM for the Orr-Sommerfield equation*, Int. J. Num. Meth. Fluids **32** (2000) pp 119–137.

[55] Krishnamurti R. *Convection induced by selective absorption of radiation: A laboratory model of conditional instability*, Dyn. Atmos. Oceans **27** (1997) pp 367–382.

[56] Larson VE. *Stability properties of and scaling laws for a dry radiative-convective atmosphere*, Quart. J. Royal Meteo. Soc. **126** (2000) pp 145–171.

[57] Larson VE. *The effects of thermal radiation on dry convective instability*, Dyn. Atmos. Oceans **34** (2001) pp 45–71.

[58] Lehoucq RB, Sorenson DC & Yang C. *ARPACK Users' Guide: Solution of Large Scale Eigenvalue Problems with Implicitly Restarted Arnoldi Methods*, Phildelphia: SIAM, 1998.

[59] Lombardo S, Mulone G & Straughan B. *Non-linear stability in the Bénard problem for a double-diffusive mixture in a porous medium*, Math. Meth. App. Sci. **24** (2001) pp 1229–1246.

[60] Lu WS & Shao HY. *Generalized nonlinear subcritical symmetric instability*, Adv. Atmos. Sci. **20** (2003) pp 623–630.

[61] Mahidjiba A, Vasseur P & Bilgen E. *Multiple solutions for double-diffusive convection in a vertical porous enclosure*, Int. J. Heat Mass Transfer **38** (1995) pp 1787–1798.

[62] Mahidjiba A, Mamou M & Vasseur P. *Onset of double-diffusive convection in a rectangular porous cavity subject to mixed boundary conditions*, Int. J. Heat Mass Transfer **43** (2000) pp 1505–1522.

[63] Mahidjiba A, Robilland L & Vasseur P. *Linear stability of cold water saturating an anisotropic porous medium - effect of confinement*, Int. J. Heat Mass Transfer **46** (2003) pp 323–332.

[64] Mamou M, Hasnaoui M, Amahmid A & Vasseur P. *Stability analysis of double-diffusive convection in a vertical Brinkman porous enclosure*, Int. Comm. Heat Mass Transfer **25** (1998) pp 491–500.

[65] Martys NS. *Improved approximation of the Brinkman equation using a lattice Boltzman method*, Phys. Fluids **13** (2001) pp 1807–1810.

[66] Martys NS, Bentz DP & Garboczi EJ. *Computer simulation study of the effective viscosity in Brinkman's equation*, Phys. Fluids **6** (1994) pp 1434–1439.

[67] McKay G. *Onset of buoyancy-driven convection in superposed reacting fluid and porous layers*, Jnl. Engng. Maths. **33** (1998) pp 31–46.

[68] McKay G. *Double-diffusive convective motions for a saturated porous layer subject to modulated surface heating*, Continuum Mech. Thermodyn. **12** (2000) pp 69–78.

[69] McKay G & Straughan B. *The influence of a cubic density law on patterned ground formation*, Math. Mod. App. Sci. **1.1** (1991) pp 27–39.

[70] Mercier JF, Weisman C, Firdaouss M & Le Quere P. *Heat transfer associated to natural convection flow in a partly porous cavity*, J. Heat Transfer **124** (2002) pp 130–143.

[71] Merrikh AA & Mohamad AA. *Non-Darcy effects in buoyancy driven flows in an enclosure filled with vertically layered porous media*, Int. J. Heat Mass Transfer **45** (2002) pp 4305–4313.

[72] Mitrinovic DS. *Analytic Inequalities*, Springer-Verlag: New York, 1970.

[73] Moler CB & Stewart GW. *An algorithm for generalized matrix eigenproblems*, SIAM J. Numer. Anal. **10** (1973) pp 241–256.

[74] Mulone G. *On the nonlinear stability of a fluid layer of a mixture heated and salted from below*, Continuum Mech. Thermodyn. **6** (1994) pp 161–184.

[75] Mulone G & Rionero S. *Unconditional nonlinear exponential stability in the Bénard problem for a mixture: necessary and sufficient conditions*, Rend. Mat. Acc. Lincei **9** (1998) pp 221–236.

[76] Nield DA. *Convection in a porous medium with an inclined temperature gradient: additional results*, Int. J. Heat Mass Transfer **37** (1994) pp 3021–3025.

[77] Nield DA & Bejan A. *Convection in Porous Media*, 2nd ed. New York: Springer Verlag, 1999.

[78] Payne LE, Song JC & Straughan B. *Continuous dependence and convergence results for Brinkman and Forchheimer models with variable viscosity*, Proc. R. Soc. Lond. A **455** (1999) pp 2173–2190.

[79] Payne LE & Straughan B. *Unconditional Nonlinear Stability in Temperature-Dependent Viscosity Flow in a Porous Medium*, Stud. App. Math. **105** (2000) pp 59–81.

[80] Pop IS. *A stabilized approach for the Chebshev-tau method*, Studia Univ. Babes-Bolyai, Mathematica **42** (1997) pp 67–79.

[81] Pop IS. *A stabilized Chebyshev-Galerkin approach for the biharmonic operator*, Bul. Stint. Univ. Baia Mare, Ser. B, Matematica-Informatica **16** (2000) pp 335–344.

[82] Poulikakos D. *Double-diffusive convection in a horizontally sparsely packed porous layer*, Int. Comm. Heat Mass Transfer **13** (1986) pp 587–598.

[83] Saloff-Coste L. *Aspects of Sobolev-Type Inequalities*, Univeristy Press: Cambridge, 2002.

[84] Saravanan S & Kandaswamy P. *Convection currents in a porous layer with gravity gradient*, Heat Mass Transfer **39** (2003) pp 693–699.

[85] Shen J. *Efficient spectral-Galerkin method I. Direct solvers of second and fourth order equations using Legendre polynomials*, SIAM J. Sci. Comput. **15** (1994) pp 1489–1505.

[86] Shen J. *Efficient spectral-Galerkin method I. Direct solvers of second and fourth order equations using Chebyshev polynomials*, SIAM J. Sci. Comput. **16** (1995) pp 74–87.

[87] Sneddon IN. *Special functions of Mathematical Physics and Chemistry*, 3rd ed. London and New York: Longman, 1980.

[88] Straughan B. *Mathematical aspects of penetrative convection*, Pitman Research Notes in Mathematics, Vol. 288: Longman Publishing Co., 1993.

[89] Straughan B. *Global stability for convection induced by absorption of radiation*, Dyn. Atmos. Oceans **35** (2002) pp 351–361.

[90] Straughan B. *The energy method, stability, and nonlinear convection*, 2nd ed. New York: Springer Verlag, 2004.

[91] Straughan B & Walker DW. *Two very accurate and efficient methods for computing eigenvalues and eigenfunctions in porous convection problems*, J. Comput. Phys. **127** (1996) pp 128–141.

[92] Theofilis V. *Advances in global linear instability analysis of nonparallel and three-dimensional flows*, Prog. Aerosp. Sci. **39** (2003) pp 249–315.

[93] Tien H & Chiang K. *Non-Darcy flow and heat transfer in a porous insulation with infiltration and natural convection*, J. Marine Sci. Tech. **7** (1999) pp 125–131.

[94] Tracey J. *Stability analysis of multi-component convection-diffusion problems*, PhD. Thesis, Univ. of Glasgow, 1997.

[95] Trevisan OV & Bejan A. *Combined Heat and Mass Transfer by Natural Convection in a Porous Medium*, Adv. Heat Transfer **28** (1990) pp 1587–1611.

[96] Tse KL & Chasnov JR. *A Fourier-Hermite pseudo spectral method for penetrative convection*, J. Comput. Phys. **142** (1998) pp 489–505.

[97] Whitaker S. *The Forchheimer equation: A theoretical development*, Trans. Porous Med. **25** (1996) pp 27–62.

[98] Young WH. *On classes of summable functions and their Fourier Series*, Proc. Roy. Soc. A **87** (1912) pp 225–229.

[99] Zhang KK & Schubert G. *Teleconvection: remotely driven thermal convection in rotating stratified spherical layers*, Science **290** (2000) pp 1944–1947.

[100] Zhang KK & Schubert G. *From penetrative convection to teleconvection*, Astrophys. J. **572** (2002) pp 461–476.